TÉCNICO LISBOA

Project of control software and antennas for an indoor UWB localization system

Duarte Nuno Rodrigues Varandas Gouveia

Thesis to obtain the Master of Science degree in

Electrical and Computer Engineering

Supervisor: Prof. António Manuel Restani Graça Alves Moreira

Examination Committee

Chairperson: Prof. José Eduardo Charters Ribeiro da Cunha Sanguino
Supervisor: Prof. António Manuel Restani Graça Alves Moreira
Member of the Committee: Prof. António José Castelo Branco Rodrigues

May 2016

Dedicated to my Family and Friends

Acknowledgments

To begin with, I would like to express my gratitude towards Prof. António Moreira for his support on my thesis supervision as well as his patience and willingness.

I would also like to thank Eng. António Almeida for helping me with laboratory set-up for practical tests of the developed localization system and antenna measurements. It helped me begin my development and acquaintance in an Antenna Laboratory as well as become aware of some measurement practices.

Additionally, I express my gratitude towards Eng. Carlos Brito who manufactured my antenna prototype and thoroughly explained and demystified the development of printed circuits bringing me along in the entire process.

Also, I am thankful to Instituto de Telecomunicações, specially to Prof. Carlos Fernandes for providing and letting me handle the hardware ranging modules that compose the main building blocks of the localization system developed in this work.

Thank you to my parents and closest family members for supporting me on my educational journey. Also, a sincere thank you to my brother Luís Miguel who was there for me all these years.

Resumo

O interesse pelos sistemas de localização em tempo real (RTLS) tem sido cada vez mais pertinente na última década. A necessidade para uma solucão de *tracking* em ambientes *indoor* é importante e, garantir que o sistema tem agilidade, boa performance, resiliência e alta capacidade de adaptação, são os principais objectivos para o desenvolvimento de sistemas de localização.

Este trabalho consiste no desenvolvimento de um software de controlo, adaptável e stand-alone para uma solução comercial existente de módulos que estimam a distância entre si usando impulsos Ultra Wide Band (UWB). Para isso, foram analisados vários algoritmos de localizacão baseados no método dos mínimos quadrados não linear, aproximação por série de Taylor e ainda outros métodos não iterativos. Também foi desenvolvido, para este sistema, um modelo de estados para um filtro de Kalman de forma a mitigar os efeitos do ruído nas medições.

Após uma análise dos resultados, concluiu-se que a aproximação por série de Taylor é o algoritmo que gera um melhor compromisso entre tempo de execução e resultados em termos de erro médio e accuracy. Conjuntamente com o desenvolvimento da aplicação, sugere-se uma antena UWB dimensionada para a frequência de funcionamento dos módulos. Após um teste da sua aplicação, concluiu-se que o uso da antena proposta causa uma diminuição da variância das medições de distância face ao monopolo usado como referência, mas é no aumento do Indicador de Sinal Recebido (RSSI) que mais se destaca. Estes resultados incentivam a sua utilização em sistemas de ranging, como é o caso.

Palavras-chave: Sistemas de localização indoor, sistemas de localização em tempo real, antena Ultra Wide Band (UWB), *tracking*, UDP, *ranging*

Abstract

In the last decade, the Real-time Localization Systems (RTLS) have been increasingly relevant. Simple and efficient solutions for indoor tracking are important for several real-world applications.

The objective of this work is to provide a fully functional UWB indoor localization system making use of four Time Domain PulsOn P400 ranging modules for which a corresponding controlling software and antenna were developed. The software implements techniques based on Non-Linear Least Squares, Taylor Series approximation and other linear methods that were reviewed. Also, to improve the software tracking abilities, a Kalman filter state model for the system was proposed. After a careful analysis to the gathered results, it has been concluded that the Taylor Series Approximation algorithm establishes a fair compromise between *Tracking Algorithm* iteration time and consistent results in terms of mean error relative to the true target position and accuracy.

Alongside the development of the application, a UWB reflector antenna is also proposed. This antenna presents a high directivity and has been designed to operate in the frequency band of the modules. It competes directly with the existent omni-directional antennas used by the modules. After evaluating the antenna performance in a real ranging scenario, it has been observed that the variance of the measurements has decreased compared to the reference omni-directional monopole. Moreover, the observed increase in Received Signal Strength Indicator (RSSI) readings suggests the application of this antenna in ranging systems.

Keywords: Indoor localization systems, Real-time Localization Systems (RTLS), Ultra Wide Band (UWB) Antenna, tracking, UDP, ranging

Contents

Acknowledgments v
Resumo vii
Abstract ix
List of Tables xv
List of Figures xix
List of Acronyms xxii

1 Introduction **1**
1.1 Motivation and objectives 1
1.2 Contents 2

2 Outline of localization systems **5**
2.1 Introduction 5
2.2 Technical aspects of location systems 6
2.2.1 Network topology 6
2.2.2 Accuracy and precision 7
2.2.3 Location techniques 7
Received Signal Strength Indicator (RSSI) 7
Time of Arrival (ToA) 9
Time Difference of Arrival (TDoA) 11
Round-trip Time of Flight (RToF) 13
Angle or Direction of Arrival (AoA or DoA) 13
Proximity 14
2.3 Overview of deployed wireless location systems 14
2.3.1 Contact-based systems 15
2.3.2 Contact-less systems 15

3 Antennas for indoor location **19**
3.1 Introduction 19
3.2 Technical overview 19
3.2.1 Antenna requirements 19
3.2.2 Antenna types 20

3.3 Antennas for RSSI based systems . . . 21
3.4 Antennas for ToA or TDoA based systems . . . 24
3.5 Antennas for AoA based systems . . . 28

4 Development of a reflector UWB Antenna 31
4.1 Introduction . . . 31
4.2 Antenna Design . . . 32
4.2.1 Base model . . . 32
4.2.2 Parameter analysis . . . 34
4.3 Performance Analysis . . . 37
4.3.1 Measurement of reflection coefficient . . . 38
4.3.2 Performance measurement in a ranging system . . . 39
4.4 Summary . . . 41

5 Location techniques and solvers 43
5.1 Linear Approaches . . . 44
5.1.1 Simple Geometric Pinpoint . . . 44
5.1.2 Linearized Least Squares Approximation . . . 45
5.2 Non-Linear Approaches . . . 48
5.2.1 Non-linear least squares . . . 48
5.2.2 Taylor-Series Approximation . . . 49
5.3 Noise model . . . 50
5.4 Real-Time Tracking and path smoothing . . . 51
5.5 The Tracking Algorithm . . . 54
5.6 Performance Analysis . . . 54
5.6.1 Static target . . . 55
5.6.2 Target moving on a straight path . . . 59
5.7 Summary . . . 61

6 System architecture 63
6.1 Introduction . . . 63
6.2 Hardware description . . . 64
6.2.1 The PulsOn P400 Modules . . . 64
Communication and Controlling Interfaces . . . 65
Round-trip Time of Flight Ranging . . . 66
6.2.2 Network environment and communication . . . 66
Network Layout . . . 66
Transmitted packet types . . . 68
6.3 Software description . . . 70
6.3.1 Application structure . . . 71

Tracker class 71
Packet class 72
Solver class 73
6.4 Summary 74

7 Conclusion and future work **77**
7.1 Future Work 78

References **81**

A Connector model **87**

B Radiation patterns of UWB antenna **89**

C Software User Interface **91**
C.1 Main User Interface 91
C.2 Advanced Options 92
C.3 New base station layout 93
C.4 Smoothing options 93
C.5 Simulation console 93
C.6 Tracking report 94

D Example of layout input file **97**

List of Tables

2.1 Overview of presented technologies. 17

5.1 Data for Point A. 57
5.2 Data for Point B. 58
5.3 Data for Point C. 58
5.4 Data for straight line path A to B. 61

6.1 Classes present in the application. 72

C.1 Fields of tracking log file. 95

List of Figures

1.1 Illustration of a simple localization system. 2

2.1 Illustration of network operating modes. 7
2.2 Fingerprinting: Unknown node's location P is estimated according to off-line RSSI measurements 8
2.3 Positioning based on RSSI and ToA measurements. 11
2.4 Positioning using the time difference of arrival of an RF and an ultrasound signal. 11
2.5 TDoA positioning (only the relevant branch of the hyperbola is shown for each measurement). 12
2.6 AoA positioning. 14
2.7 Examples of devices used in two presented location systems. 16

3.1 Antenna types for indoor location 21
3.2 Examples of Inverted F and Meander antennas. 23
3.3 Meander antenna for RFID Tag 23
3.4 Microstrip rectangular and circular patch. Antenna excitation from underneath via probe feed. 24
3.5 Illustration of received power in a multipath environment. 25
3.6 Typical UWB monopoles design. 27
3.7 Illustration of two UWB circularly polarized antennas. 28
3.8 Depiction of the dielectric loading sandwich technique. 28
3.9 Examples of smart antennas design. 30
3.10 Cylindrical conformal array of UWB Antennas. 30

4.1 Stock UWB monopole variation. 32
4.2 Base model for the proposed UWB antenna design - reflector plane and SMA connector not shown (dimentions in mm). 33
4.3 Perspective and side view of the antenna model with reflector plane and SMA connector (dimensions in mm). 34
4.4 Sweep for the parameter we. Left: S_{11} in dB, Right: Directivity in dBi 34
4.5 Sweep for the parameter m. Left: S_{11} in dB, Right: Directivity in dBi 35
4.6 Sweep for the parameter at. Left: S_{11} in dB, Right: Directivity in dBi 35

4.7 Sweep for the parameter vc. Left: S_{11} in dB, Right: Directivity in dBi . . . 35
4.8 Sweep for the parameter alt. Left: S_{11} in dB, Right: Directivity in dBi . . . 36
4.9 Reflector inclination dependent on angle α. . . . 36
4.10 Sweep for the parameter α. Left: S_{11} in dB, Right: Directivity in dBi . . . 37
4.11 S_{11} and Directivity for the final parameters. . . . 37
4.12 Antenna prototype. . . . 38
4.13 S_{11} measurement. . . . 38
4.14 S_{11} measurement and simulated results. . . . 39
4.15 Measurement scheme. . . . 39
4.16 Picture of reference and proposed antenna on their respective nodes. . . . 40
4.17 Standard deviation for proposed and reference antenna. . . . 40
4.18 RSSI difference between proposed and reference antenna. . . . 40

5.1 Cluster of ToA estimation. . . . 44
5.2 Measured standard deviation and interpolated noise model. . . . 50
5.3 Simplified block diagram of the *Tracking Algorithm*. . . . 55
5.4 Base station and target positions. . . . 56
5.5 Photo of measurement set up. . . . 56
5.6 Straight line path to be tested. . . . 59
5.7 Main user interface during target detection. . . . 60
5.8 LLS and TS/LSS performance visualization. . . . 61

6.1 System architecture. . . . 64
6.2 One of the four identical RCMs. . . . 65
6.3 Network of RCMs. . . . 67
6.4 Network Layer 3 and Layer 4 structure (target not shown). . . . 68
6.5 System packet transmission. . . . 69
6.6 Block diagram of stage A of the *Tracking Algorithm*. . . . 73
6.7 4th time slot is skipped due to delay on stage A, B or C of the *Tracking Algorithm*. . . . 74
6.8 Block diagram of stage B, C and D of the *Tracking Algorithm*. . . . 75

A.1 SMA connector. . . . 87
A.2 CST model of SMA connector. . . . 87

B.1 Antenna spherical coordinate system. . . . 89
B.2 $f = 3.1GHz$ for $\phi = 0$. . . . 89
B.3 $f = 4.3GHz$ for $\phi = 0$. . . . 89
B.4 $f = 5.3GHz$ for $\phi = 0$. . . . 90
B.5 $f = 3.1GHz$ for $\phi = 90°$. . . . 90
B.6 $f = 4.3GHz$ for $\phi = 90°$. . . . 90
B.7 $f = 5.3GHz$ for $\phi = 90°$. . . . 90

C.1 Main User Interface. 91
C.2 Advanced configuration interface. 92
C.3 Set new base station layout interface. 93
C.4 Kalman filter options interface. 93
C.5 Simulation console interface. 94
C.6 Save tracking report window. 94

List of Acronyms

AoA	Angle of Arrival
AP	Access Point
API	Application Programming Interface
BIA	Burned-In Address
BS	Base Station
CDMA	Code-Division Multiple Access
Cell-ID	Cell Identification
CLWLS	Constrained Linear Weighted Least Squares
CPW	Coplanar Waveguide
CRLB	Cramér-Rao Lower Bound
DHCP	Dynamic Host Configuration Protocol
DoA	Direction of Arrival
DSSS	Direct Sequence Spread Spectrum
GNSS	Global Navigation Satellite System
GPS	Global Positioning System
GUI	Graphical User Interface
LLS	Linear Least Squares
LoS	Line of Sight
LS	Least Squares
LWLS	Linear Weighted Least Squares
MAC	Media Access Control
MDE	Mean Distance Error
ML	Maximum Likelihood
mps	Measurements per Sample
MSE	Mean Squared Error
NIC	Network Interface Controller
NLLS	Non-Linear Least Squares
NLoS	Non Line of Sight
NLWLS	Non-Linear Weighted Least Squares
OSI	Open Systems Interconnection

PCB	Printed Circuit Board
PIFA	Planar Inverted-F Antenna
RCM	Ranging and Communications Module
RF	Radio Frequency
RFID	Radio Frequency Identification
RSSI	Received Signal Strength Indicator
RTLS	Real-Time Localization System
RToF	Round-trip Time of Flight
SAA	Sectorized Antenna Array
SGP	Simple Geometric Pinpoint
SNR	Signal-to-Noise ratio
T.A.	Tracking Algorithm
TDoA	Time Difference of Arrival
ToA	Time of Arrival
TS	Taylor Series Approximation
UDP	User Datagram Protocol
UHF	Ultra-High Frequency
UWB	Ultra Wide Band
VLAN	Virtual Local Area Network
VNA	Vector Network Analyser
Wi-Fi	Wireless Fidelity

Chapter 1

Introduction

1.1 Motivation and objectives

Since the inception of wireless propagation, but specially in the last 10 to 15 years, there has been a non-stop development in the area of location techniques. The capacity growth of devices that help locate someone or something on a given site has been tremendous. More and more the utilities and capabilities of wireless propagation techniques have become increasingly relevant in this scientific field.

Antennas are one of the most important components in a localization system. They are the entrance and exit points for information when it's transmitted wirelessly. Improvements in the area are almost limitless and there is still a lot of research to be done. Today with modern simulation techniques one can almost develop a full working model on the computer by means of advanced simulation software. However, the testing phase cannot be left aside. The usefulness of the fine tuning ensuing the testing phase is indubitably as relevant. The potential of these methods and their ability to adapt to new scientific challenges is one of the reasons why this subject is so interesting and promising.

Alongside the development of a localization system there's the need for developing software that analyses, processes and presents the user with human readable and useful information. The variety of possibilities in regards to programming language, platforms and environments allow for a very versatile and complete solution.

The purpose of localization systems is vast and concerns many scientific fields and services such as medical and healthcare monitoring, inventory location, global positioning or even personal tracking. These fields have developed a need for the so-called Location Awareness. The constant improvement of such systems is imperative as they must keep up with constant new challenges and necessities. Overall, the goal is to reduce complexity, increase resilience and maintain operation capacity throughout usage time despite external factors such as interference, user interaction or physical damage.

Figure 1.1 illustrates de concept of a complete localization network or system and its central functions. First, the network wireless signals enter the physical interface. They are then processed according to the system's needs and finally presented to the user. The objective of this work is to provide a fully functional Ultra Wide Band (UWB) indoor localization system making use of four Time Domain PulsOn

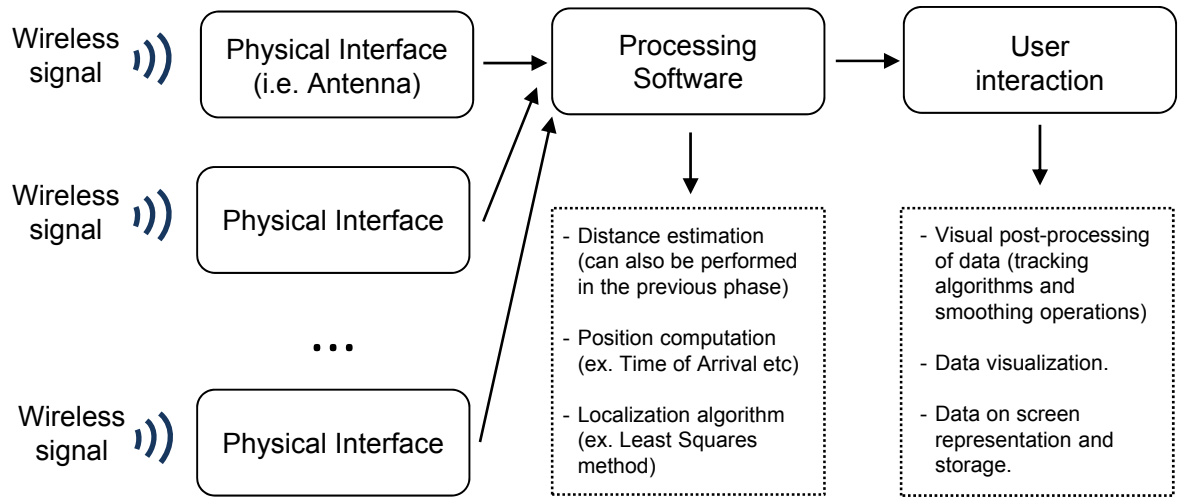

Figure 1.1: Illustration of a simple localization system.

P400 ranging modules linked together in an Ethernet network for which a corresponding controlling software and antenna were developed.

The proposed control software consists of a Graphical User Interface (GUI) developed in Visual C# 2012 which communicates via User Datagram Protocol (UDP) packets with the PulsOn P400 modules which are capable of determining distance between themselves by request using a Round-trip Time of Flight (RToF) protocol via UWB pulses. Positioning, localization and visual post-processing of data algorithms were developed with the aid of the Math.NET Numerics toolkit and MATLAB R2015a which then are used by the software via shared pre-compiled libraries provided by the MATLAB Runtime software package. For intra-module communication a unidirectional, UWB antenna (optimized for the band 3.1 to 5.3 GHz) was developed and tested in an indoor localization scenario. Moreover, the validity of existing Time of Arrival (ToA) localization estimation algorithms is tested and their performances compared, in the scope of the developed indoor Real-Time Localization System (RTLS).

1.2 Contents

Chapter 2 starts off by giving an overview of the current state-of-the-art of wireless localization systems focused on the indoor case. It is given special attention to the RTLSs. Position estimation techniques like ToA, Time Difference of Arrival (TDoA) or Angle of Arrival (AoA)/Direction of Arrival (DoA) amongst others are also analysed. Also, a comprehensive overview on deployed wireless location systems is presented along with the definition and examples of contact-based and contact-less systems.

In chapter 3, antennas for indoor localization are presented along with their functionality and properties. In section 3.2 the antenna types and requirements are detailed. In the following sections antennas for position estimation techniques presented earlier are discussed. The advantages and disadvantages on the application of the presented antennas are examined. The significance of antennas for UWB is also stressed.

In chapter 4, an UWB antenna for ranging communication is proposed. The idea behind a new design lies on the use of a metallic reflector plane which concentrates power on a given direction. Optimization details and performance are also evaluated.

In chapter 5, the localization and tracking algorithms used by this system are introduced. Various proposals are made to be used in the RTLS. In addition, by using the developed control software, the algorithms are tested and its performance commented on.

In chapter 6, the system architecture is presented. Not only the hardware and network parts are explained, but also the software development and its usefulness are demonstrated.

In chapter 7, the final conclusions about the work are drawn. Also, future work topics are suggested.

Chapter 2

Outline of localization systems

In this chapter, the definition and application of a general localization system as well as an overview of the underlying localization estimation techniques are introduced. The concept of a Real Time Localization System is also presented. Furthermore, the current knowledge in this field, recent developments that have occurred and some already developed location systems are exposed.

2.1 Introduction

A location or localization system is a set of operational devices which possess specific hardware and software to compute and locate the position of a moving or stationary object in a given site. These systems are made of nodes that can represent devices to be located (unknown nodes, dark nodes or target nodes) or reference points whose location is known (reference nodes or base stations). The goal of such systems is to provide a more-or-less precise and accurate location of the object depending on its characteristics and function. A system that does this in real-time is called an RTLS. One application of the RTLSs is the already mentioned medical services, for example. More in-depth, location estimation within hospitals or outdoor ambulance tracking helps the medical emergency service to function more efficiently. Another application of RTLS is the very classic navigation. An RTLS such as the Global Positioning System (GPS) [1] can be used to simply find directions or, in a more complex scenario, to aid traffic management.

Moreover, tracking services also employ RTLSs. These can include people, vehicle, personnel or product tracking [2]. As an example, a study presented in [3] reveals that through user localization in indoor construction environments, immediate and opportune access to project relevant information can be useful for time efficiency and cost reduction. Other social services, where mostly outdoor RTLS can be implemented, include information, marketing and billing [2].

A location system can be differentiated by specific characteristics or properties. As expected, despite the physical properties of the system and its applications, the required estimation accuracy and precision varies significantly depending on the goal the system is trying to achieve and the hardware used. Moreover, the working environment, whether it is indoor or outdoor, is also an important characteristic.

Similarly, the system can be either contact of contact-less based. Finally, the used location techniques are also an important aspect.

In what follows, the mentioned characteristics will be analysed in detail. Along with the analysis, examples of currently deployed systems will be presented and referenced in the scope of each property. A special emphasis will be given to the location techniques, since it's one of the main subjects of this dissertation.

2.2 Technical aspects of location systems

In this section, several technical aspects are presented. These include the concept of operation mode, accuracy and precision as well as basic location techniques.

The estimation of localization can be divided into three categories or steps: Distance/angle estimation, position computation and visual post-processing. Information gathered by the sensors or devices will travel these 3 steps in order. In section 2.2.3 it will be given special attention to distance/angle estimation which is the component responsible for computing the distance or angle between two nodes. In the same section, position computation techniques like Fingerprinting, Tri- and Multilateration will be introduced. Additionally, some position estimation algorithms, which will compute the nodes location with respect to existing reference nodes or points, will be mentioned. Visual processing is part of the developed software which will be briefly mentioned in posterior Chapters.

2.2.1 Network topology

Location systems are based on an underlying network regardless of the technology used. According to [4] one can distinguish between three major types of fundamental topologies or operation modes.

Infrastruture mode. The devices used in such an operation mode are part of an infrastructure of previously placed reference nodes which the devices are connected to. There is no direct communication between devices. This allows for a flexible connection/disconnection of nodes to or from the network because they do not depend on each other. However, this added complexity requires more equipment and configuration necessities. In Wireless Fidelity (Wi-Fi) networks, for example, the reference nodes are Access Points (AP) to which Wi-Fi enabled devices connect to. An example of network operating in an infrastructure mode is presented in Figure 2.1 a).

Ad-hoc mode. In this operation topology the devices or sensors do not depend on a previously existing network to communicate or on any central administration. The communication is done in a peer-to-peer fashion. Because each device acts as its own router, network management and fault detection is a difficult task to accomplish [5]. The ZigBee standard [6] supports this operation mode and is an example of recent application. Figure 2.1 b) depicts an ad-hoc network composed of mobile devices.

Deduced or dead reckoning. This is an operation mode where the system estimates an object's current position by inferring it from the last previous known location together with speed and trajectory information. The device estimates its own location by itself, without external communication. Inertial

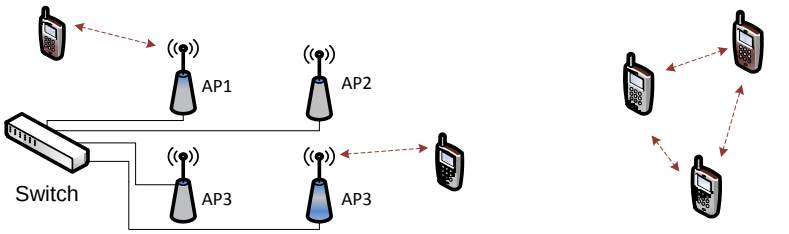

a) Infrastructure mode b) Ad-hoc mode

Figure 2.1: Illustration of network operating modes.

Navigation [7] is a currently used form of dead reckoning.

2.2.2 Accuracy and precision

The rigour of a location estimation system is a characteristic of great importance. In the literature, by introducing the concept of Accuracy and Precision, it can be classified how well the location estimation system behaves [8].

Accuracy, or granularity, denotes how close an estimation is to the real value. In the case of location systems, a higher accuracy (finer granularity) means a lower spatial error margin relative to the true location. It is expressed in units of length and it usually arises in the form of a range of values. Precision denotes how likely it is for the estimated value to lie within a certain accuracy interval or above a threshold.

Accuracy of location systems vary within orders of magnitude. It typically ranges from centimetres up to kilometres depending on propagation environment (indoor or outdoor) as well as on their application goal and available technology. Table 2.1 summarizes the expected accuracy and precision for some of the briefly presented location systems in section 2.3.2.

2.2.3 Location techniques

In what follows, special attention will be given to basic techniques for location determination in which methods like Received Signal Strength Indicator (RSSI), ToA, TDoA, AoA/DoA and RToF are included. Along with the analysis the most used estimation algorithms are briefly mentioned.

Received Signal Strength Indicator (RSSI)

The RSSI can be used to estimate a distance between two nodes using only the measured signal strength (or a value proportional to it) received from one of the nodes. A common model to relate the average received power with the distance travelled by the signal is given by [9]

$$\overline{P}(d) = P_0 - 10n \times log_{10}(d/d_0) \tag{2.1}$$

where P_0 is the power in dB received at the reference distance d_0 and n is called the path loss exponent. Despite this model's simplicity, the instantaneous power received is subject to multipath effects such as reflection, scattering and diffraction which foment a rapid received power variation over short time intervals or distances. This effect can be mitigated by computing the mean of the power received over a certain period of time T. However, there can be no Line of Sight (LoS) and so the signal suffers from shadowing and a slower power variation still occurs around its mean [9]. Signal power variation in linear units caused by this fading can be modelled by a log-normal distribution with a certain mean and variance σ^2. Propagation conditions depend on a constant scenario variation when the node to be located constantly moves. This makes it difficult to properly define an accurate path loss exponent n and variance σ^2. The type of antenna and node orientation must also be taken into account. These effects corrupt the measured quantity; therefore, the distance estimation is mostly inaccurate using solely this method.

Most available receivers are able to measure the RSSI without any special additional hardware [10]. This means that systems based in RSSI can have a reduced cost. This brings a problem however, although a RSSI based location can be a inexpensive solution, low-cost modules commonly possess poorly calibrated components. This not only affects RSSI readings but also the transmitted power. As an example, an experiment in [11] obtained estimation accuracies in the order of a few metres using WINS Sensor nodes [12] placed at ground level. The same experiment shows that RSSI can be very unpredictable and highly dependable on distance between reference nodes.

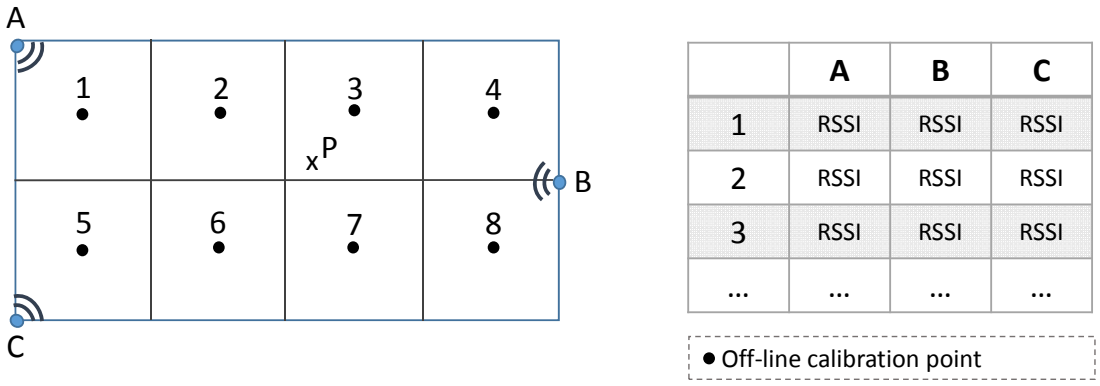

Figure 2.2: Fingerprinting: Unknown node's location P is estimated according to off-line RSSI measurements

A known application for the use RSSI information in a technique called Fingerprinting [13]. Such a system is depicted in Figure 2.2. This technique involves two phases: off-line and on-line phase. In the off-line phase, the area of operation of the location system is scanned in order to collect signal features from the various reference nodes like RSSI information. These data are stored in a database. In the on-line phase, Fingerprinting-based location algorithms compare the target node's current readings with the stored information in the off-line phase and computes its position. These algorithms include, for instance, the kNN - Nearest Neighbour estimation algorithms [14], Neural Networks [4], Probabilistic approaches based on Bayesian inference [14] or Dempster-Shafer [15].

Figure 2.2 depicts an case where there are 3 reference nodes and 8 off-line calibration points. At

each point, RSSI information from reference nodes A to C has been gathered and stored in the table. The main advantage of Fingerprinting is that RSSI reading errors caused by the application environment have already been taken into account in the off-line phase. It is this a priori calibration that makes this technique suitable for indoor environments. Nevertheless, the need for a central system for database storage, off-line calibration, which needs to be updated in case of environment changes and algorithms complexity, render the solution complex and time-consuming.

Time of Arrival (ToA)

The distance between two nodes can also be measured in terms of the time it takes for the signal to travel between them. Supposing v is the propagation speed of the signal, then $d = v \times (t_2 - t_1)$ where d is the distance between the nodes and t_1 and t_2 are the times at which the signal was sent and received, respectively. This technique can provide highly accurate results [10]. However, the calculation of d requires the times t_1 and t_2 to be measured by different nodes in the network. This implies time stamp information transfer between devices as well as prior clock synchronization of the network. These aspects will rise hardware complexity and system cost.

Assuming that all transmitters emit a pure sinusoidal wave, the ToA can be measured by identifying the phase of arrival of the carrier signal. Some type of synchronism must be present, for example, emission with a known phase offset. Nevertheless, this method is highly susceptible to multipath fading which is a common occurrence in indoor environments. For this reason, narrowband signals are inadequate to be used in this method. More complex techniques like Direct Sequence Spread Spectrum (DSSS) or UWB contribute to reduce the effects of multipath due to their short duration in the time domain. Therefore, these signals are more suitable for a ToA based location estimation [16, 17]. The use of UWB for ToA applications is analysed in detail in section 3.4.

Conventional ToA estimation involves the use of correlators or matched filter receivers [9]. The former correlates the received signal with a template signal for various time delays. The time delay that produces the correlation peak is the estimated ToA. The latter works by using a filter matched to the transmitted signal which outputs its largest value at the instant of signal reception. Both methods are subject to errors due to electromagnetic and hardware noise. In the absence of LoS, first-path detection algorithms like in [18] or [19] must be applied in order to detect the first arriving signal, rather than possibly stronger multipath originating copies which would impose false correlator and filter outputs [9].

ToA measurements merely infer the time it takes for a signal to arrive at a node so that a distance can be computed. However, the direction of signal arrival is still unknown. Trilateration is a technique for locating an unknown point based on distances to other points whose location is known. Trilateration makes use of at least three distance measurements (in 2D) to three reference nodes. The distance estimates are obtained through ToA or RSSI measurements, for example. In an ideal case (absence of noise in the measured value and no multipath effects), a circumference around each reference node is created where the target node might be located.

The estimated distance d_i between the target node and the i-th reference node is given by

$$ct_i = d_i = f_i(x_i, y_i) + \epsilon_i \qquad i = 1, 2, \ldots, M \tag{2.2}$$

where t_i is the actual ToA measurement, c is the speed of light, ϵ_i denotes the measurement error or noise and

$$f_i(x_i, y_i) = \sqrt{(x - x_i)^2 + (y - y_i)^2} \qquad i = 1, 2, \ldots, M.$$

Equation 2.2 is actually a system of equations where (x_i, y_i) are coordinates of the i-th reference node, M the number of reference nodes and (x, y) the coordinates of the target node. For $\epsilon_i = 0$, when three of these circumferences intersect, a fixed location is obtained. This procedure is depicted in Figure 2.3 a). The location is obtained by solving the system for (x, y).

However, in a real system, reference node position and distance estimation inaccuracies occur. These are modelled by the noise variable ϵ_i. This variable introduces the probabilistic characteristic of this problem and so a new approach has to be applied, i.e. the position (x, y) has to be estimated. The circumferences, which denote a possible position for the target node, will intersect at different points forming an area of uncertainty where the true location lies on - Figure 2.3 b). Moreover, the system 2.2 is overdetermined and non-linear.

To solve this statistics problem, the Maximum Likelihood (ML) method can be applied [20]. Under the assumption that the noise ϵ_i is normally distributed, has zero mean, variance σ_i^2, the estimator $\hat{\boldsymbol{\theta}}_{ML} = [\hat{x}, \hat{y}]^T$ asymptotically achieves the Cramér-Rao Lower Bound (CRLB) [1] [21]. In a real system, M will be finite so, in general, the ML estimator will be biased and have a non-optimal variance greater than the CRLB. The final expression for $\hat{\boldsymbol{\theta}}_{ML} = [\hat{x}, \hat{y}]^T$ corresponds to the following Non-Linear Weighted Least Squares (NLWLS) problem [20]

$$\hat{\boldsymbol{\theta}}_{ML} = [\hat{x}, \hat{y}]^T = \underset{x,y}{\operatorname{argmin}} \sum_{i=1}^{M} \frac{(d_i - f_i(x, y))^2}{\sigma_i^2}. \tag{2.3}$$

It is noteworthy that the variance of the noises ϵ_i (i.e. σ_i^2) are dependent on i. For each of i measurement there is a different variance because a different channel is used. However, σ_i^2 is also distance dependent, i.e. the noises are heteroeskedastic [22]. To improve performance, a basic variance model based on real distance measurements is developed for the location system developed in this work.

The absence of a closed form solution to the NLWLS problem in (2.3) implies the use of iterative and computationally intensive algorithms, such as the method of Gauss-Newton or Leverberg-Marqvardt. Although providing accurate results, these approaches require good parameter initialization to avoid diverging or converging to local minima and minimize iterative steps. Initialization parameters for these algorithms can be obtained via Simple Geometric Pinpoint (SGP) or via linearization techniques. The latter can also be used to obtain an approximate closed form solution to the NLWLS problem. Both SGP and linearization are introduced and discussed in detail in Chapter 5.

[1] The CRLB expresses a lower bound to the variance of an unbiased estimator. It states that this variance is at least as high as the inverse of the Fisher Information matrix.

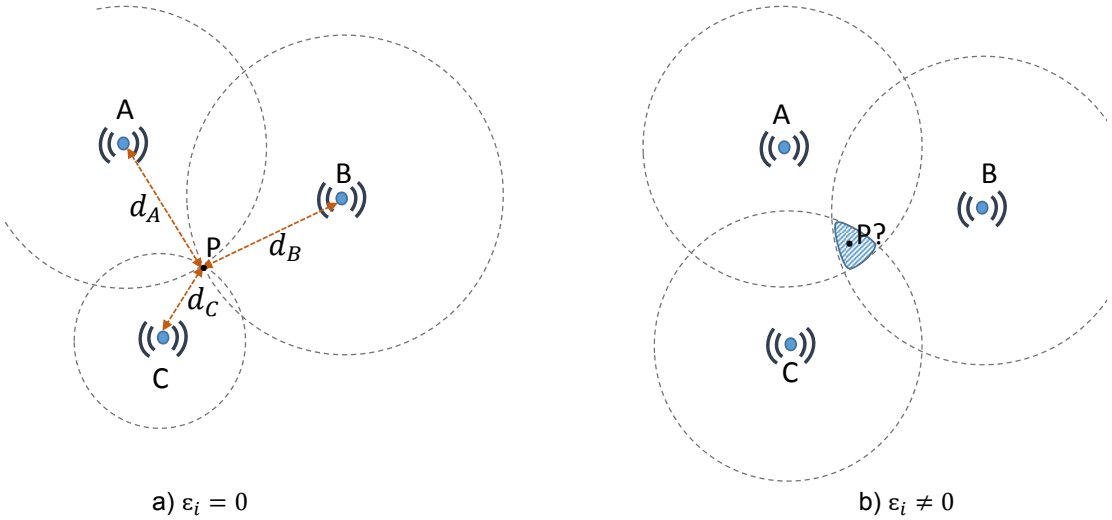

a) $\varepsilon_i = 0$ b) $\varepsilon_i \neq 0$

Figure 2.3: Positioning based on RSSI and ToA measurements.

Time Difference of Arrival (TDoA)

This method can essentially be divided in two.

- A: The difference in multiple, different signal arrival times from one node at another node.
- B: The difference in signal arrival times from two or more nodes at a single node.

A. The first method consists of sending two signals simultaneously with different and known propagation speeds v_1 and v_2. For example, a system may use Radio Frequency (RF) and ultrasound simultaneously [23]. The first one usually contains the information packet and the last one being a control signal only [9]. Using basic geometry, the distance between the sending and receiving node is given by $d = (v_1 - v_2)(t_1 - t_2)$. This concept is depicted in Figure 2.4.

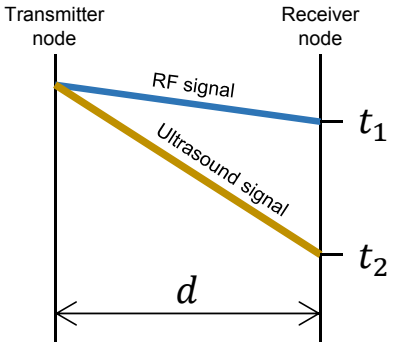

Figure 2.4: Positioning using the time difference of arrival of an RF and an ultrasound signal.

This solution does not require synchronization of the network because the distance estimate does not depend on the absolute time the signal was sent, only on the arrival difference. However, it requires an additional cost in hardware due to the necessity on being able to transmit and receive two types of signals.

An application of this method, using RF/Ultrasound, was able to reach an accuracy of 2 centimetres with a node distance of 3 metres [11]. This solution provides high accuracy and is well suited for wireless sensor networks [10].

B. In the second type of TDoA, the target node can listen to signals from nearby transmitters or reference nodes, compute their ToA and calculate the time difference of arrival for each different pair of signalling transmitters. For example, with three transmitters A, B and C one would have the TDoA of A-B, A-C and B-C. On that note, a TDoA measurement is, in its essence, just the composition of two ToA measurements. Considering equation (2.2) for ToA, a TDoA measurement can be expressed as

$$c(t_i - t_k) = d_i - d_k = \sqrt{(x - x_i)^2 + (y - y_i)^2} - \sqrt{(x - x_k)^2 + (y - y_k)^2} + \epsilon_{ik} \tag{2.4}$$

where i and k denote reference units and ϵ_{ik} the error or noise in the measured distance differences $d_i - d_k$. These can be obtained by multiplying the measured time differences $t_i - t_k$ by c, the speed of light. If every transmitter has a unique signal, each TDoA measurement will define a hyperbola, whose foci are the location of the reference nodes (x_i, y_i) and (x_k, y_k) of the current measurement [24]. Points on this hyperbola represent locations where the time differences of arrival of the signals from a reference node pair (i, k) are the same - thus, they exhibit possible locations for the target node. Figure 2.5 a) depicts such a case where the target node is represented by the point P.

A second TDoA measurement with a third transmitter must be performed so that two hyperbolas can intersect for a location fix to be determined. This positioning method is called Multilateration and it can be visualized in Figure 2.5 b). In the event of the two hyperbolas intersect at two distinct points, a third measure has to be done (for example, TDoA between nodes B and C) or one of the possible locations is discarded by means of a priori scenery information.

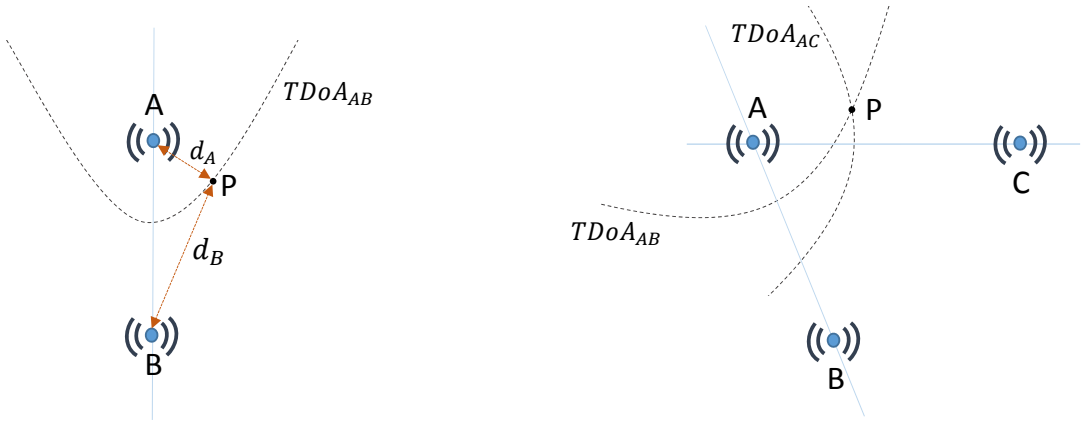

a) 1 measurement

b) 2 measurements

Figure 2.5: TDoA positioning (only the relevant branch of the hyperbola is shown for each measurement).

In contrast to ToA, in TDoA at least one reference node takes part of at least two measurements. This means that the errors ϵ_{ik} should not be considered independent. In this case, not all off-diagonal

elements of the covariance matrix for ϵ_{ik} are null and the ML estimator degenerates in a Non-Linear General Least-Squares problem [20].

The method described is a self-positioning system. This means that it is the target node who listens and processes signals. The inverse is also possible where the system collects the ToA of a signal sent from the target node to nearby receiving units. This is called a remote positioning system. Based on these results, the system can determine the various TDoA and perform the same method as before. An important requirement for a TDoA system, regardless of self-positioning operation or remote positioning, is that there must be a precise time synchronization of the reference nodes in order to avoid estimation bias errors.

Round-trip Time of Flight (RToF)

Another ToA based technique is the RToF which resembles the classical radar. The measuring unit (for example, a reference node) measures the total time a sent signal takes to travel to the target node and travel back. The signal can be subject to processing before being sent back [13]. Deviations in processing time causes a delay that can be significant when compared to travel time of the signal. For small indoor networks, precise processing time must be taken into account to achieve high accuracy. Moreover, distance estimation in RToF is performed the same way as in ToA as a result of RToF being essentially only two ToA measures between two nodes. In contrast to previous cases, this solution does not need a tight synchronization of the entire network. Two-Way Ranging Protocols [25] can provide the necessary synchronism by, for instance, sharing clock information prior to measurement. This concept is used to measure distances between two PulsOn P400 ranging modules employed in the development of the localization system of this work. Further discussion on details of this system is presented in section 6.2.

Angle or Direction of Arrival (AoA or DoA)

Using Angle or Direction of Arrival one can estimate the target node location by intersecting straight lines from the signal path from the target node to the reference nodes. These lines compose a certain angle against a known direction, either using an electronic compass or a second signal from another node. The angle can be measured using, for instance directional antennas or antenna arrays with help of beamforming techniques [10, 26] and implementation of array signal processing algorithms like MUSIC [27] and ESPRIT [28]. Estimation by AoA in a 2D scenario only requires two reference nodes - this is an advantage towards TDoA. On the other hand, the complex hardware requirements rise the cost of these systems. Moreover, accuracy heavily depends on multipath effects, on the propagation in Non Line of Sight (NLoS) conditions and on the distance between reference nodes and target nodes [14].

Figure 2.6 a) depicts a case of position estimation from a signal received from the target node P at the two reference units which measure the AoA.

It is also possible for a target node to receive signals form the reference nodes and compute its

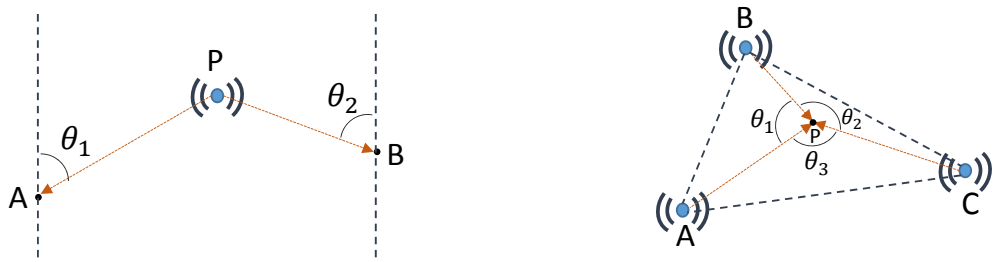

a) Distributed estimation

b) Local estimation

Figure 2.6: AoA positioning.

position locally, this is the case of Figure 2.6 b). In this case, however, a minimum of three reference nodes are needed. In any case, using simple trigonometric relationships the measured angles can be used to calculate the distances between all the nodes and compute the target node's position - this technique is called Triangulation.

Hybrid possibilities such as combination of AoA/T(D)oA and AoA/RSSI are also possible [29, 30]. The primary advantage of such systems is the improved accuracy and the possibility of using only a single reference node (also called single-anchor). This solution reduces system cost and complexity significantly.

Proximity

Proximity based location is a primitive localization technique which involves simply associating the position of a node with the location of the reference node to which it is connected. An example is the so-called Cell Identification (Cell-ID) location system which simply locates the mobiles devices by the cell they're connected to. This method greatly simplifies the location mechanism. By detecting several cells at its range, the target node can connect itself, for example to the one which has the higher RSSI [13]. However, despite high precision, the maximum accuracy is the range of the cell. In an indoor environment, due to multipath and shadowing, the range of a cell is difficult to determine, which can worsen cell range overlap and cause unexpected RSSI readings.

2.3 Overview of deployed wireless location systems

In this section, an overview of currently deployed wireless location systems is presented. At first, the contact-based systems and some of their basic properties and uses are introduced. Moreover, it is given special emphasis to contact-less systems, specially those created for an indoor environment. The advantages and disadvantages are also evaluated. This section is meant to provide a state-of-the-art approach to solutions based on the previously described techniques.

2.3.1 Contact-based systems

These location methodologies require the object, whose estimation is to be located, to have physical contact with the sensor. It is clear that these location methods present a major drawback which is, they need an extensive amount of sensors to achieve a fine granularity, i.e. to achieve high accuracy. The complexity and cost rise by consequence. However, this aspect can be seen as an advantage since the amount of sensors is proportional to the desired accuracy - such approach for granularity improvement cannot be applied to wireless systems since they are always subject to propagation effects.

The Smart Floor [31], developed at the Georgia Institute of Technology is a tracking method which consists of floor tiles equipped with a sensor that measures the Ground Reaction Force. This force along the tile forms a unique footstep profile, composed by the measurements of the force exerted by the heel once the foot touches the floor until the tip of the toes leave the floor. In a scenario where replicas of these sensors are spread across the floor, a system is obtained that not only estimates one's location but also identifies each individual. Since each profile is unique, this solution can also be applied to biometrics.

2.3.2 Contact-less systems

Contact-less systems are based either on image processing techniques or wireless sensoring. Image processing based methods rely on advanced image scanning and identification algorithms to estimate an object's or person's location. One example of a system based on this technique is the EasyLiving [32]. This project developed by Microsoft accomplishes a solution which uses stereo colour cameras to achieve person-tracking within a room with refresh rates of about a few Hertz. Although being able to do much more than just locating (e.g. surveillance), the ability for the system to recognize people's faces or gestures or even certain objects is a major challenge because it requires real-time assessment of the surrounding scenario needing a high performance processing. By consequence, the cost and the complexity rises substantially.

Wireless sensoring involves all systems that estimate position based on electromagnetic waves. Besides radio, also optical or acoustic are wireless possibilities and therefore fall in this category. In this chapter, special attention to radio based solutions is given. This section is virtually almost only dedicated to these technologies. A thorough analysis of indoor localization is made followed by examples of currently deployed systems as well as a brief historical overview.

In contrast to outdoor localization, indoor localization has several important differences. This environment is much more restrictive in terms of spatial operation range and it is designed to work within a building or a small venue like stadiums [33] or campuses which include buildings and other structures where the use of Global Navigation Satellite System (GNSS) or another aforementioned outdoor technique is either unavailable or too inaccurate [13].

The first indoor localization systems used an infra-red sensor network to estimate an object's current position [2]. The Active Badge [34] system developed by AT&T Cambridge, used infra-red beacons mounted on the wall or ceiling listening to periodic identification transmissions from a, so-called badge

worn by a person. The system could then approximate their current position based on the beacon they were receiving the signal on. The use of infra-red is obviously very limited since every non-transparent object can easily block the signal. This solution is also only limited to a couple of metres, impractical for large open room areas. The Active Bat, a subsequent solution, used ultrasound to compute the location of the object based on ToA [8, 33].

The Radio Frequency Identification (RFID) technology has had a significant importance in the last decade as well. These systems consist of a transponder (colloquially called and RFID-Tag), a reader and a controlling application. Depending on the desired performance, the RFID-Tag can be active or passive. Active tags possess their own power source which give them more range than passive ones which rely on energy sent off by the readers [35]. These tags usually transmit an identification or serial number which is received by the reader and subsequently its location is estimated associating the tag's position to the reader. Ranges differ from approximately 1 meter for passive tags and 100 metres for active tags [36].

Bluetooth (IEEE 802.15.1) technology is also an option when considering indoor location. Specially designed for data transfer under short distances, that is up to 100 meters depending on the class of the used devices [37], Bluetooth is an ubiquitous technology in recent mobile devices. This fact makes this technology very interesting for cheap location systems such as, for instance, ZONITH [38]. This solution only requires a mobile device with Bluetooth feature turned on. The system uses a grid of Bluetooth beacons (Figure 2.7 b)) which detect the presence of a nearby device and estimates its location by proximity techniques or Cell-ID analogous to the outdoor solution.

Furthermore, the ZigBee standard (IEEE 802.15.4) has also played a role in the field of wireless positioning in recent years. The underlying protocol is designed to build an ad-hoc based mesh-oriented network which is not found in every standardized wireless solution [6]. This makes it ideal for sensor networks. Combined with low-power consumption, high endurance of the modules, robustness and scalability of the mesh-network, one can achieve a solution that makes it possible for it to be used in position estimation that does not require very high precision [4].

a) Ubisense tag

b) ZONITH Bluetooth beacon

Figure 2.7: Examples of devices used in two presented location systems.

More recently, localization systems have become more and more complex. An example for this is the recent Ubisense solution, developed by the University of Cambridge, known for its elevated precision.

It consists of base stations equipped with UWB receivers and the so-called Ubitags (Figure 2.7 a)). The latter are small active devices meant to be worn by people. The tags send wireless pulses to be detected by the pre-installed base stations. The Ubisense allows for a full-duplex communication between the base station and the tags which is not a common feature in location networks. Tags can also be equipped with multiple user relevant functions, such as built-in Wi-Fi capability. All these functions make this system highly desirable. However, the relative high cost of UWB receivers and complexity of the underlying infrastructure are very limiting factors [4, 39].

Table 2.1 summarizes the described technologies along with an example system. Additionally, information on precision and accuracy is given for a proper comparison.

Table 2.1: Overview of presented technologies. [1, 4, 13, 14, 40]

	Wireless form	**System**	**Underlying technology**	**Precision and Accuracy**
Outdoor	Radio	GPS	Satellite Location (ToA)	95% within 7.8 m
Indoor	Optical	Active Badge	Infra-Red (Cell-ID)	100% within Cell range
	Accoustic	Active Bat	Ultrasound (ToA)	95% within 8cm
	Radio	AeroScout	RFID (RSSI / TDoA)	N/A
		RADAR by Microsoft	Wireless Fidelity (RSSI)	50% within 2.5m
		ZONITH	Bluetooth (Cell-ID)	100% within Cell range
		TI Location Engine CC2431	ZigBee (RSSI)	95% within 5m
		Ubisense	UWB (TDoA / AoA)	99% within 0.3m

In conclusion, for indoor, RFID technology brings simplicity to the system by mostly relying on proximity techniques for location estimation, thus leaving aside high computation requirements. Additionally, network scalability is provided by simply adding more readers to the network. Furthermore, tags' price is low due to the reduced need of electronics and lack of power supply in passive RFID. However, the use of proximity techniques and the very limited range, specially with passive tags, make this system less competitive when compared to other solutions.

Bluetooth and Wi-Fi can deliver accurate indoor location systems depending on what technique is used. In addition, systems based on these technologies can make use of the wide implementation on almost every mobile device which render these technologies promising candidates for indoor location. Moreover, the computational power of these devices (cell-phones or computers) can be used to process more complex estimation algorithms which provide more accuracy. Nevertheless, the power consumption of these standards make these options inappropriate for lightweight, small hand-held or wearable

sensors.

The ZigBee standard is designed for low-rate data intermittent communication which is a factor that contributes to ultra-low power consumption of available modules. In addition, the mesh topology provided by the underlying protocol aids the data communication between nodes directly. UWB technology also provides a low-power solution when applied to sensor networks. The use of wideband signals due short duty-cycle pulses of UWB are able to better handle multipath effects and, coupled with a low data-rate requirements of a location system, one is able to achieve a trade-off between spectral efficiency and energy consumption [41]. These solutions, when compared to Bluetooth or Wi-Fi are low-power oriented which affect the ability for a high range estimation.

Chapter 3

Antennas for indoor location

3.1 Introduction

In the previous chapter, the properties of location systems such as application environment, location techniques, positioning algorithms, underlying protocols and technologies were discussed. The overall performance of these systems also strongly depends on the properties of the antennas used, as it is the hardware element responsible for the signal emission and reception, which is one of the core components of radio-based location estimation.

In this chapter, the antennas designed and used for indoor location systems will be presented. Important characteristics such as gain, directivity, radiation pattern, bandwidth and polarization will be discussed. Furthermore, some applications and recent developments will be exposed as well.

Location techniques discussed earlier will be addressed again in this chapter. First, a brief technical overview of relevant properties of antennas and details will be presented. Section 3.3 will address antennas designed and specialized for RSSI techniques such as the dipole/monopole and printed antennas. In section 3.4 antennas for ToA/TDoA techniques will be discussed. The details of UWB will be analysed as it is the major technology used with this technique. Finally, in section 3.5 antennas for AoA techniques will be explored. Several examples of Smart Antennas will be presented and their properties analysed.

3.2 Technical overview

3.2.1 Antenna requirements

When modelling a location system, special attention is required to several important details of antennas that will influence their design, project and final goal. Antenna parameters must be chosen adequately to satisfy location technique requirements, to maximize accuracy, precision and overall performance. These parameters can be classified as follows [42]:

- **Frequency selection and bandwidth.** Location systems may work on different frequencies or

bands. Antennas have to be properly adapted to the potential use of several channels as well as impedance matched over the whole bandwidth. Antenna efficiency has also to be taken into consideration.

- **Coverage.** Depending on the environment the system will be located in, coverage requirements are a major factor on the estimation rigour. Radiation patters to study gain and directivity (necessity of ground plane or reflector, for example) have to be carefully adjusted to the goals of the application.
- **Mobility.** User mobility has to be taken into account specially when designing antennas for mobile unknown nodes. In contrast to reference nodes, mobile nodes constantly move, change positions and are much more likely to suffer damage. Resilient construction materials and good protection are required.
- **Antenna position and orientation.** Partially also due to user mobility, antennas' possible working position may constantly change. This is specially relevant for mobile nodes or wearable sensors. Proper polarization mode must be chosen to minimize mismatches in the communication between node antennas.
- **Size.** Antenna dimensions have to be kept in view, particularly for mobile nodes or even wearable antennas whose goal is to be as small and as discrete as possible. The choice for the type of antenna should be evaluated accordingly.
- **Power requirements.** Adaptable to the propagation environments, power usage should be adjusted not to interfere with other systems or surpass legal requirements.
- **Cost.** Ideally an appropriate performance-price trade-off should be found when taking into consideration all of the aforementioned parameters on the design of the antennas in order to minimize cost and maximize profitability.

3.2.2 Antenna types

Antenna design diversity is introduced to enhance location system performance and robustness. These, can essentially be categorized in four main groups [13]. The last two groups apply only for antennas for reference nodes.

- **Omnidirectional antennas**. These type of antennas are primarily suited for Tri-/Multilateration techniques or Fingerprinting. The lack of directivity makes these antennas independent of user or node orientation and therefore are immune to environment changes and user mobility given a proper polarization. The coverage capability is also one of the main advantages specially due to the reduced need of nodes.
- **Directive antennas**. Primarily used in the scope of RFID systems for tag identification, these antennas are well suited for proximity techniques due to their narrow beam and operating range, avoiding interference with other readers.

- **Sectorized Antenna Array (SAA)**. Mostly used due to its multipath mitigation capability, these antennas offer a sectorized coverage which allows not only range control but also the possibility for implementation on AoA techniques, by being able to measure the direction of arrival from a directive source.

- **Phased Array**. These antennas have the ability to control radiation pattern on-the-fly as well as improved signal-to-noise ratio. They provide precise measurements for AoA besides their high directivity, which can be used to perform radiation beam sweeps to better locate signal direction of arrival.

These antenna types and their radiation characteristic examples are depicted in Figure 3.1.

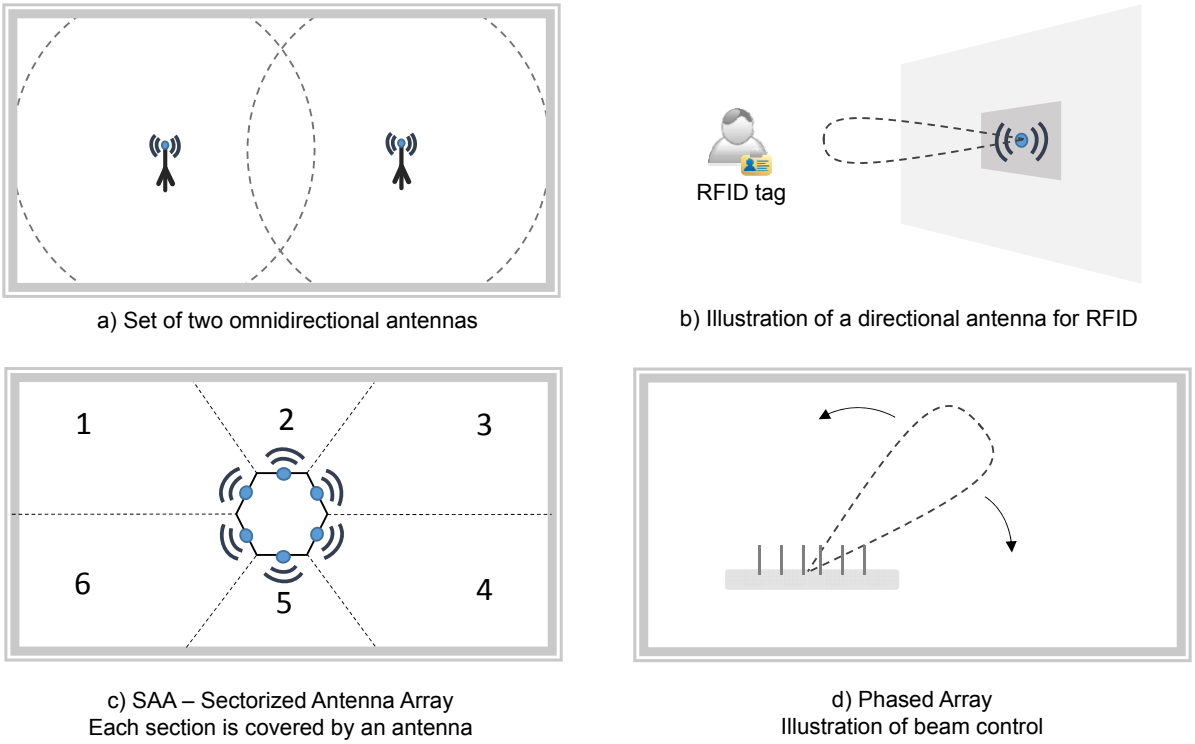

a) Set of two omnidirectional antennas

b) Illustration of a directional antenna for RFID

c) SAA – Sectorized Antenna Array
Each section is covered by an antenna

d) Phased Array
Illustration of beam control

Figure 3.1: Antenna types for indoor location. [13]

In what follows, each of these parameters will be analysed in detail for each major location technique: RSSI, ToA/TDoA and AoA. Antennas available for these techniques will be presented and discussed. Their physical and technical properties will be described as well as their advantages and disadvantages in the scope of indoor location.

3.3 Antennas for RSSI based systems

In this section, antennas designed for RSSI techniques will be discussed. The RSSI location technique was thoroughly analysed in section 2.2.3. Trilateration, Fingerprinting and Proximity positioning methods were described using RSSI. It was concluded that RSSI measurements suffered from multipath

effects specially in the case of NLoS. Measurement inaccuracies due to low-quality receivers and interference also influence RSSI readings. As such, antennas designed for this case must take into account and try to minimize these factors.

Inherent to all location systems, antennas in mobile nodes are subject to continuous movement due to user mobility. Antenna placement on someone's body must be carefully taken into consideration. This is specially relevant for RSSI techniques that use Trilateration or Fingerprinting methods although the latter should ideally not depend on antenna configuration, given that the same antennas are used in both on-line and off-line phases [13].

According to [13], to overcome the user mobility problem, an isotropic radiative element could ideally be implemented. Thereby, no orientation would be preferred against another. In a real scenario however, the closest simplest element that approximates an isotropic radiator are dipoles or monolopoles. Most used solutions include the classical half-wavelength dipole or quarter-wavelength monopole due to their omnidirectional radiation characteristic.

If the body's vertical position of a user carrying along a mobile unit is assured, then relative low motion in the elevation plane is expected. This makes linear vertically polarized antennas, for either mobile nodes and reference nodes the simplest and the least expensive solution. Location applications based on RSSI primarily apply these type of antennas [13]. Other solutions like collinear arrays of half-wavelength dipoles for higher gain and directivity in the azimuthal plane are also possible.

Cases where user's body vertical position is not assured, the use of circular polarization on the reference node's side provides robustness to the system as it's taking into account possible unexpected body movements. For example, in the case of antennas placed on a wrist, the constant up and down movement of the arm could compromise co-polarization between the mobile and reference node.

The use of external half-wavelength dipoles, commonly seen in Wi-Fi or ZigBee applications, specially on the side of access points or reference nodes, provides good performance and low-cost [13]. However, the size of these antennas is a limiting factor for mobile applications.

A more compact solution is achieved by the use of Printed Circuit Board (PCB) technology. These solutions contemplate for example the Planar Inverted-F Antenna (PIFA) or a variation of these, the Meander antennas. These designs are the results of printed monopole variations. Two examples from [43] and [44] can be seen in Figure 3.2 a) and b), respectively.

The PIFA can be seen as a monopole that was tilted towards the ground plane. The proximity to the ground plane reduces efficiency and input resistance. A stub along the width of the monopole is used to minimize this effect and so the F shape takes form. This antenna is used extensively primarily due to its simpleness, good efficiency, omnidirectional pattern and high gain in both vertical and horizontal polarization modes which make this antenna appropriate for RSSI based location methods [45]. The PIFA is resonant at a quarter-wavelength and combined with its low-profile characteristic it allows for small scale device integration, which makes it a good candidate for location technologies.

Another PCB antenna option is the meander antenna. In this antenna, the wire is folded back and forth, i.e. it is meandered, and it can be built in a half-wavelength or quarter-wavelength monopole format. Example of the latter is depicted in Figure 3.2 b). By doing so, the resonance frequency is

a) TI CC2430 ISM 2,4GHz Inverted F antenna.

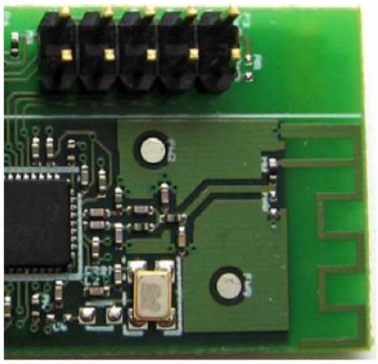

b) TI CC2511 USB-dongle for Wi-Fi ISM 2,4GHz Meander antenna.

Figure 3.2: Examples of Inverted F and Meander antennas.

achieved in a much more compact structure [45]. The downfall towards the classical inverted F antenna include bandwidth, efficiency and input resistance drop but preserves its fairly omnidirectional radiation pattern [46].

As discussed in section 2.2.3, proximity-based systems fix a user's location by being in range of a certain reference node or reader. This is an example application for RFID technology. The mobile RFID unit or tag once it's in the reader's range of operation it will become associated with the location of that reader. Primarily used for authentication or stock tracking, proximity based on RFID must rely on small sized tags meaning small sized antennas and, if possible, planar. Reduced production cost, high efficiency and reliability are also priorities. Composition of RFID passive tags in its very basic contain an RFID integrated circuit and an antenna as power source as well as for receiving and transmitting the RF signal. Due to its simplicity and low-cost, dipole or dual dipole antennas are present in most Ultra-High Frequency (UHF) RFID (300MHz to 3GHz) systems [47]. In the latter case, two dipoles form a cross shape and are fed at the middle mitigating tag's orientation dependency. Other solution feasible for UHF RFID Tags is the use of the already mentioned meander antennas as depicted in Figure 3.3.

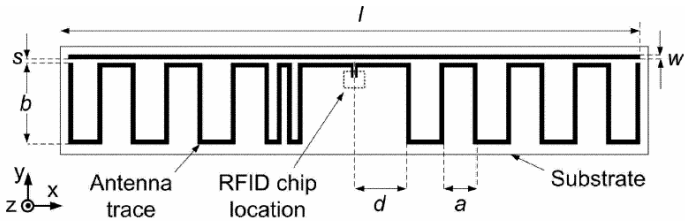

Figure 3.3: Meander antenna for RFID Tag. The additional bar and furthered meandered left section improved impedance matching to the RFID chip. [48]

An alternative solution to the size constraint present in location systems involves the microstrip antennas. In its most simple form, a microstrip antenna consists in a radiating element on one side of a dielectric (relative permittivity ϵ_r and loss tangent $tan(\delta)$) which has a ground plane on the other side [49]. The radiating elements can assume the form of rectangular, circular or ring patches among others depending on required radiation characteristics. An example of a rectangular and circular patch is

depicted in Figure 3.4.

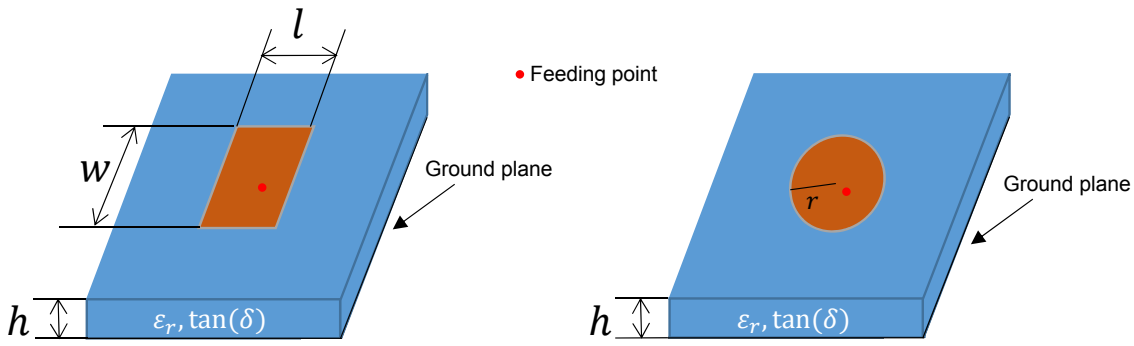

a) Rectangular patch b) Circular patch

Figure 3.4: Microstrip rectangular and circular patch. Antenna excitation from underneath via probe feed.

Microstrip antennas are low-profile, light and inexpensive. Depending on patch design and feeding methods, microstrip antennas provide polarization diversity which is a major advantage regarding location systems. For example, in the case of the rectangular patch, perturbation corner cuts/truncation or added strips are used to suitably differentiate the two orthogonal modes at resonant frequency so that the patch radiates a circularly polarized wave [50]. Provided the existence of a ground plane, these antennas can easily be optimized for operation on RFID readers, which need semi-hemispherical radiation profile [51], as illustrated in Figure 3.1 b).

An application of microstrip antennas for RFID is proposed in [52], where a meandered patch is produced for an RFID reader underneath a conveyor belt. Other solutions include different designs such as a truncated corners patch array to achieve high gain, directional radiation and circular polarization for RFID readers proposed in [53]. Further examples on circularly polarized microstrip antennas for RFID supporting multi-band are presented in [54].

3.4 Antennas for ToA or TDoA based systems

Systems based on ToA or TDoA are location systems based on time intervals. It is the measurement of this time interval that defines the accuracy of the system as explained in section 2.2.3. One way to achieve high accuracy in ToA and TDoA based localization systems is by using UWB technology [13]. Ultra Wide Band, formerly known as pulse radio, relies on the transmission of very narrow pulses in the time domain covering a very wide bandwidth in the frequency domain. The frequency spectrum allocated for UWB ranges from 3.1 to 10.6 GHz and a UWB signal has at least 500 MHz bandwidth or 20% of its centre frequency [55]. The high time resolution prominent from UWB is what makes this technology considered to be a high resolution solution for location systems [56]. As such, UWB technology offers very high bitrate transfer (in the order of several hundred Mbps reaching up to Gbps) but only through very short distances (1 to 10 meters) due to the low power requirements set by the

Federal Communications Commission and the European Telecommunications Standards Institute as not to cause unwanted interference to devices operating on the same band. Moreover, UWB signals present relative immunity to multipath effects due to reduced signal overlap at the receiver and grant an extremely fine time and range solution even through opaque media [55].

Overall, ToA estimation with or without UWB is influenced by the following common error sources [71]:

- **Multipath effects**. Indoor environments are specially susceptible to multipath effects due to the high obstacle density between transmitter and receiver. A transmitted pulse in a narrowband system overlaps with other multipath originating copies at the receiver. In the case of correlator receiver, this effect causes a shift in the correlation peak and introduces a large estimation error. High computational effort has to be employed to mitigate these effects with the help of super-resolution techniques [57]. The short duration of UWB pulses avoids the need for such computational requirements as the pulse duration is much shorter than the interval of arrival of the multipath components.

- **Interference**. Interference in a multiuser environment (or in a multinode environment in the case of a location system) can impose severe limitations. Multiple access techniques like time slot attribution or frequency band allocation can help mitigate interference.

- **LoS vs NLoS**. Due to LoS obstruction the direct signal may not be the strongest arriving at the receiver. In extreme situations the direct signal power may be below the receiver's sensibility which makes it undetectable. In the latter case, ToA estimation will be estimated with a bias error since the first arriving signal is not the direct component. This case is depicted in Figure 3.5 b). Figure 3.5 a) demonstrates the LoS case for comparison.

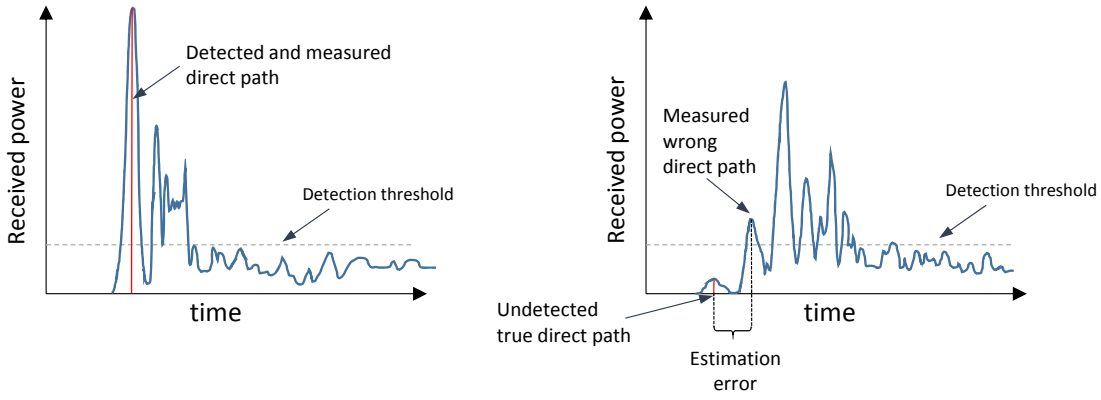

a) Received power in LoS

b) Received power in NLoS

Figure 3.5: Illustration of received power in a multipath environment.

NLoS situations may be recognized and its effects mitigated by employing appropriate LoS reconstruction algorithms [9].

- **High-time resolution of UWB signals**. Due to the short UWB pulse duration, node's clock synchronization jitter plays a role in ToA estimation errors. Also, a low sampling rate is required to achieve a low power design [25].

Besides the requirements mentioned in section 3.2.1, the design of UWB antennas must consider the following aspects, according to [13]

- **Bandwidth**. For conventional UWB, antennas must present a minimum 500 MHz operational bandwidth. For robustness the antennas should ideally cover the entire UWB band.
- **Radiation patten**. Similar to antennas for RSSI based location, UWB antennas should possess a high omnidirectional radiation pattern.
- **Operation uniformity**. The antennas should operate uniformly throughout the entire operational bandwidth. A stable phase centre at all operation frequencies is required as not to deform the shape of UWB pulses [58].
- **Dimensions and cost**. UWB antennas should be planar and have low-profile characteristics to allow small device integration and the lowest cost.
- **Radiation efficiency**. Due to the low power nature of UWB technology, antennas must present high efficiency. Typically greater than 70% [13].
- **Linear phase**. Coupled with operation uniformity over the total bandwidth, phase response of antennas for UWB should be a linear function of the frequency as not to distort the shape of UWB pulses.

Antennas for ToA or TDoA with UWB technology share many of the required characteristics with antennas for RSSI. As such, there are many proposed designs for UWB antennas fulfilling these requirements [59–66]. In the past, horn structures, crossed or rolled antennas were developed for UWB applications. However, these structures did not meet the low-profile requirements for small scale integration despite their high bandwidth and omnidirectional radiation pattern required for ToA or TDoA based localization systems [60]. To overcome this problem, PCB solutions are implemented. A typical design example in [62], similar to the rectangular patch, proposes a printed circular monopole antenna fed by a microstrip line which can be seen in Figure 3.6 a). This antenna presents a fairly simple design yet it has robust UWB properties due to its omnidirectional radiation pattern and return loss less than -10dB over the whole UWB bandwidth [62]. Nevertheless, the antenna has a linear polarization which renders this antenna non-optimal for localization systems.

In order to achieve the required characteristics, different patch designs must be implemented. Solutions include circular, rectangular, triangular, elliptical, spiral, fractal design or some combination of these [61]. These designs are optimized for high bandwidth, omnidirectional radiation patterns and desired polarization. Feeding techniques like coplanar waveguide, microstrip, via probes or a variation of these are also possible to tune input impedance [63] and refine polarization characteristics [13].

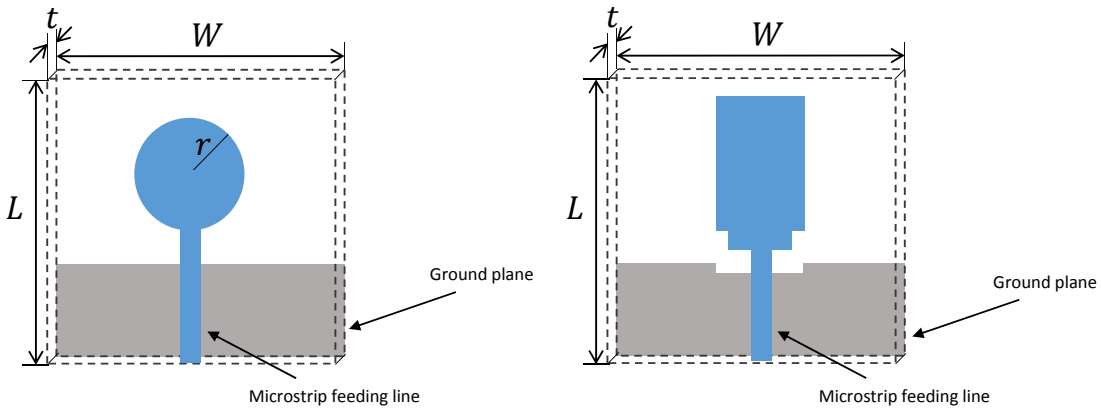

a) Circular printed monopole.

b) Rectangular printed monopole with lower corners and ground plane notches.

Figure 3.6: Typical UWB monopoles design.

To illustrate possible patch variations, Figure 3.6 b) depicts a printed rectangular monopole proposed in [64]. This antenna was designed for UWB with a microstrip feed, notch structures in the two lower corners and truncated ground plane. Impedance bandwidth enhancement occurs from the implementation of these notches as they affect the electromagnetic coupling between the radiating element and ground plane. The latter is truncated before it reaches the monopole patch which acts as impedance matching element to control the impedance bandwidth [64]. The notch structure is also embedded in the ground plane.

Often considered for UWB applications are the planar spiral antennas due to their inherent circular polarization and frequency independent behaviour [58]. A UWB circularly polarized equiangular spiral antenna is proposed in [66] and is presented in Figure 3.7 a). This antenna possesses a bidirectional radiation pattern with opposite polarization with an axial ratio below 3dB from 3 to 14.5Ghz. This design produces minimal pulse distortion which is of major importance for ToA or TDoA applications using UWB. Moreover, due to the balanced nature of spiral antennas with more than one arm, a microstrip-to-coplanar stripline tapered balun is used integrated in one arm of the spiral achieving a completely planar structure. Although the dimensions of the structure (75.8 mm by 84.26 mm) render this antenna unsuitable for mobile integration, it can still play a significant role in UWB ToA or TDoA based location systems by being installed on reference nodes.

An important drawback of UWB systems follows precisely from one of its advantages. Due to the occupied bandwidth, the system performance may be compromised by interference from other narrowband and high power wireless standards the occupy portions of the UWB band. One such case are the IEEE 802.11a bands that are operated by Wi-Fi applications. As a result, notch frequencies were introduced in the frequency response of UWB antennas to help mitigate interference problems. One such example is the design proposed in [65] and depicted in Figure 3.7 b). By introducing the U-shaped slot in the circular radiative element, the antenna rejects the 4.8 to 6 GHz band to achieve minimal interference with systems operating at these frequencies. Also, the introduction of frequency rejection bands on antenna design avoids the use of external microwave filters or signal post-processing which simplifies the circuit

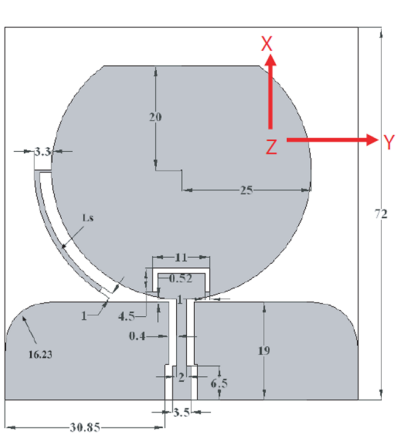

a) Circularly polarized printed monopole.

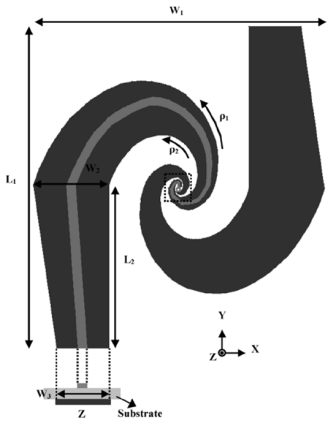

b) Circularly polarized spiral antenna.

Figure 3.7: Illustration of two UWB circularly polarized antennas.

and allows substantial size and cost reduction of the overall module [61].

Another solution to reduce the effect of interference sources and to be able to control the rejection bands more easily relies on the so-called dielectric loading sandwich technique [67]. A padding patch, printed on a substrate layer, is glued on top of the radiative element of the UWB antenna. This procedure is depicted in Figure 3.8.

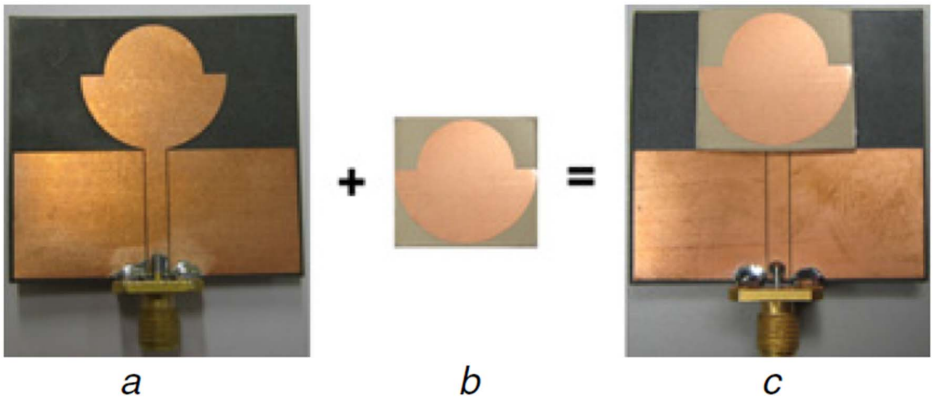

Figure 3.8: Depiction of the dielectric loading sandwich technique. [67]

The upper and lower semicircles resonate at one distinct frequency, respectively. The existent padding patch causes destructive interference at these two frequencies and so two separate notches occur in the frequency response of the antenna. Additionally, the notch bandwidth can be controlled by varying the substrate thickness of the padding patch.

3.5 Antennas for AoA based systems

In systems based on AoA measurements, the angle or direction of arrival of a signal transmitter from an unknown node is estimated. These estimations are performed by implementing antenna arrays or directional antennas. Their configuration will allow the system to achieve the desired accuracy,

connectivity and spectral efficiency [13].

Measuring the angle of arrival of a signal on a reference node is far more complex than the previous location estimation options. Antennas developed for this purpose occupy more space, when compared to other techniques, due to the need of arrays or more than one antenna to cover certain regions in a 3D space. Additionally, a fixed space reference for accurate location estimation is needed. As such, antennas developed for AoA systems are placed in base station or reference nodes where user mobility is not required.

The Smart Antennas have been an emerging technology to cover AoA estimation necessities [29]. These antennas provide the possibility to control some of its properties like polarization and radiation pattern in real time. Included in this group are the SAA [29, 30, 68] and Phased Arrays [69–71]. The former consists of a set of directional antennas oriented in such a way for each to cover a certain solid angle achieving a distributed coverage of the space. The latter consists in a antenna array where the phase of the signals is controlled in such a way as to re-enforce the radiated energy in a desired direction and to cancel in others. Phased arrays also allow other forms of beam control which will be discussed later on.

With this is mind, the development of antennas for AoA estimation the following aspects must be taken into consideration [29]

- **Position**. An unobtrusive position to the users is desired to minimize visual and spatial impact. The antenna should be placed preferably in the centre of the covered room in order to achieve maximum coverage and reduce dark spots.

- **Interference**. In dense networks, where several systems may be working on the same frequency bands, spatial selectivity is advised for interference reduction.

- **Spatial arrangement**. The spatial arrangement of the antennas constituting the array should maximize 3D space coverage preferably equally and enable spatial re-usability. In the case of SAA, antenna coupling should be reduced as not to deform the radiation pattern.

- **Radiation pattern**. Depending on the antenna type and coupled with spatial arrangement, antennas for AoA should be able to receive and send signals almost isotropically.

- **Polarization**. AoA estimation is heavily affected by multipath effects. It has been referred to in the literature that circular polarization for these antennas can help mitigate these effects [29].

- **Cost**. Antenna design should take into account the network topology and operation environment. To achieve low-cost production, PCB antennas should be preferred.

A Smart Antenna and system for location-aware applications is proposed in [29]. The structure of the antenna can be seen in Figure 3.9 a).

This antenna is composed of six equal circularly polarized printed antennas placed on the surfaces of a half dodecahedron intended to be mounted on the ceiling to provide 3D space coverage. This is a

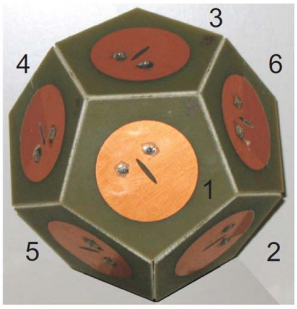

a) Switched beam antenna.

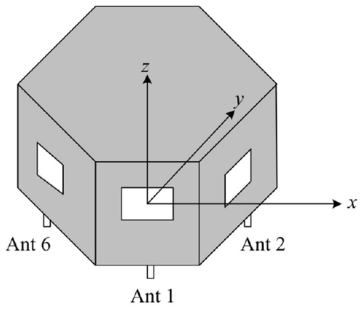

b) Sectorized Antenna Array for UWB.

Figure 3.9: Examples of smart antennas design.

switched beam sectorized antenna array and narrowband system where each radiating element is selected by a multiplexing circuit. This antenna allows 2D location estimation by providing both the azimuth and elevation angles of the incoming signal. RSSI readings on each antenna provide the necessary information for the array signal processing algorithm, in this case the MUSIC algorithm [27], to estimate the angle of arrival. Performance tests showed that this system can estimate a location with an average error of 1.7m [29].

UWB solutions are also present in AoA estimation. Antenna requirements for these systems are similar to those for UWB in ToA estimation [13]. In [30] a UWB antenna and hybrid AoA/ToA system for high accuracy positioning is proposed. An hexagonal monopole antenna array of six elements facing different directions is used for omnidirectional coverage. The antenna is depicted in Figure 3.9 b). The proposed system estimates the angles of arrival based on amplitude difference of the tag reflected UWB pulse arriving at the different array antennas similar to the mono-pulse radar operation. Due to the ease of signal amplitude measurements and the high precision provided by UWB technology as discussed earlier, this system can achieve an accuracy up to 2cm, proving how well hybrid solutions such as AoA/ToA perform. Similar to this concept, another solution presented in [72] which proposes a cylindrical conformal array of UWB antennas to achieve the same goal. The proposed antenna is depicted in Figure 3.10.

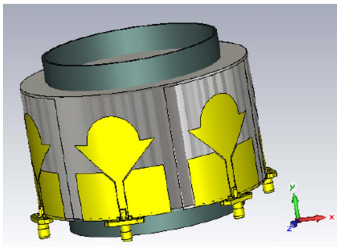

Figure 3.10: Cylindrical conformal array of UWB Antennas. [72]

Chapter 4

Development of a reflector UWB Antenna

In this chapter a UWB antenna to be used in the developed localization system is proposed. First, basic concepts like antenna type and its relevance are introduced. In section 4.2 the antenna design is described along with parameter optimization. Then, in section 4.3 the test results of the antenna prototype are presented. At last, in section 4.4 some conclusions are drawn related to the design and antenna testing phase.

4.1 Introduction

As previously discussed in Chapter 3, printed UWB antennas have been of major importance lately due to their wideband characteristic, low cost and reduced dimensions. In this chapter, a UWB antenna is proposed, taking advantage of its properties for implementation on an RTLS system. The RTLS system for which the antenna is designed consists of four identical hardware PulsOn P400 active modules from Time Domain which perform ranging measurements. With four available modules the RTLS system is composed of three static base stations and one free target.

The original stock antennas (Figure 4.1) for each module are variations of a UWB monopole, which offers a nominal 3dBi gain in all directions perpendicular to the antenna. This omnidirectional radiation characteristic is optimal when orientation of the target is not known or when signals are expected to arrive from any direction, which is the case. However, for static base station antennas, their spacial orientation can be set and remain unchanged throughout the operation of the system. Consequently, a UWB monopole may not be the optimal antenna for a static base station if the target remains in a confined area. To improve Signal-to-Noise ratio (SNR) and possibly decrease measurement variance, a more directional and high gain antenna is developed and tested. Additionally, the more directivity, the less multipath effects on received and sent signals.

The main idea behind the development of the proposed high gain, directive UWB antenna relies on the use of a reflector metallic plane placed near the antenna so that the radiated power can be narrowed

Figure 4.1: Stock UWB monopole variation.

down to a specific direction. Different reflector plane distances to the antenna will be tested to achieve best impedance matching and maximize directivity particularly for the 3.1 to 5.3GHz band which is the P400 module working frequency.

4.2 Antenna Design

4.2.1 Base model

There are many printed antenna designs for UWB applications. Several examples were discussed in section 3.5, some of which include spiral, monopole or slot antennas. The choice for the antenna design relies on its desired radiation characteristics which are formalized below for the RTLS system developed in this work.

- **Directivity and Gain**. Antenna application requires high directivity to maximize radiated power in the spatial direction of interest. In this case the antenna is designed to achieve maximum possible directivity in the z direction (see Figure 4.2).
- **Polarization**. The developed RTLS system is designed to perform on a 2D plane which includes base stations and target antennas. Therefore, circular polarization is not a requirement. Besides, the target antenna is linearly polarized. As such, to avoid polarization mismatches, the proposed antenna is designed to be linearly polarized as well.
- **Impedance matching**. A common impedance matching criterion is

$$P_r/P_i \leq 0.1 \tag{4.1}$$

where P_r is the reflected power and P_i is the incident power. The last equation can be described in terms of the antenna reflection coefficient, which can be expressed by the scattering parameter S_{11}

$$|S_{11}| \leq -10dB. \tag{4.2}$$

The proposed antenna is designed to have the S_{11} parameter below the threshold in the frequency band of interest (3.1 to 5.3 GHz).

The printed antenna design is inspired by the monopole design depicted in Figure 3.6. However, to better control geometrical dimensions of the antenna without making it too large as well as to keep metallic surface as small as possible to minimize losses, the upper half of the circumference was left out. The start design point is depicted in Figure 4.2. Also an inverted triangle was cut out on the top of the stub to compensate for surface current path on lower frequencies. Its effect will be parametrized and analysed to find the optimal dimensions, in order to achieve the best impedance matching.

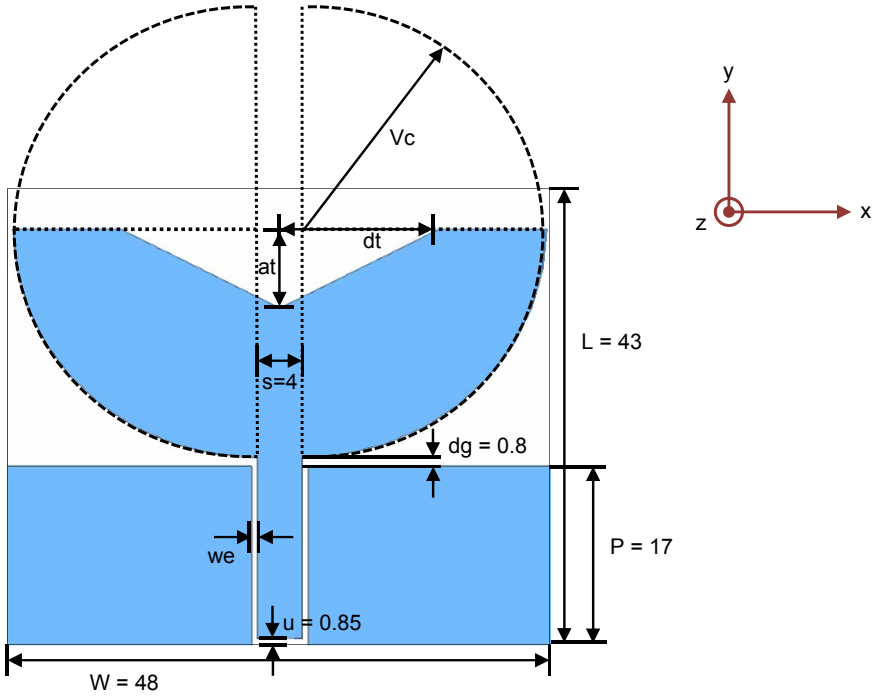

Figure 4.2: Base model for the proposed UWB antenna design - reflector plane and SMA connector not shown (dimentions in mm).

As it is shown in Figure 4.2, the antenna is fed by a Coplanar Waveguide (CPW). In this feeding technique, the ground conductors and the feed line are on the same plane. The substrate used is the Rogers 5880 laminate with 0.787mm thickness and dielectric constant $\epsilon_r = 2.2$. All metallic parts and surfaces (conductors, connector and reflector plane) are modelled by lossy copper with conductivity 5.8×10^7 S/m. The software tool used to simulate antenna behaviour is the CST Microwave Studio 2015 and the model produced in this software is depicted in Figure 4.3. The connector model is shown in Appendix A.

The distance from the reflector plane to the antenna is $\lambda_c/4$ where λ_c if the wavelength correspondent to the centre frequency ($f_c = 4.3Ghz$) of the band of interest.

$$\lambda_c/4 = \frac{c}{4f_c} = \frac{2.998 \times 10^8}{4 \times 4.3 \times 10^9} mm = 17.43mm. \tag{4.3}$$

The parameter m is added to the distance $\lambda_c/4$ and is initially assumed to be zero. In order to observe the influence on the scattering parameter S_{11} of the distance from the antenna to the reflector plane, a sweep on this parameter will be carried out together with the parameters at, we and vc - all other parameters remain constant.

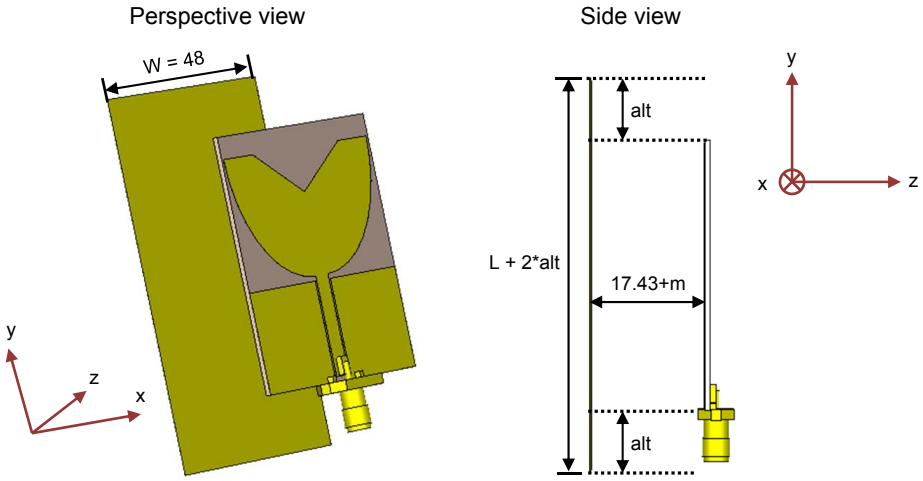

Figure 4.3: Perspective and side view of the antenna model with reflector plane and SMA connector (dimensions in mm).

4.2.2 Parameter analysis

In Figure 4.4 a parameter sweep of we is carried out between 0.1 and 0.6mm in a 0.5mm step where $at = m = 0mm$, $vc = 21.45mm$ and $alt = 10mm$. It can be concluded that $we = 0.5mm$ leads to an S_{11} below -10dB for the band 2.5-5.5GHz and produces a significant resonance at 3.8GHz.

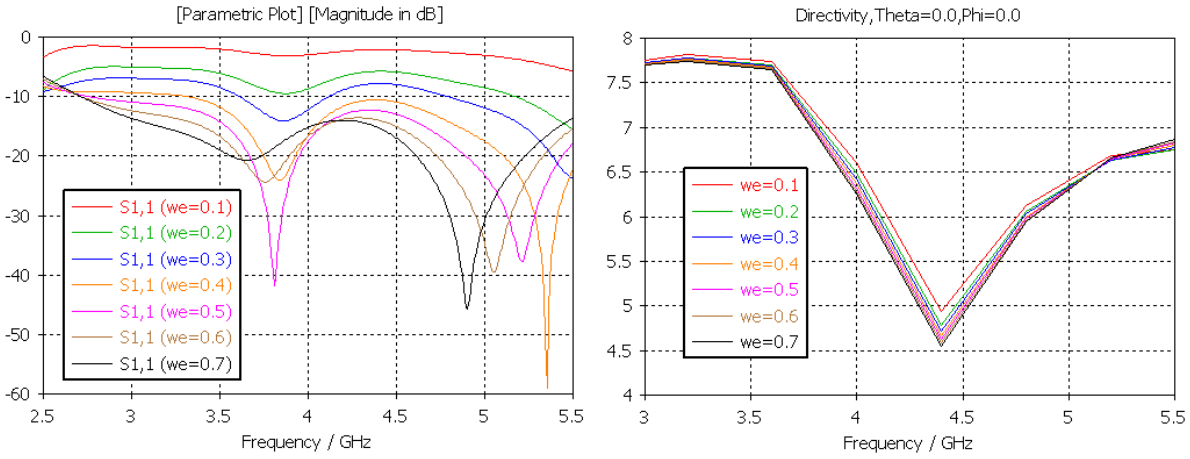

Figure 4.4: Sweep for the parameter we. Left: S_{11} in dB, Right: Directivity in dBi

Next, a sweep on the m was performed between -1 and 2mm. The other parameters were kept constant: $we = 0.5mm$, $at = m = 0mm$ and $vc = 21.45mm$. The result is depicted in Figure 4.5. It can be observed that the best impedance matching for the whole band is found at $m = -1mm$ which makes this the value chosen for m.

Additionally, a sweep was performed on the parameter at. The result is depicted in Figure 4.6. It can be concluded that the cut out triangle on the metallic surface of the antenna with height at has a little influence on the reflection coefficient S_{11}. However, despite the minor influence, the value $at = 11.85mm$ is adopted as it still minimizes S_{11}.

Moreover, a sweep on the radius vc was performed. The results are presented in Figure 4.7. It

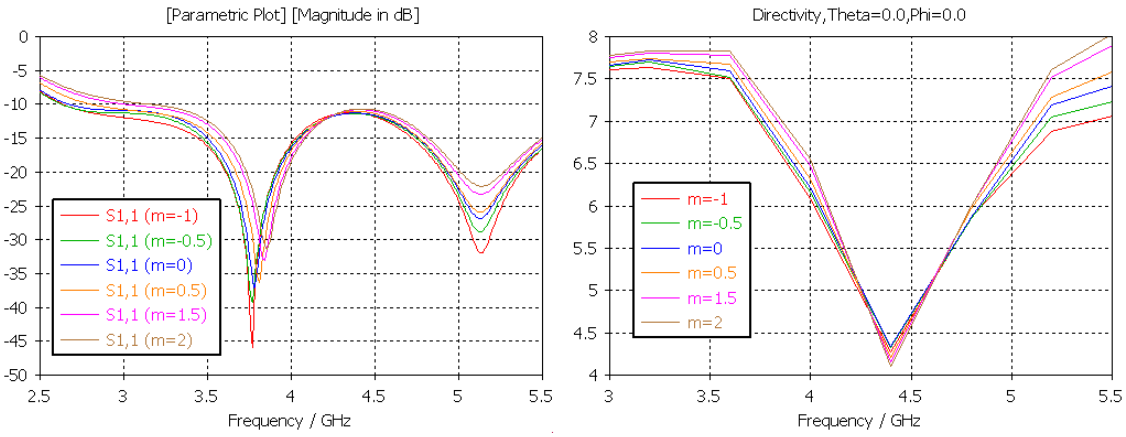

Figure 4.5: Sweep for the parameter m. Left: S_{11} in dB, Right: Directivity in dBi

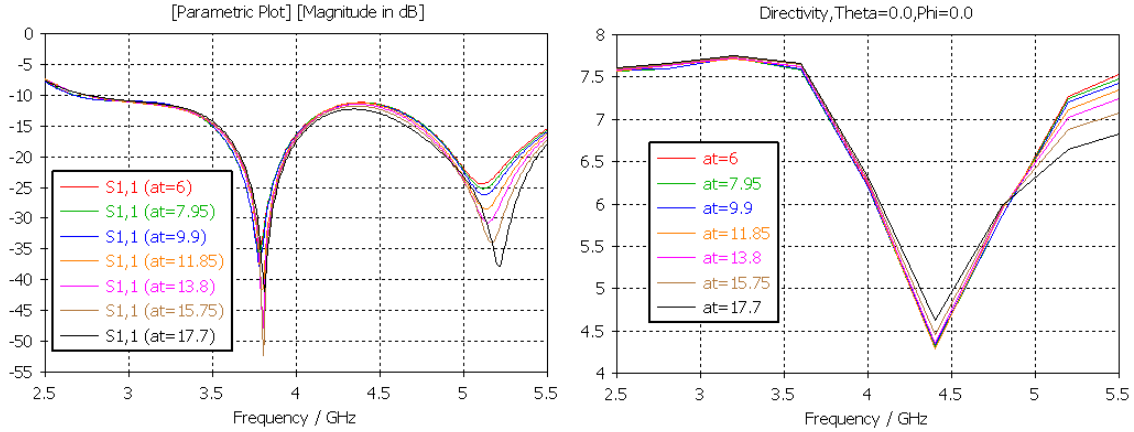

Figure 4.6: Sweep for the parameter at. Left: S_{11} in dB, Right: Directivity in dBi

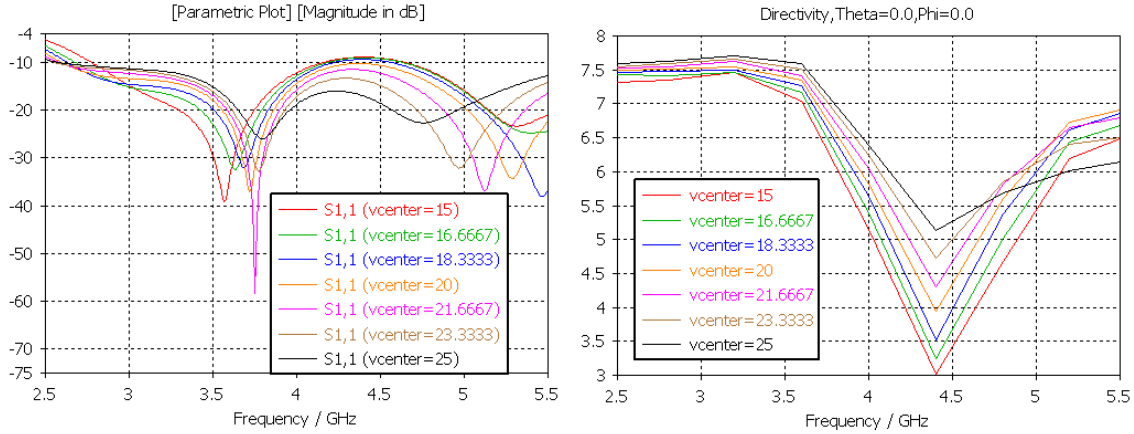

Figure 4.7: Sweep for the parameter vc. Left: S_{11} in dB, Right: Directivity in dBi

can be concluded that this parameter has a strong influence on the reflection coefficient. Such an effect was expectable since the physical properties of region where the surface current is high are being changed, namely the gap between the ground and the stub. Furthermore, taking into account the Gain dependency depicted in Figure 4.7, the value $vc = 23.33mm$ was chosen for this parameter.

In addition, the effect on reflector height alt was investigated. The results can been seen in Figure

4.8.

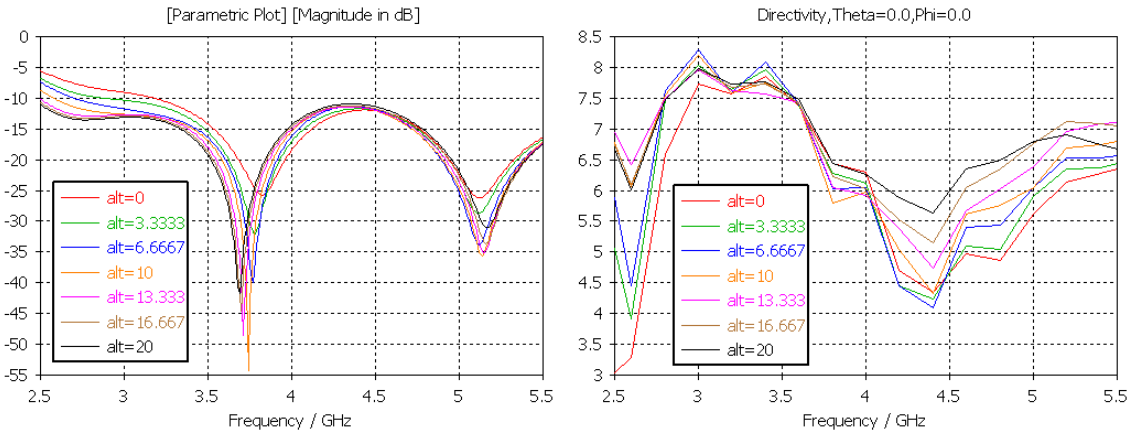

Figure 4.8: Sweep for the parameter alt. Left: S_{11} in dB, Right: Directivity in dBi

Analysing Figure 4.8, clearly the best result in terms of S_{11} and Directivity stability is achieved when $alt = 20mm$. However, this would mean a reflector plane 4cm longer than the actual antenna. A fair compromise can be found setting $alt = 10mm$.

Finally, the influence of reflector incline was analysed. Figure 4.9 depicts the various possible reflector positions depending on the angle α. The results of the performed sweep can be seen in Figure 4.10.

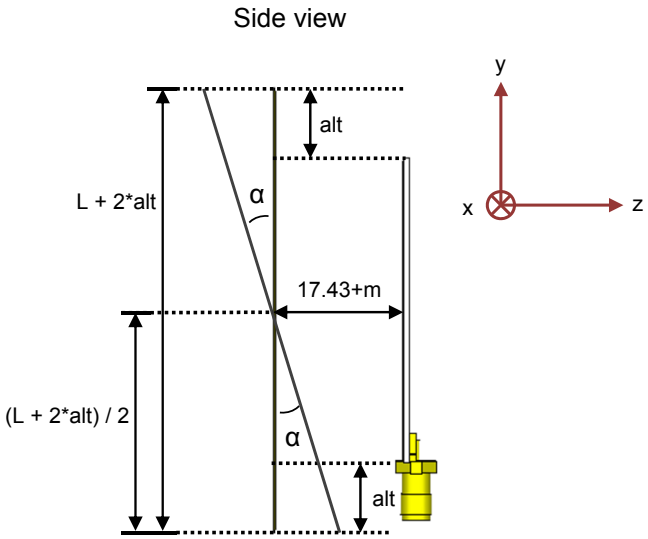

Figure 4.9: Reflector inclination dependent on angle α.

From Figure 4.10 it can be concluded that there is no significant influence of α on the reflection coefficient. Although it does change antenna directivity, the manufacturing process requires an additional step which is to make sure the reflection plane is placed at the right angle. This step will introduce errors which are in order of magnitude of the optimal angle ($\alpha = -10°$) compromising the optimization. As such, the reflector plane remains parallel to the antenna substrate ($\alpha = 0°$).

The Directivity and the reflection coefficient S_{11} for the chosen parameters are depicted in Figure

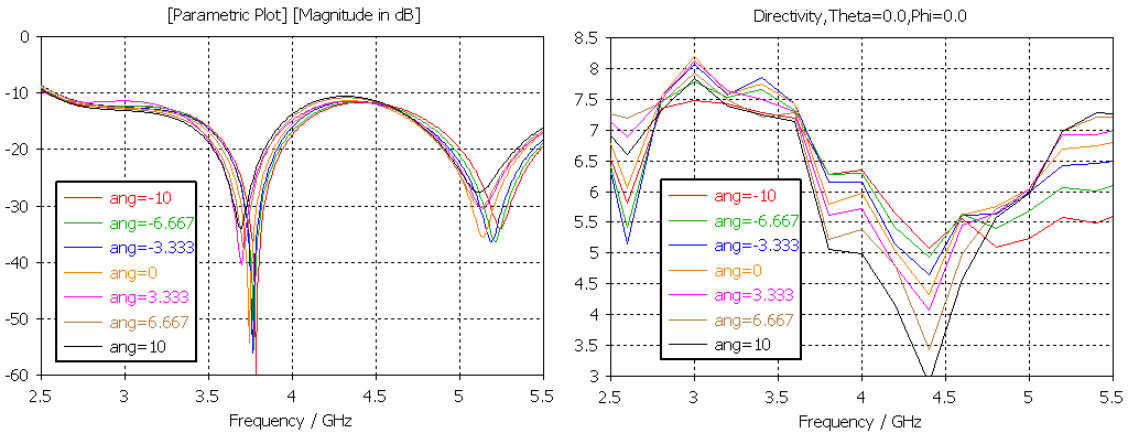

Figure 4.10: Sweep for the parameter α. Left: S_{11} in dB, Right: Directivity in dBi

4.11 for the band 2-10Ghz.

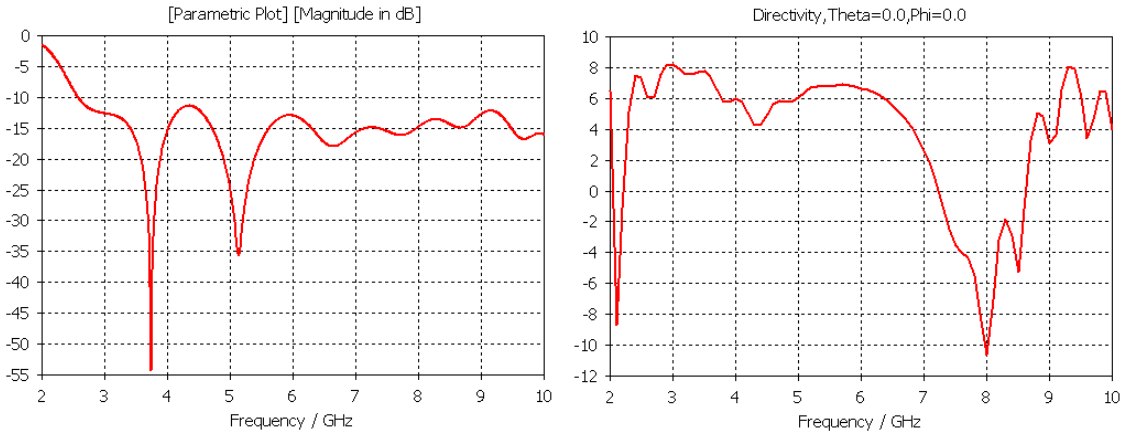

Figure 4.11: S_{11} and Directivity for the final parameters.

Although the antenna has been optimized to work in the band 3.1-5.3GHz, it can been seen from Figure 4.11 that the antenna completely fulfils impedance matching requirements up to 10GHz, meaning that it allows applications that work outside the range of frequencies the antenna was originally designed for. Nevertheless, from Figure 4.11 it can be concluded that above 6GHz the antenna ceases to be directive in the z direction and is no longer optimal for ranging applications. Radiation patterns for the frequencies 3.1, 4.3 and 5.3GHz are presented in Appendix B.

4.3 Performance Analysis

A prototype of the developed antenna model was produced so that it could be tested in a real world scenario. The substrate and connector used were the same as the simulated materials. To build the reflector plane, a rectangular piece of brass was cut and fastened to a block of Roofmate Styrofoam. The good electrical properties ($\epsilon_r \approx 1$) and lightness of this material make it a good option to emulate an air gap between the reflector and the substrate which was placed in the opposite side of the block. This Styrofoam block also acts as solid structure to hold the prototype parts in place. A picture of the finished

prototype is presented in Figure 4.12.

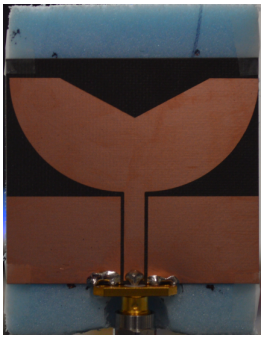

Figure 4.12: Antenna prototype.

Two procedures are carried out in this performance analysis. First, the antenna reflection coefficient S_{11} is measured to obtain impedance matching data. Lastly, the prototype is tested in the scope of a ranging system, specifically distance measurement with the PulsOn P400 modules from TimeDomain, which are also the hardware building blocks of the indoor localization system developed in this work.

4.3.1 Measurement of reflection coefficient

To perform impedance matching measurements, the prototype antenna was connected to the Vector Network Analyser (VNA) E5071C of Agilent Technologies and placed on top of absorbent material to minimize reflections. Also, to help mitigate coaxial cable effects, a strip of absorbent material was wrapped around the cable near the connector. Measurement set-up is depicted is Figure 4.13.

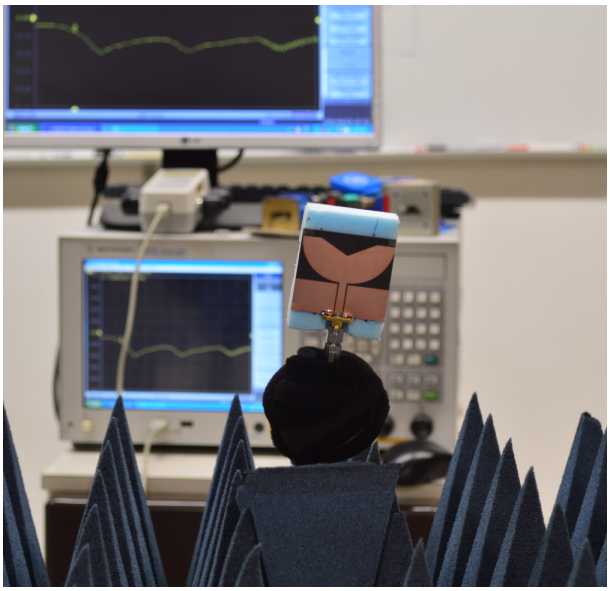

Figure 4.13: S_{11} measurement.

A frequency sweep from 2GHz to 10GHz was conducted and the S_{11} results are plotted in Figure 4.14.

By analysing the obtained results, it can be concluded that the antenna is matched for the band 3.3GHz to 10GHz which corresponds to the simulated results except for the lower frequencies. The

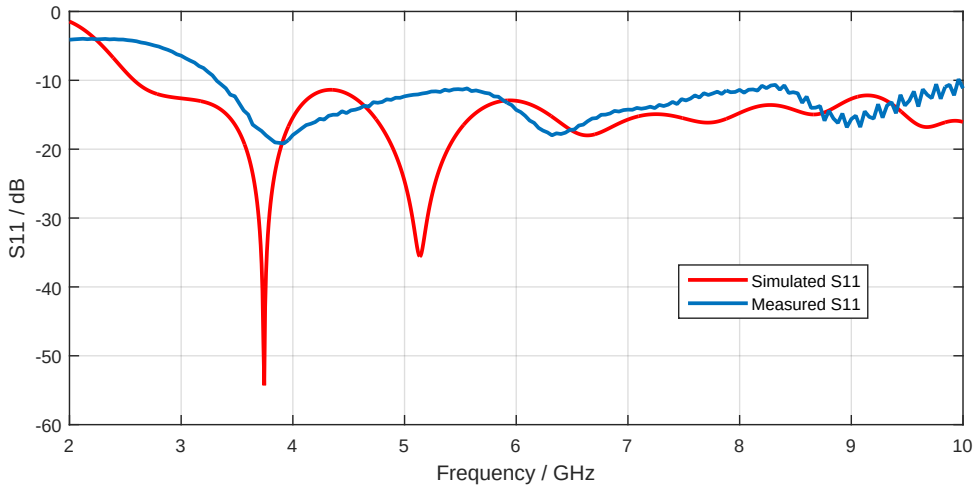

Figure 4.14: S_{11} measurement and simulated results.

lower band of the prototype in contrast to the theoretical model, can be explained by several factors not accounted for in the simulation. First, it can be seen in Figure 4.5 that good impedance matching is highly sensible to the distance between the substrate and the reflector. The sub-millimetre precision required to get optimal experimental results cannot be reached in practice, therefore the results are subject to error. Moreover, coaxial cable to connector mismatch will affect input impedance which will in turn worsen S_{11} results. Furthermore, substrate misalignments relative to the ground plane will also negatively influence results.

At the beginning of the band of interest (3.1GHz) the antenna prototype as an S_{11} equal to -7.5dB which is an acceptable value nonetheless. Additionally, the prototype still has very favourable expected directivity. This fact makes it a good candidate for ranging applications which will be tested next.

4.3.2 Performance measurement in a ranging system

To evaluate performance in a real ranging system, three PulsOn P400 modules were used: One target and two base stations. The proposed antenna was attached to one of the base stations. The other two modules use the stock 3dBi omni-directional monopole antenna [73], which will act as the reference antenna. The measurement set-up is depicted in Figure 4.15. A picture of base station nodes is also presented in Figure 4.16.

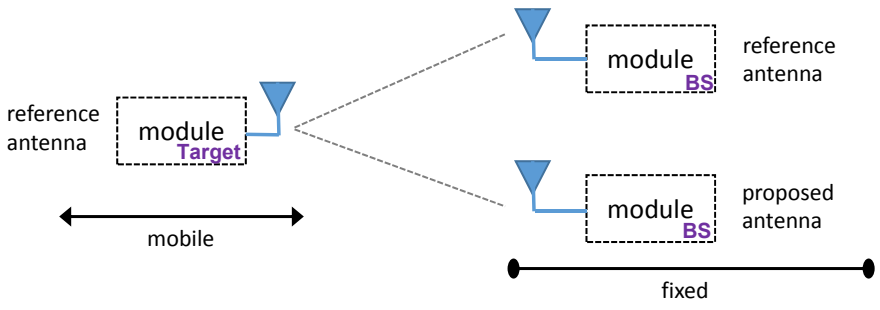

Figure 4.15: Measurement scheme.

The objective of this test is to compare distance measurement variance between antennas as well as to obverse the change in RSSI for both base stations. To achieve this, 1000 distance samples between the target and the base stations were taken in 0.3m steps from 0.6m to 4.8m. Measurement variance was computed and plotted in Figure 4.17.

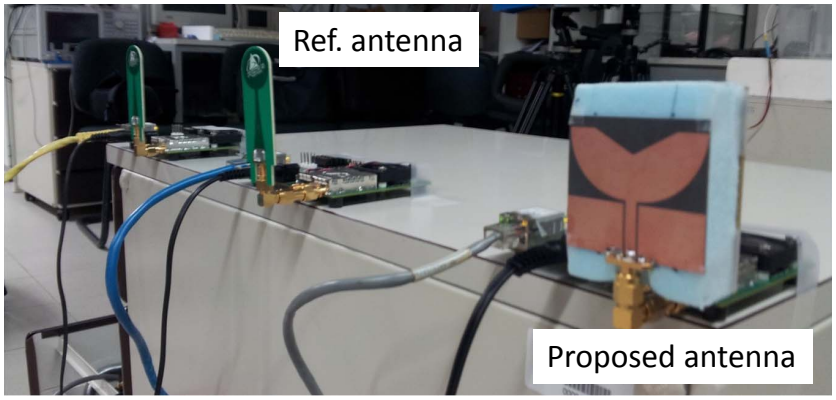

Figure 4.16: Picture of reference and proposed antenna on their respective nodes.

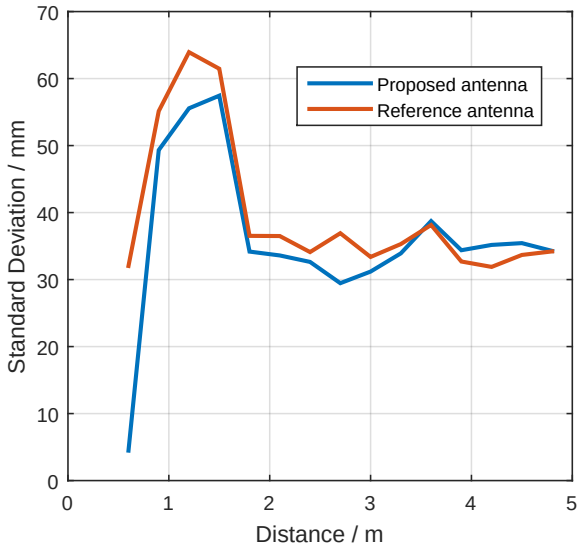

Figure 4.17: Standard deviation for proposed and reference antenna.

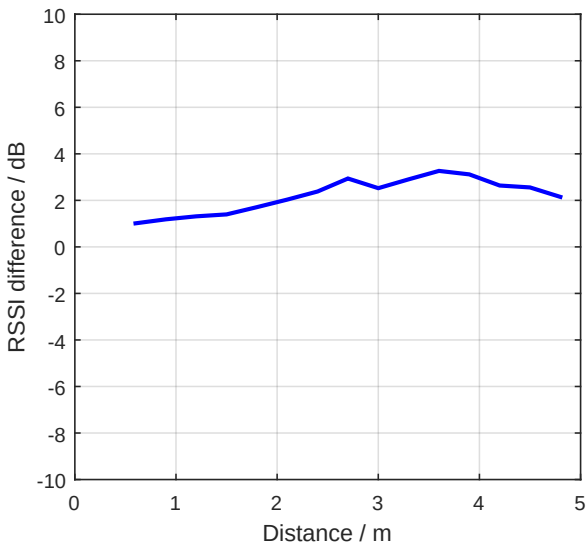

Figure 4.18: RSSI difference between proposed and reference antenna.

In can be seen that the proposed antenna manages to slightly improve measurement variance specially for small distances when compared to the reference antenna. In Figure 4.18, the difference in RSSI in dB from both base stations is plotted. It can be seen that, although both antennas perform similarly in terms of measurement variance, the proposed antenna improves RSSI at the target up to 3.3dB. On average, RSSI increases 2.27dB. This result indicates system range improvement as well as higher capability and compatibility for application in RSSI based localization systems.

It is worth to mention that the presented results only apply for the commercial system in study. Performance may vary if the proposed antenna is used in other systems. This is because signal post-processing algorithms vary from system to system. In this specific case, they are not known to the user and they too have influence on measurement variance. Moreover, UWB pulse distortion caused by the

antenna will also affect variance results - antenna fidelity factor [74] measurements were not carried out due to time constraints.

4.4 Summary

A new UWB antenna with reflector has been proposed for UWB ranging applications to replace the omni-directional 3dBi stock antennas provided in the commercial set of Time Domain P400 modules. This new antenna makes use of a reflector plane, whose angle and distance was studied to maximize directivity in the z direction. Moreover, the antenna is matched up to 10GHz, which can be of interest for other applications outside the band of interest to this work (3.1 - 5.3GHz). However, the radiation pattern is not optimized for frequencies above 5.3GHz.

One example of the application environment for this antenna consists on its use for localization system in active base stations located on the same plane as the target. The high directivity of the proposed antennas illuminates only a certain and well defined region of space concentrating the radiated power in a specific direction and, at the same time, mitigating the effects of other multipath signals arriving from other directions.

The prototype of the proposed antenna was fabricated and put under test. First, the reflection coefficient S_{11} was measured. It could be observed that, in the lower frequencies, the antenna was above the -10dB threshold, which can be caused by manufacturing imperfections and connector mismatch issues. However, from 3.3 up to 10GHz the antenna is matched as expected. Lastly, the prototype was attached to one ranging module acting as base station for measurement variance comparison with the stock 3dBi omni-directional antennas for this system. A slight improvement has been observed specially for short distances. Moreover, the difference RSSI was computed. It has been concluded that the proposed antenna increases RSSI at the target up to 3.3dB, which can improve system range and compatibility with RSSI based localization systems.

Chapter 5

Location techniques and solvers

Distance measuring in real-word localization scenarios is subject to inaccuracies that require the use of algorithms that try to mitigate the effects of errors in the measurements and deliver the best approximate result. The software developed in this work makes use of these algorithms to process target position estimation. The challenge is to find the most appropriate method to solve the following non-linear and (possibly) overdetermined system of equations that describes ToA localization

$$d_i(x,y) = \sqrt{(x-x_i)^2 + (y-y_i)^2} + \epsilon_i \qquad i = 1, 2, \ldots, M \tag{5.1}$$

where d_i is the measured distance, M is the number of measurements (often coincides with the number of base stations), (x_i, y_i) are the coordinates of the i-th reference node and ϵ_i is the measurement error or the residual. The parameter processed by the algorithms in the developed software is the measured distance d_i and not the ToA itself - however, the two only differ by the factor c, the speed of light, so the problem formulation remains unchanged.

Computational performance and accuracy are two ideal concepts that are, unfortunately, at opposite sides of the spectrum and are, as such, impossible to achieve simultaneously. A trade-off between these two essential goals has to be found based on the system's needs. Based on the research conducted in Chapter 2, the algorithms can be separated into two main categories:

- **Linear approach**. Typically involves linearized versions of the Least Squares method, which produces fast results with a minimum of mathematical operations although not guaranteed to be near the correct result. Improved versions take into account the variance of the measurements to produce a Linear Weighted Least Squares problem which are discussed in this work. Further linear methods are also mentioned in section 5.1.2.

- **Non-linear approach**. Non-linear approaches generally involve iterative algorithms that may reach the correct solution to the non-linear problem within a few steps given proper initialization which can be done by implementing a previous linear approach. Although accurate to the desired precision level, these algorithms are computationally intensive. Further characteristics on iterative algorithms are detailed in section 5.2.1.

The software developed in scope of this work makes use of the aforementioned Linear and Non-Linear approaches to estimate target position. In this section, the mathematical models for the methods used to estimate target localization are presented along with the proper modifications for implementation on an indoor Real-Time Localization System.

5.1 Linear Approaches

5.1.1 Simple Geometric Pinpoint

The SGP is a simple and direct positioning method. For three base stations, the case of interest, the SGP consists in finding the target position based on the centroid of the triangular shape formed by the three most closed points, known as cluster points, corresponding to the intersection of the range circles provident from a ToA based range estimation. Figure 5.1 depicts the location of the target node (black cross), cluster points (red) and ToA circles for two intersection scenarios.

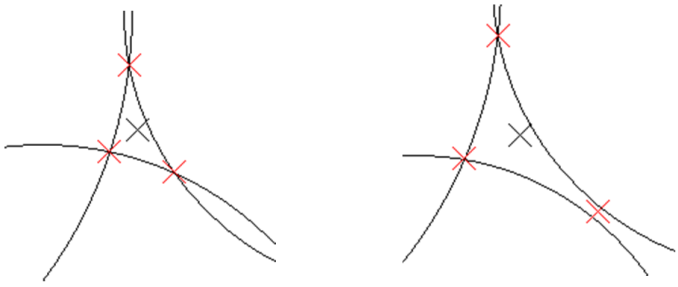

a) Evey ToA circle intersects one another.

b) At least one pair doesn't intersect one another.

Figure 5.1: Cluster of ToA estimation.

The intersection points of two ToA circles are obtained by solving the following system of equations

$$\begin{cases} r_1^2 = (x - x_1)^2 + (y - y_1)^2 \\ r_2^2 = (x - x_2)^2 + (y - y_2)^2 \end{cases}$$

Where (x_1, y_1) and (x_2, y_2) are base station coordinates and r_1 and r_2 are distance estimates to target. The solution set (x_{c1}, y_{c1}), (x_{c2}, y_{c2}) exists when both circles intersect and both points are candidates to cluster points, Figure 5.1 a). To determine which of the two intersections belongs to the cluster, the distance differences from the two intersection points to the circle defined by the measurement of the third base station are computed. The point whose distance difference is the smallest belongs to the cluster. In case the ToA circles only intersect at one point, there is only one solution to the system of equations and the corresponding point (x_c, y_c) is automatically a cluster point. The third case, Figure 5.1 b), occurs when two ToA circles don't intersect at all. In this case the cluster point is a point where the distance to either circles is minimized.

The centroid of the triangle formed by the cluster points can be found by averaging the x and y coordinates of the cluster points. Let x_{c1}, x_{c2}, x_{c3} and y_{c1}, y_{c2}, y_{c3} be the x and y coordinates of the

cluster points, respectively. Then, the centroid denoting target final position (x_T, y_T) is:

$$x_T = \frac{x_{c1} + x_{c2} + x_{c3}}{3} \qquad\qquad y_T = \frac{y_{c1} + y_{c2} + y_{c3}}{3}$$

The SGP can be applied to any system where the Base Station (BS) number is larger than 1 and is useful for course localization measurements that don't require much accuracy. The fact that it has a closed form solution, makes this a low resource method which is favourable for computation time. The points provided through SGP may serve as initialization points for more advanced and computer intensive statistical approaches like Least Squares (LS). Still, it is not guaranteed that SGP points will be close to the optimal LS solution, which can increase computational requirements compared to other initialization techniques. This issue is addressed in the next section, where linear and non-linear least squares approximations are presented.

5.1.2 Linearized Least Squares Approximation

Linear solutions consist on modifying the involved equations so that they depend linearly on the parameters to be estimated, in this case x and y, the coordinates of the target position. To begin with, ToA is employed so the non-linear equation system is as follows:

$$ct_i = d_i = f_i(x, y) + \epsilon_i \qquad i = 1, 2, \ldots, M \tag{5.2}$$

where d_i is the estimated distance between the target node and the i-th reference node, t_i is the actual ToA measurement, c is the speed of light, ϵ_i denotes the measurement error, residual or noise and

$$f_i(x, y) = \sqrt{(x - x_i)^2 + (y - y_i)^2} \qquad i = 1, 2, \ldots, M.$$

Following the linearization proposed in [75], squaring both sides of (5.2) gives

$$xx_i + yy_i - \frac{1}{2}R^2 = \frac{1}{2}(x_i^2 + y_i^2 - f_i^2) \qquad i = 1, 2, \ldots, M \tag{5.3}$$

with $R = \sqrt{x^2 + y^2}$.

Writing the system of equations in (5.3) in the matricial form $\boldsymbol{A}\vec{\gamma} = \vec{b}$

$$\boldsymbol{A} = \begin{bmatrix} x_1 & y_1 & -\frac{1}{2} \\ x_2 & y_2 & -\frac{1}{2} \\ \vdots & \vdots & \vdots \\ x_M & y_M & -\frac{1}{2} \end{bmatrix}, \vec{\gamma} = \begin{bmatrix} x \\ y \\ R^2 \end{bmatrix}, \vec{b} = \frac{1}{2}\begin{bmatrix} x_1^2 + y_1^2 - f_1^2 \\ x_2^2 + y_2^2 - f_2^2 \\ \vdots \\ x_M^2 + y_M^2 - f_M^2 \end{bmatrix}.$$

The system

$$\boldsymbol{A}\vec{\gamma} = \vec{b} \tag{5.4}$$

can be solved recurring to the known standard least squares estimation

$$\hat{\vec{\gamma}} = \underset{\hat{\vec{\gamma}}}{\operatorname{argmin}}(\boldsymbol{A}\hat{\vec{\gamma}} - \vec{b})^T(\boldsymbol{A}\hat{\vec{\gamma}} - \vec{b}) = (\boldsymbol{A}^T\boldsymbol{A})^{-1}\boldsymbol{A}^T\vec{b}. \tag{5.5}$$

In case there are only three measurements (one from each base station, ie. $M = 3$), the system in (5.4) is determined and has a trivial solution which is given by

$$\vec{\gamma} = \boldsymbol{A}^{-1}\vec{b}. \tag{5.6}$$

Although simple, the method in (5.5) still has two problems. First, the restriction $R = \sqrt{x^2 + y^2}$ is not accounted for and secondly, in case $M > 3$, the variance of the errors σ_i^2 is also ignored. The latter means that independent of variance, all measurements will have the same weight on determining the final LS solution. Also the value of f_i is unknown and will have to be replaced by d_i for implementation.

To improve the estimator, the variances of the errors can be taken into account. Given (5.2),

$$f_i^2 = (d_i - \epsilon_i)^2 \tag{5.7}$$

and, for sufficiently small σ_i^2,

$$(d_i - \epsilon_i)^2 \approx d_i^2 - 2d_i\epsilon_i. \tag{5.8}$$

Defining $\vec{p} = [-d_1\epsilon_1, -d_2\epsilon_2, -d_3\epsilon_3]^T$ and updating vector $\vec{b}$ to take into account this approximation one gets

$$\vec{b} = \frac{1}{2}\begin{bmatrix} x_1^2 + y_1^2 - d_1^2 \\ x_2^2 + y_2^2 - d_2^2 \\ \vdots \\ x_M^2 + y_M^2 - d_M^2 \end{bmatrix}$$

and also the system in (5.4) becomes

$$\boldsymbol{A}\vec{\gamma} + \vec{p} = \vec{b}. \tag{5.9}$$

Vector $\vec{p}$ is a random vector and, according to [76], its covariance matrix is a diagonal matrix given by

$$\boldsymbol{C_p} = diag(f_i^2\sigma_i^2, ..., f_M^2\sigma_M^2) \approx diag(d_i^2\sigma_i^2, ..., d_M^2\sigma_M^2) \tag{5.10}$$

since the errors are assumed to be uncorrelated. This assumption is generally accepted for ToA estimation [20] and is here tested for indoor scenarios.

The adopted Linear Weighted Least Squares (LWLS) estimator for $\hat{\vec{\gamma}}$ in (5.9) is [76]

$$\hat{\vec{\gamma}} = \underset{\hat{\vec{\gamma}}}{\operatorname{argmin}}(\boldsymbol{A}\hat{\vec{\gamma}} - \vec{b})^T\boldsymbol{W}(\boldsymbol{A}\hat{\vec{\gamma}} - \vec{b}) = (\boldsymbol{A}^T\boldsymbol{W}\boldsymbol{A})^{-1}\boldsymbol{A}^T\boldsymbol{W}\vec{b} \tag{5.11}$$

with $\boldsymbol{W} = \boldsymbol{C_p}^{-1}$.

Still, the restriction $R = \sqrt{x^2 + y^2}$ is not accounted for in (5.11) and also f_i is approximated by d_i which makes this solution generally suboptimal [21]. A more complete but more computationally intensive Constrained Linear Weighted Least Squares (CLWLS) solution that takes into account the restriction $R = \sqrt{x^2 + y^2}$ and still has a negligible bias is proposed in [75] but it's not applied in this work. In contrast, the presented LWLS, is less computationally intensive and its solution can be applied to initialize subsequent iterative algorithms. Other Linear Least Squares solutions involving equation subtraction and averaging are presented in [21].

In addition, it is worth to mention that in practice the entries of the covariance matrix $\boldsymbol{C_p}$ are not known and have to be estimated, in particular the variances σ_i^2. Applying these weights to LS estimation only makes sense if one makes sure the propagation characteristics of the channel i remain approximately constant, so that they can be correctly modelled by σ_i^2 during detection. If the target moves, σ_i changes unpredictably and so the system model will have to be corrected. Therefore, to obtain the values of σ_i^2 a noise model has been developed for this system which is presented in section 5.3.

Both systems (5.11) and (5.6) can be solved using the iterative Gaussian elimination algorithm to avoid computing the matrix inverses. However, a new system has to be solved each time a position has to be estimated. This means that Gaussian elimination or other solving techniques have to be performed each of those times. This is the case of LWLS estimator since the matrix $\boldsymbol{A}^T\boldsymbol{W}\boldsymbol{A}$ depends on d_i. However, for the non-weighted case in (5.6), the matrix $\boldsymbol{A}$ only depends on the positions of the reference nodes which remain constant throughout the whole positioning process. To minimize computation time, the use of iterative algorithms can be avoided by decomposing $\boldsymbol{A}$ into the multiplication of an orthogonal ($\boldsymbol{Q}$) and an upper triangular matrix ($\boldsymbol{R}$) known as QR decomposition.

The equation

$$\boldsymbol{A}\hat{\vec{\gamma}} = \vec{b} \tag{5.12}$$

becomes

$$\boldsymbol{Q}\boldsymbol{R}\hat{\vec{\gamma}} = \vec{b} \tag{5.13}$$

which can be rewritten as

$$\boldsymbol{Q}^T\boldsymbol{Q}\boldsymbol{R}\hat{\vec{\gamma}} = \boldsymbol{Q}^T\vec{b} \tag{5.14}$$

and since $\boldsymbol{Q}$ is orthogonal, $\boldsymbol{Q}\boldsymbol{Q}^T = 1$. This means

$$\boldsymbol{R}\hat{\vec{\gamma}} = \boldsymbol{Q}^T\vec{b}. \tag{5.15}$$

Since $\boldsymbol{R}$ is upper triangular, the system can be solved each time without Gaussian elimination and contribute to the algorithm's computational efficiency.

5.2 Non-Linear Approaches

5.2.1 Non-linear least squares

As discussed in section 2.2.3 for ToA, the optimal solution to the target position (x, y) in the problem (5.1) can be estimated through the Method of Maximum Likelihood which degenerates into a Non-Linear Least Squares (NLLS) problem given by

$$S = \frac{1}{2}\sum_{i=1}^{M} W_{ii}\epsilon_i^2. \tag{5.16}$$

where

- M is the number of measurements.
- W_{ii} is a weighting diagonal matrix equal to $1/\sigma_i^2$. Is it important to note that the errors are assumed to be uncorrelated which is generally accepted for ToA estimation [20].
- ϵ_i is the residual error and $\epsilon_i = d_i - f_i(x, y)$ where d_i is the measured distance and $f_i(x, y) = \sqrt{(x - x_i)^2 + (y - y_i)^2}$ where (x_i, y_i) are the position of the base stations to which the i-th measurement was taken.

The goal of the Least Squares method is to find the values of (x, y) that minimize the sum of the squares of the residuals, i.e. minimize the quantity S. Defining $\vec{\gamma} = (x, y)^T$ and computing the derivative of S with respect to γ_j where $j = 1, 2$ and setting it to zero gives

$$\frac{\partial S}{\partial \gamma_j} = \sum_{i=1}^{M} W_{ii}\epsilon_i J_{ij} = 0 \tag{5.17}$$

where $J_{ij} = \partial\epsilon_i/\partial\gamma_j$ is the Jacobian matrix.

In contrast to the trivial linear least squares, the matrix $\boldsymbol{J}$ actually depends on the parameters to be estimated so there is no closed form solution to (5.17). Evaluating $\boldsymbol{J}$ gives,

$$J_{ij}(x, y) = \begin{bmatrix} -\frac{x-x_1}{h_1} & -\frac{y-y_1}{h_1} \\ \vdots & \vdots \\ -\frac{x-x_M}{h_M} & -\frac{y-y_M}{h_M} \end{bmatrix} \tag{5.18}$$

where $h_i = \sqrt{(x - x_i)^2 + (y - y_i)^2}$.

As opposed to the linear approaches and the Taylor-Series approximation described next, the software developed in this work makes use of the already programmed and optimized iterative non-linear least squares solver available in the Optimization Toolkit which can be accessed via the MATLAB Runtime package to solve equation (5.17) - this is the only employed localization method which needs external software. The command for the used solver is the known MATLAB command `lsqnonlin` with the default iterative algorithm Trust-Region Reflective, since there are no constraints on the parameters

(x, y) and the system is overdetermined. To reduce the amount of function evaluations within the execution of the command, each time the solver is called, the Jacobian (5.18) is computed beforehand and provided to MATLAB Runtime engine each time a location estimation is carried out.

5.2.2 Taylor-Series Approximation

The Taylor Series Approximation (TS) for ToA is an iterative method that locally linearizes the function

$$f_i(x, y) = \sqrt{(x - x_i)^2 + (y - y_i)^2} \qquad i = 1, 2, \ldots, M. \tag{5.19}$$

in the neighbourhood of an initial target position estimate (x_e, y_e), which can be obtained through SGP or other Linear Least Squares approach. Approximating (5.19) by a first order Taylor series expansion gives

$$f_i(x, y) \approx f_i(x_e, y_e) + \theta_x \frac{\partial f_i(x, y)}{\partial x}(x_e, y_e) + \theta_y \frac{\partial f_i(x, y)}{\partial y}(x_e, y_e) \tag{5.20}$$

where $\theta_x = x - x_e$ and $\theta_y = y - y_e$ and where

$$\frac{\partial f_i(x, y)}{\partial x}(x_e, y_e) = \frac{x_e - x_i}{h_{ei}} \qquad\qquad \frac{\partial f_i(x, y)}{\partial y}(x_e, y_e) = \frac{y_e - y_i}{h_{ei}}$$

with $h_{ei} = \sqrt{(x_e - x_i)^2 + (y_e - y_i)^2}$, equation (5.19) can be expressed as

$$\boldsymbol{A}\vec{\theta} = \vec{b} \tag{5.21}$$

where

$$\boldsymbol{A} = \begin{bmatrix} \frac{x_e - x_1}{h_{e1}} & \frac{y_e - y_1}{h_{e1}} \\ \vdots & \vdots \\ \frac{x_e - x_M}{h_{eM}} & \frac{y_e - y_M}{h_{eM}} \end{bmatrix}, \vec{\theta} = \begin{bmatrix} \theta_x \\ \theta_y \end{bmatrix}, \vec{b} = \begin{bmatrix} f_1(x, y) - f_1(x_e, y_e) \\ \vdots \\ f_M(x, y) - f_M(x_e, y_e) \end{bmatrix}.$$

According to (5.2), and since the value of $f_i(x, y)$ is unknown, it is replaced by $d_i - \epsilon_i$. Updating $\vec{b}$ and defining $\vec{p} = [\epsilon_1, ..., \epsilon_M]^T$ gives

$$\vec{b} = \begin{bmatrix} d_1 - f_1(x_e, y_e) \\ \vdots \\ d_M - f_M(x_e, y_e) \end{bmatrix}$$

also the system in (5.21) becomes

$$\boldsymbol{A}\vec{\theta} + \vec{p} = \vec{b} \tag{5.22}$$

The minimum amount of measurements is $M = 3$, since there are three base stations, which means the system in (5.22) is always overdetermined. Moreover, $\vec{p}$ is a random vector whose covariance matrix is given by

$$\boldsymbol{C_p} = \mathbb{E}[\vec{p}\vec{p}^T] = diag(\sigma_1^2, ..., \sigma_M^2) \tag{5.23}$$

where $\mathbb{E}[\ ]$ is the expectation operator and, once again, the errors are assumed to be uncorrelated [20].

According to [77], the best linear unbiased estimator for $\hat{\vec{\theta}}$ in (5.22) is given by the following LWLS problem

$$\hat{\vec{\theta}} = \underset{\hat{\vec{\theta}}}{\operatorname{argmin}} (\boldsymbol{A}\hat{\vec{\theta}} - \vec{b})^T \boldsymbol{C}_p^{-1} (\boldsymbol{A}\hat{\vec{\theta}} - \vec{b}) = (\boldsymbol{A}^T \boldsymbol{C}_p^{-1} \boldsymbol{A})^{-1} \boldsymbol{A}^T \boldsymbol{C}_p^{-1} \vec{b}. \tag{5.24}$$

Equation (5.24) is then solved using QR decomposition. The variances of equation (5.23) are obtained via the suggested noise model in section 5.3.

5.3 Noise model

The variance of distance measurement between a base station and a target depends on several factors such as system bandwidth, clock jitter - which remain constant - and distance dependent ones such as the SNR. This means that the expected measurement variance actually depends on the parameter being estimated. There are several methods to address this problem [20, 22] that are based on SNR variation applied to indoor path loss models. A variance or noise model is important when using Weighted algorithms as it should be given less importance to more noisy measurements so that target detection occurs more precisely. The hardware (Time Domain P400 modules) used to produce distance measurements is part of a commercial product, so the post-processing algorithms used internally are not available to the user and no noise model is given. As a result, a more empiric approach had to be employed in order to develop a simple noise model for this system.

The measured variance results graphed in Figure 5.2, are taken from the proposed antenna performance test in section 4.3.2. However, the plotted results are from the reference omni-directional monopole antenna as this is the antenna used for all upcoming system performance tests. The polynomial Least Squares fit carried out in MATLAB is plotted in Figure 5.2 as well and it is given by (5.25). Measurements under 300mm are considered to have a constant 19mm standard deviation.

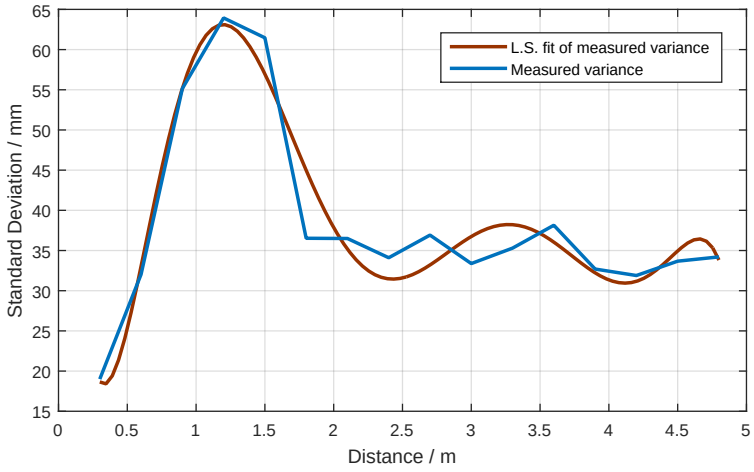

Figure 5.2: Measured standard deviation and interpolated noise model.

This model is the default noise model for the control software developed in this work and can be modified if information is available from manufacturer or on special propagation conditions.

$$\sigma(d) = \begin{cases} 19, & \text{if } d \leq 0.3m \\ (-0.01d^7 + 0.2d^6 - 1.5d^5 + 5.5d^4 - 11.5d^3 + 11.1d^2 - 4.4d + 0.8) \times 10^2, & \text{if } d > 0.3m \end{cases} \quad (5.25)$$

5.4 Real-Time Tracking and path smoothing

Target detection consists on the first phase of a localization system. The next phase consists in employing a data processing technique that can deal with the following four central problems that follow:

- **Smoothing.** Target detection is subject to errors that corrupt the estimates i.e. introduce noise in the measurements. These errors have a certain probability distribution, generally unknown. According to a given system model, this noise can be filtered to produce a smoothed path.

- **Failures in measurements.** A localization system can work at a specific pace (for example, one measurement per second or, more generally, one measurement per one arbitrary time step). However, such pace is subject to abnormalities inherent to the hardware used to retrieve the measurements which is not guaranteed to work for every request. Post-processing algorithms must be capable of dealing with time steps where there is a lack of a measurement in a robust manner, somehow predicting how the system would behave based on a given model.

- **Unmeasurable variables.** The only variable the developed localization system retrieves is the 2D position of the target corrupted with noise. It is important to estimate other relevant system parameters such as the velocity or acceleration. Post-processing of the data should be able to estimate these parameters as simply and as accurate as possible.

- **Computational efficiency.** It has to be taken into account the fact that the developed localization system is real-time. This means that all of the aforementioned criteria for a post-processing algorithm have to be fulfilled and must produce tangible results within an a priori user-given interval.

In order to achieve the stated requirements for signal post-processing, a Kalman Filter was chosen. The Kalman Filter is a linear optimal[1]-state estimation technique which minimises the mean squared error of the estimated parameters. It is used, for instance to keep track of objects by GPS, in processed images or radar. It also has applications in Economics and other Data Fusion processes. The Kalman Filter is an iterative process that estimates the state of a linear system based on corrupt measurements affected by noise. Only the last state is needed to estimate a new state which makes this a computational efficient algorithm when compared to other batch techniques which require data from all previous time steps. It produces an estimated state output which is a weighted average between the prediction based on the given linear model for system behaviour and the noisy measurement. Moreover, in the absence of measurements, the filter can continue to produce results based only on the given system model. Such a feature enables the user not to lose track of the target even when a measurement fails. Allied to the

[1]Given that all errors are normally distributed

fact that this technique attempts to minimize the Mean Squared Error (MSE) of the estimated system state, it produces a continuous - even when measurements of certain time steps fail - and smoothed - in the sense that attempts to filter out the noise - state estimation. In the case of the current localization system, a ”system state” is represented by the following state vector

$$\vec{x} = \begin{bmatrix} x \\ y \\ \dot{x} \\ \dot{y} \end{bmatrix}$$

in which x and y are position coordinates and $\dot{x}$ and $\dot{y}$ are the velocities in the x and y direction, respectively. The Kalman linear state transition equation is given by [78]

$$\vec{x}_k = \boldsymbol{A}\vec{x}_{(k-1)} + \boldsymbol{B}\vec{u}_{(k-1)} + \vec{w}_{(k-1)} \tag{5.26}$$

where $\boldsymbol{A}$ and $\boldsymbol{B}$ are the state transition and control input matrices, respectively; $\vec{x}_{k-1}$ and $\vec{u}_{k-1}$ are the state and control input vectors at time step $k-1$ respectively and $\vec{w}_{k-1}$ is the noise vector at time step $k-1$. According to Newton's Laws of Motion and assuming constant acceleration between time step $k-1$ and k, the position in the x direction at time step k is given by

$$x_k = \frac{1}{2}[\dot{x}_{(k-1)} + \dot{x}_k]\Delta t + x_{(k-1)} \tag{5.27}$$

where Δt is the time step period. The velocity $\dot{x}_k$ is given by

$$\dot{x}_k = \dot{x}_{(k-1)} + \Delta t \times a_{(k-1)_x} \tag{5.28}$$

where $a_{(k-1)_x}$ is the acceleration in the x direction at time step $k-1$. Substituting (5.28) in (5.27) gives

$$x_k = x_{(k-1)} + \Delta t \times \dot{x}_{(k-1)} + \frac{\Delta t^2}{2} \times a_{(k-1)_x}. \tag{5.29}$$

Equations (5.28) and (5.29) define the model of the system for the coordinate x. Calculations for the y coordinate are analogous. Writing the system of equations formed by (5.28) and (5.29) in matrix format gives

$$\vec{x}_k = \begin{bmatrix} 1 & 0 & \Delta t & 0 \\ 0 & 1 & 0 & \Delta t \\ 0 & 0 & 1 & 1 \\ 0 & 0 & 0 & 1 \end{bmatrix} \begin{bmatrix} x_{(k-1)} \\ y_{(k-1)} \\ \dot{x}_{(k-1)} \\ \dot{y}_{(k-1)} \end{bmatrix} + \begin{bmatrix} \frac{\Delta t^2}{2} a_{(k-1)_x} \\ \frac{\Delta t^2}{2} a_{(k-1)_x} \\ a_{(k-1)_y} \Delta t \\ a_{(k-1)_y} \Delta t \end{bmatrix} = \boldsymbol{A}\vec{x}_{(k-1)} + \vec{w}_{(k-1)}. \tag{5.30}$$

The target is assumed to be moved by random forces in the x and y direction which produce a random, constant acceleration a_x and a_y from time step to time step. These are considered to be normally distributed with zero mean and variance σ_a. As a result, the vector on the second term of

(5.30) can be interpreted as the random noise vector $\vec{w}_{(k-1)}$ of the Kalman filter state transition equation with covariance $\boldsymbol{Q}$ given by

$$\boldsymbol{Q} = \mathbb{E}[\,\vec{w}_{(k-1)}\,\vec{w}_{(k-1)}^{T}\,] = \begin{bmatrix} \frac{\Delta t^4}{4} & 0 & \frac{\Delta t^3}{2} & 0 \\ 0 & \frac{\Delta t^4}{4} & 0 & \frac{\Delta t^3}{2} \\ \frac{\Delta t^3}{2} & 0 & \Delta t^2 & 0 \\ 0 & \frac{\Delta t^3}{2} & 0 & \Delta t^2 \end{bmatrix} \sigma_a^2$$

and $\boldsymbol{B} = \vec{u}_{(k-1)} = 0$.

The next step is to define the filter measurement equation which is given by

$$\vec{z}_k = \boldsymbol{H}\vec{x}_k + \vec{v}_k \tag{5.31}$$

where $\vec{z}_k$ is the measurement vector of the true state $\vec{x_k}$ corrupted by the noise vector $\vec{v}_k$. Matrix $\boldsymbol{H}$ is the observation model and given that the only measured values are the x and y position coordinates, $\boldsymbol{H}$ is given by

$$\boldsymbol{H} = \begin{bmatrix} 1 & 0 & 0 & 0 \\ 0 & 1 & 0 & 0 \end{bmatrix}.$$

The covariance matrix of the noise vector $\vec{v}_k$, $\boldsymbol{R}$ is

$$\boldsymbol{R} = \mathbb{E}[\,\vec{v}_k\,\vec{v}_k^{T}\,] = \begin{bmatrix} \sigma_d^2 & 0 \\ 0 & \sigma_d^2 \end{bmatrix}$$

where σ_d^2 is measurement error variance in both the x and y direction, which for this simple Kalman filter application are assumed to be independent and identical independently of the chosen solver.

The Kalman filter algorithm has two stages: the predict and update stage which are given by the following set of equations

- Prediction

  Predict system state: $\hat{\vec{x}}_k = \boldsymbol{A}\tilde{\vec{x}}_{(k-1)}$

  Predict process noise covariance $\boldsymbol{P}$: $\hat{\boldsymbol{P}}_k = \boldsymbol{A}\boldsymbol{P}_{(k-1)}\boldsymbol{A}^T + \boldsymbol{Q}$

- Update

  Calculate the Kalman gain $\boldsymbol{K}$: $\boldsymbol{K}_k = \hat{\boldsymbol{P}}_k\boldsymbol{H}^T(\boldsymbol{H}\hat{\boldsymbol{P}}_k\boldsymbol{H}^T + \boldsymbol{R})^{-1}$

  Update system state prediction with current measurement: $\tilde{\vec{x}}_k = \hat{\vec{x}}_k + \boldsymbol{K}_k(\vec{z}_k - \boldsymbol{H}\hat{\vec{x}}_k)$

  Update process noise covariance: $\boldsymbol{P}_k = (\boldsymbol{I} - \boldsymbol{K}_k\boldsymbol{H})\hat{\boldsymbol{P}}_k$

The Kalman filter parameters, such as the initial values for system state $\vec{x}_0$ and process covariance $\boldsymbol{P}_0$, as well as the time invariant $\boldsymbol{R}$ and $\boldsymbol{Q}$, can be defined manually in the user interface of the software as they are dependent on target movement behaviour and have to be adjusted accordingly. During system performance analysis, in section 5.6, several values for these parameters are tested.

5.5 The Tracking Algorithm

The *Tracking Algorithm* is the aggregation of four stages the software performs each time a new target location estimation is carried out. The four stages A, B, C and D can be described as follows.

- **A - Get distances in sequence.** At this stage the software requests each base station sequentially for a measurement to the target. After receiving packets from all base stations, the algorithm proceeds. If this stage fails the next two stages are skipped.
- **B - Initialization.** If an iterative algorithm is selected an initialization has to be performed. This can be achieved executing one linear approach. The stage is skipped if a linear approach is used as solver.
- **C - Solving.** The solving stage is where the solving algorithm is executed to produce a target location estimation. This stage (as well as the initialization stage) is executed once the *Tracking Algorithm* has gathered all measurements for the current sample[2]. It is otherwise skipped.
- **D - Smoothing.** At this stage the target estimate coordinates or sample from the solver are fed to the Kalman filter. This stage is executed when the solver terminates successfully or when there is a measurement failure in the first stage. If the latter occurs, the filter outputs a location estimation based solely on the prediction generated from the given system model.

The *Tracking Algorithm* repeats itself subject to a user specified sampling frequency until it is cancelled by user interaction, the solver fails or one of the following, previously set, stop criteria is met.

- **Time limit**. The tracking takes place for a certain time interval independently of samples taken.
- **Successful samples limit.** The tracking takes place up to the point where a certain amount of samples have been gathered successfully (no errors in the measurement process or processing steps) independently of the total time taken.

The *Tracking Algorithm* stages can be described in the block diagram in Figure 5.3. It is noteworthy that this is a simplified algorithm description. Error verification such as failure on thread creation (stage A and B), consecutive measurement request failure (stage A), errors due to invalid input parameters (stages B, C and D), other general system failures and algorithm stop criteria that are also accounted for in the software are not represented in this description for simplification reasons. A more technical in-depth explanation of a complete iteration of the target algorithm is presented in section 6.3.1.

5.6 Performance Analysis

In this section the performance of the system employing the localization algorithms in section 5.1 and 5.2 is measured. Taking into account what was discussed in these two sections, the following Linear Approaches were implemented:

[2]A sample is the output of the localization algorithm executed by the solver. The inputs are (apart from initialization samples) the distances to the base stations (refered to as 'measurements') and are always multiples of the total amount of connected base stations.

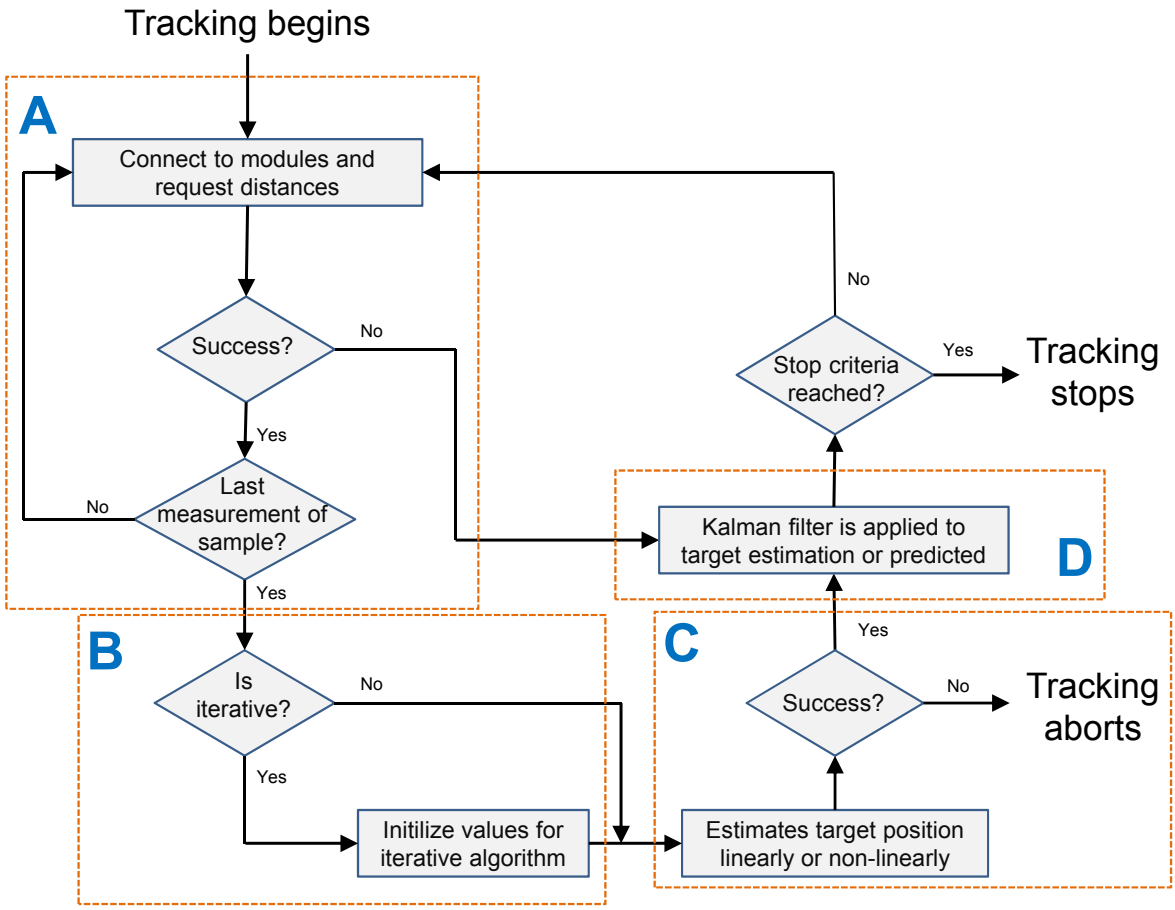

Figure 5.3: Simplified block diagram of the *Tracking Algorithm*.

- SGP - Simple Geometric Pinpoint.
- LLS - Linear Least Squares.
- LWLS - Linear Weighted Least Squares.

Additionally, the following Non-Linear Approaches were implemented:

- TS - Taylor Series Approximation.
- Non-LLS (NLLS) - Non-Linear Least Squares (MATLAB).
- Non-LWLS (NLWLS)- Non-Linear Weighted Least Squares (MATLAB).

In what follows, simulated and real RTLS system results are presented and analysed, the average solver time of the algorithms, mean error relative to true target position and system accuracy were observed and commented on. The hardware used for the test-bed and developed software, from which all experimental results were taken from, are described in Chapter 6.

5.6.1 Static target

In this test the goal is to obtain an estimation of the system accuracy and mean error depending on the algorithm and initializer used. Also, the influence on target position relative to the base stations is

analysed. All measurements were carried out with three different target positions. Figure 5.4 depicts base station layout and true target positions with a red cross. An actual photo of the measurement set up is shown in Figure 5.5.

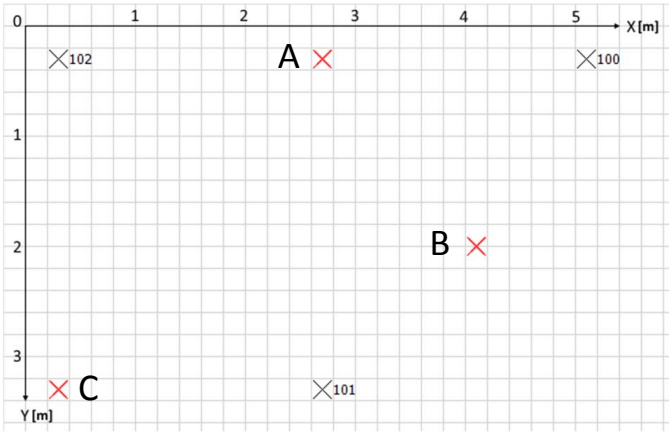

Target	X [m]	Y [m]
A	2.7	0.3
B	4.1	2
C	0.3	3.3

B.S.	X [m]	Y [m]
100	5.1	0.3
101	2.7	3.3
102	0.3	0.3

Figure 5.4: Base station and target positions.

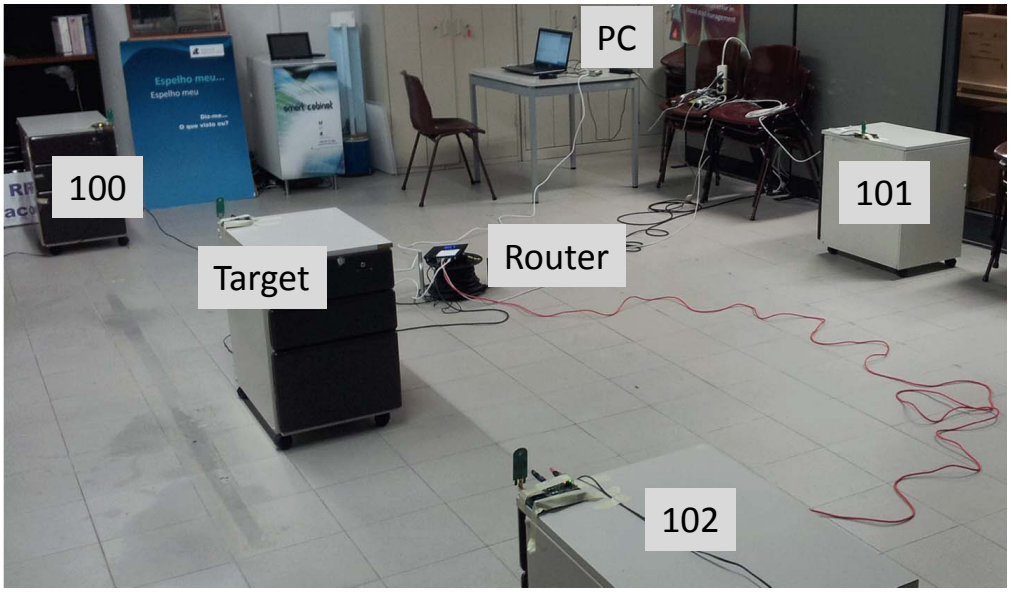

Figure 5.5: Photo of measurement set up.

Location of target points A, B and C were chosen strategically so that every limit location of the base station layout could be tested. Unfortunately, due to space limitations, points outside the rectangle defined by the base stations could not be tested although the system is prepared to do so, depending only on the employed solver algorithm. The antennas used for this test were the stock omni-directional monopoles.

The studied algorithms were tested and its performance measured in terms of the accuracy of measurements with 90% precision and the Mean Distance Error (MDE). MDE is computed as the mean

euclidean distance between position samples and the true target position and is expressed by

$$MDE = \frac{1}{M}\sum_{i=1}^{M}\epsilon_i \tag{5.32}$$

where

- M denotes the amount of successful measurements.
- $\epsilon_i = \sqrt{(x_p - x_r)^2 + (y_p - y_r)^2}$ where (x_p, y_p) are the coordinates of the estimated position and (x_r, y_r) are the real coordinates of the target.

For each combination of algorithm and initializer, 700 samples were taken. The mean solver computation time was also calculated so that the relative computational performance of the algorithms could also be evaluated. Moreover, the time for one full iteration of the *Tracking Algorithm* was computed as well. This time encloses important information about the duration of measurements which is of major importance for the overall system performance as it will limit sampling frequency. Additionally, for the applicable algorithms, two Measurements per Sample (mps) were taken for comparison purposes. Table 5.1 presents the data collected for the first measurement, point A.

Table 5.1: Data for Point A.

POINT A												
Algorithm / Initialization	**Mean solver time [ms]**		**Mean T.A. time [ms]**		**Average iterations**		**MDE [mm]**		**Maximum error [mm]**		**Accuracy** 90% precision [mm]	
	1 mps	*2 mps*	*1 mps*	*2 mps*	*1 mps*	*2 mps*	*1 mps*	*2 mps*	*1 mps*	*2 mps*	*1 mps*	*2 mps*
SGP	< 1	**	151	**	**	**	67	**	222	**	156	**
LLS	< 1	**	150	**	**	**	40	**	124	**	80	**
LWLS	**	< 1	**	301	**	**	**	35	**	105	**	65
TS/SGP	2	--	154	--	4.78	--	35	--	124	--	73	--
TS/LLS	2	2	154	309	4.77	4.77	35	25	130	70	61	44
NLLS/LLS	9	--	164	--	N/A	N/A	35	--	148	--	73	--
NLWLS/LLS	9	--	164	--	N/A	N/A	34	--	134	--	72	--

** Not aplicable -- Not computed N/A Not Available

In terms of performance with 1 mps, every tested algorithm combination except for SGP delivered good results averaging 36mm of MDE, also the accuracy is in the order of 7cm for most algorithm combinations which is a good outcome for an indoor RTLS.

It is also to note that all tested iterative algorithms performed similarly. There is almost no difference in MDE between TS and NLLS. The latter, differs in execution time taking up to ten times more than other options. However, considering *Tracking Algorithm* iteration time, the increase in mean solver time of NLLS/NLWLS compared to other algorithms is relatively small.

When taking two measurements per sample (2mps), the MDE for the linear LWLS and the iterative TS have dropped significantly compared to their 1mps counterparts. Also the maximum error in

the observed set of measurements decreased considerably. Although working at 2mps significantly improves system MDE and accuracy, it doubles mean Tracking Algorithm (T.A.) time which halves system sampling frequency.

Table 5.2: Data for Point B.

POINT B												
Algorithm / Initialization	**Mean solver time [ms]**		**Mean T.A. time [ms]**		**Average iterations**		**MDE [mm]**		**Maximum error [mm]**		**Accuracy 90% precision [mm]**	
	1 mps	*2 mps*	*1 mps*	*2 mps*	*1 mps*	*2 mps*	*1 mps*	*2 mps*	*1 mps*	*2 mps*	*1 mps*	*2 mps*
SGP	< 1	**	152	**	**	**	64	**	159	**	105	**
LLS	< 1	**	152	**	**	**	40	**	151	**	71	**
LWLS	**	< 1	**	317	**	**	**	29	**	94	**	50
TS/SGP	2	--	155	--	5.15	--	35	--	92	--	60	--
TS/LLS	2	2	154	308	4.87	4.81	36	29	100	70	65	55
NLLS/LLS	10	--	163	--	N/A	N/A	36	--	102	--	63	--
NLWLS/LLS	10	--	163	--	N/A	N/A	35	--	106	--	61	--

** Not aplicable -- Not computed N/A Not Available

Regarding point B, the all algorithms kept performance levels when compared to point A except for a generalized decrease on accuracy which can be due to the new point location and noise values. Likewise, mean solver time remained constant.

Table 5.3: Data for Point C.

POINT C												
Algorithm / Initialization	**Mean solver time [ms]**		**Mean T.A. time [ms]**		**Average iterations**		**MDE [mm]**		**Maximum error [mm]**		**Accuracy 90% precision [mm]**	
	1 mps	*2 mps*	*1 mps*	*2 mps*	*1 mps*	*2 mps*	*1 mps*	*2 mps*	*1 mps*	*2 mps*	*1 mps*	*2 mps*
SGP	< 1	**	152	**	**	**	67	**	141	**	130	**
LLS	< 1	**	150	**	**	**	53	**	214	**	100	**
LWLS	**	< 1	**	303	**	**	**	44	**	118	**	70
TS/SGP	2	--	154	--	3.96	--	41	--	120	--	65	--
TS/LLS	8	9	154	307	3.93	4.03	36	32	116	91	65	60
NLLS/LLS	10	--	164	--	N/A	N/A	41	--	136	--	64	--
NLWLS/LLS	10	--	163	--	N/A	N/A	42	--	154	--	66	--

** Not aplicable -- Not computed N/A Not Available

Point C is located the farthest way from all base stations and its effects are visible in the obtained results. Linear Least Squares (LLS) performance is the worst of all tested points in both MDE and accuracy. This can be due to the validity of the linearized model of the system which breaks down when far from the centre of the polygon formed by the base stations. Despite significant performance difference in the linearized models, all other iterative methods achieve an MDE of approximately 40mm.

In conclusion, the performance of the linearized models (including SGP) differs significantly from point to point, which was expected due to the validity of the linear models depending on target position.

Also, there was no significant difference on iterative Weighted vs. Non-weighted algorithms. The LWLS, although it is a Weighted algorithm, performed better than LLS due to the fact that it needs 2mps. It is noteworthy though, that system noise will depend on channel propagation conditions and can differ substantially in indoor scenarios, so Weighted algorithms could make a difference if the system were to be tested in other conditions, other base station configuration and employing other noise models. Another important point to be noted is that system sampling frequency is limited almost solely by the mean T.A. time - the mean solver time being much smaller - which includes 3 (at 1mps) and 6 (at 2mps) sequential measurement requests to the base stations each one taking around 50ms. This time is hardware inherent and cannot be overcome by the developed software - also, T.A. mean time remained relatively constant on all three tested points for each evaluated algorithm.

5.6.2 Target moving on a straight path

Due to the difficulty on moving an object physically with a constant velocity in a precise manner, only simulations were carried out for this test. For all algorithm combinations the tracker was configured to take 1 measurement per sample as fast as possible. This means that no particular sampling frequency was set and that the *Tracking Algorithm* will begin a new iteration without waiting for the end of a sampling period or skipping periods (see 6.3.1). The path of the target is shown in Figure 5.6.

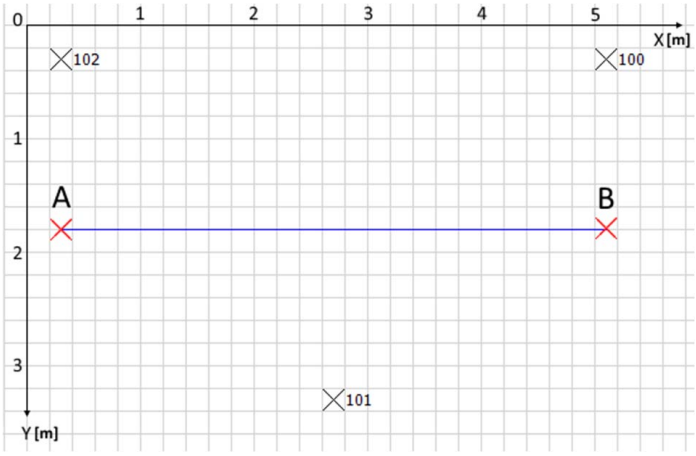

End points	X [m]	Y [m]
A	0.3	1.8
B	5.1	1.8

B.S.	X [m]	Y [m]
100	5.1	0.3
101	2.7	3.3
102	0.3	0.3

Figure 5.6: Straight line path to be tested.

The simulation details were set in the software's *Simulation Console* (see Appendix C.5).
Since the target is moving, the Kalman filter was also activated under the following initial conditions:

- Since the initial point is known, initial process covariance matrix is given by

$$\boldsymbol{P_0} = \begin{bmatrix} 0 & 0 \\ 0 & 0 \end{bmatrix}. \tag{5.33}$$

The initial system vector state can be defined as

$$\vec{x}_0 = [0.2, 5.1, 0, 0]^T. \tag{5.34}$$

- For test purposes the variance of the measurements in the x and y-direction (matrix $\boldsymbol{R}$) were defined as

$$\sigma_d^2 = 0.001m^2 \tag{5.35}$$

and for process noise covariance (matrix $\boldsymbol{Q}$)

$$\sigma_a^2 = 0.01m^2. \tag{5.36}$$

The tracking process is show in Figure 5.7 where the main user interface of the developed software is displayed. For the current test, the simulated target moves at a constant velocity of 0.25m/s on a straight path of length 4.8m between points A and B (Figure 5.6). The software also adds noise to the measurements according to the noise model defined in section 5.3. It is also to note that a 50ms delay is introduced in every measurement request to recreate real hardware response time.

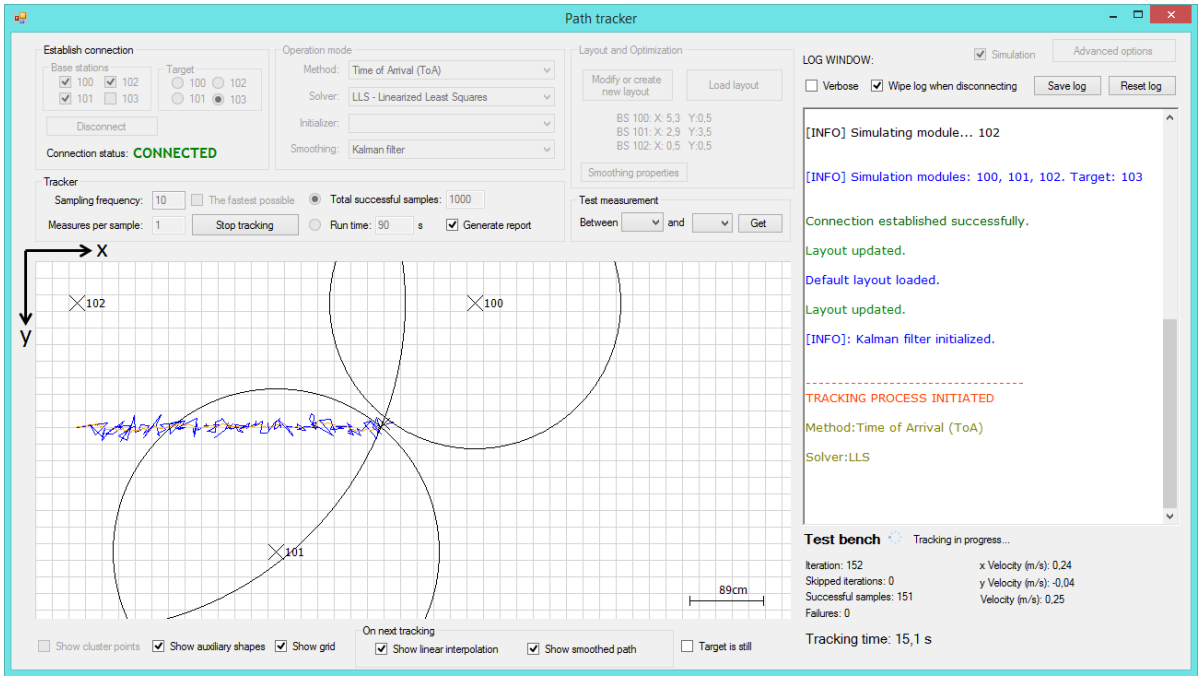

Figure 5.7: Main user interface during target detection.

Simulation results are presented in Table 5.4 where the MDE, maximum distance error and accuracy for 90% precision, for both a simple linear interpolation, and Kalman filtering are shown. Average iteration time, mean T.A. time and mean solver time were omitted since it was already concluded that these remain nearly invariant for each solver algorithm.

By analysing the collected data, it can be concluded that every algorithm combination had the same performance in terms of MDE except for SGP. Also, compared to points A, B and C there was a general increase in accuracy. Kalman filtering was able to reduce mean distance error by approximately 1 to 3 cm of the original MDE in all iterative cases. Nevertheless, the achieved values highly depend on the initial parameters of the filter, target path and measures per sample, so no conclusion can be drawn regarding the use of the filter in other cases. To provide a visualization of results from Table 5.4, Figure

Table 5.4: Data for straight line path A to B.

PATH A to B												
Algorithm / Initialization	**MDE [mm]**		**Max. error [mm]**		**Accuracy 90% precision [mm]**		**MDE [mm]**		**Max. error [mm]**		**Accuracy 90% precision [mm]**	
	Linear interpolation						**Kalman filter**					
	1 mps	*2 mps*	*1 mps*	*2 mps*	*1 mps*	*2 mps*	*1 mps*	*2 mps*	*1 mps*	*2 mps*	*1 mps*	*2 mps*
SGP	62	**	176	**	109	**	26	**	64	**	41	**
LLS	43	**	93	**	70	**	23	**	49	**	39	**
LWLS	**	40	**	73	**	72	**	29	**	50	**	45
TS/SGP	40	--	104	--	82	--	27	--	57	--	43	--
TS/LLS	41	31	111	62	75	47	23	23	53	36	36	34
NLLS/LLS	39	--	108	--	76	--	16	--	37	--	32	--
NLWLS/LLS	44	--	98	--	71	--	21	--	66	--	46	--

** Not aplicable -- Not computed

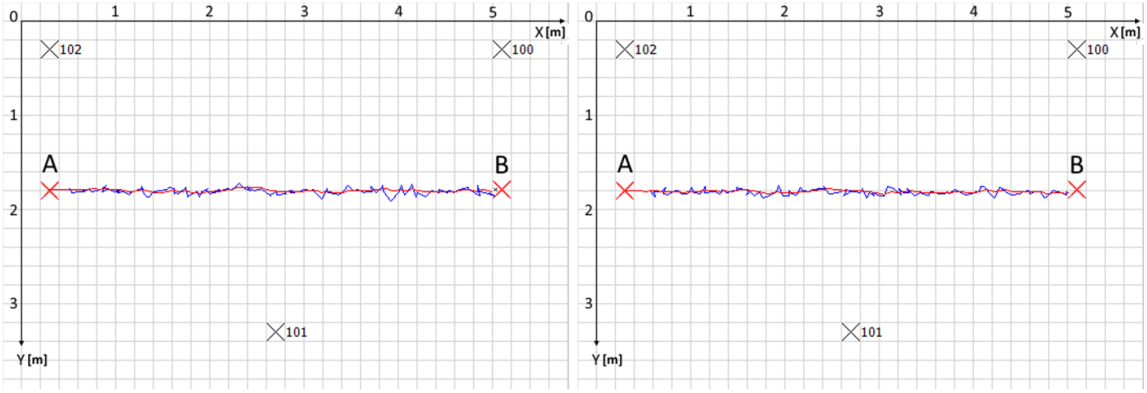

a) LLS b) TS - LLS

Figure 5.8: LLS and TS/LSS performance visualization.

5.8 illustrates the interpolated (blue) and Kalman filtered (red) target path for a) LLS algorithm and b) TS with LLS initialization. These images were taken from the software's Main User Interface (see Appendix C.1) and are generated automatically in real time.

5.7 Summary

In this Chapter, several position estimators were presented. It was given special attention to the Least Squares estimator which has both linearized and non-linear counterparts. Another iterative algorithm based on Taylor-Series Approximation was also implemented. In the case of the fixed points test, it could be concluded that algorithm performance depends on target position relative to the base stations which is explained by the noise dependency on distance. In the case of the straight path line test, all algorithms performed similarly in terms of mean distance error. Also the implemented system model for the Kalman filter was able to reduce MDE at least approximately 30% from all algorithm combinations.

It is possible to increase this value by initializing and setting the filter parameters according to predicted target behaviour. For both tests, the TS solver is the algorithm that minimizes *Tracking Algorithm* iteration time and to provide the best and most consistent results in terms of MDE and accuracy.

Moreover, the developed software was tested in both simulation and real measurements scenarios. It is able to provide tools for controlling various simulation aspects such as predefine a path, noise, Kalman filter configuration, algorithm predefinition and initialization techniques, visual representation of real-time target position as well as sample interpolation and visualization of path smoothing. The presented numerical results in sections 5.6.1 and 5.6.2 were produced automatically at the end of each tracking sequence by the report feature of the software. System architecture, network conception as well as details on *Tracking Algorithm* functioning are described in Chapter 6.

Chapter 6

System architecture

In this chapter, after introducing some basic concepts, a detailed hardware description of the system is presented. Moreover, a comprehensive explanation is given on the network configuration techniques for inferring the target localization. Finally, software programming challenges and details are described along with a thoroughly explanation of the *Tracking Algorithm*.

6.1 Introduction

As concluded in previous chapters, Real-Time Localization Systems are becoming increasingly important nowadays. To be able to build one such system, as with any sufficiently complex system, software and hardware are needed. How these two work together and their base structures is called the *system architecure*. Although this work focuses more on the software (which controls the hardware), it will be given special attention on the mechanics and Application Programming Interface (API) of the modules as this is one of the decisive elements of the system. The adopted system architecture is represented in Figure 6.1, where the arrows represent communication and information flow.

The Hardware component of the architecture can be further scrutinised and broken down in three parts:

- **4 P400 Modules**. These components are the modules itself that include the board, firmware and the two most important interfaces: Ethernet Network Interface Controller (NIC) and RF Port (Antenna).
- **Network**. This component is responsible for the communication between host and the hardware modules. It includes all the physical hardware and configuration up to the fourth layer (Transport layer) of the Open Systems Interconnection (OSI) model.
- **Host PC**. Windows machine that aggregates all information, manages module communication and runs the controlling software.

The Software component, responsible for information processing, has also three dominant components:

- **Real-time physical Localization**. This component is responsible for requesting, receiving and processing hardware commands and messages. It produces human-readable information about the target whereabouts.

- **Real-time tracking**. With data form previous measurements this component is responsible for giving current localization information and possibly predict future locations based on speed and direction of the target. Furthermore, these components are also responsible for the visual processing of the information to the user.

- **User interface**. This architecture component is where the information collected and processed by previous components is displayed. To achieve a simple yet complete interface is one of the primary goals of the work.

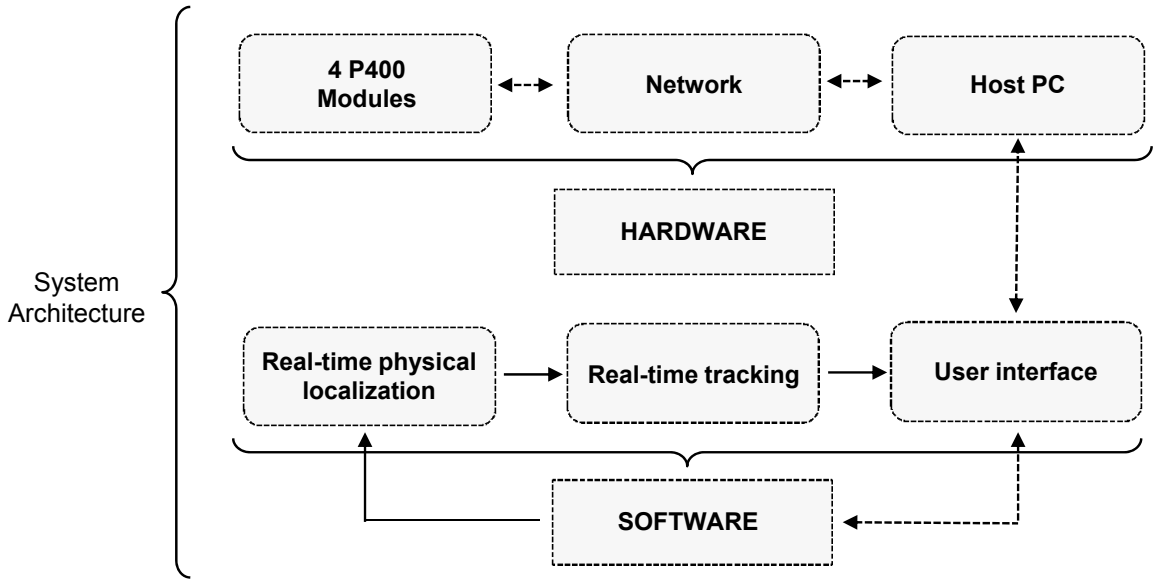

Figure 6.1: System architecture.

6.2 Hardware description

6.2.1 The PulsOn P400 Modules

This work's localization system makes use of four identical Time Domain PulsOn P400 ranging modules, hereinafter also referred to as Ranging and Communications Module (RCM). Each RCM is a radio transceiver able to measure distances between itself and another RCM via a Two-Way Time of Flight ranging mechanism, in all similar to the previously discussed RToF technique via UWB pulses (3.1 to 5.3 GHz).

Communication and Controlling Interfaces

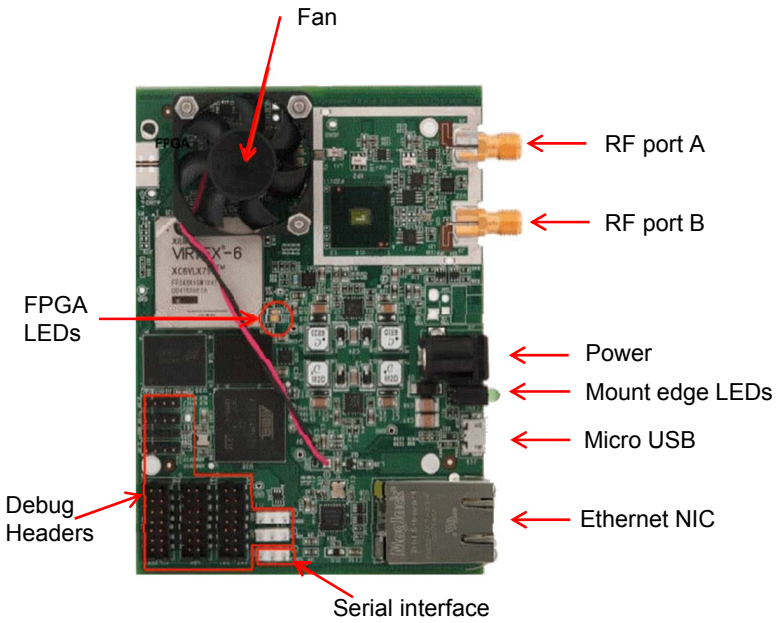

Figure 6.2: One of the four identical RCMs.

A picture of one RCM showing the physical location of the four main communication and controlling interfaces is presented in Figure 6.2.

- **Ethernet Network Interface Controller (NIC)**. Each RCM can be connected via Ethernet to an IP network to allow crossover communication (or through a switch) from/to a host PC using UDP packets.

- **Two RF ports**. Although only one port in this work is used, that is, only one antenna per module, each RCM possesses two RF ports to grant flexibility for sending and receiving UWB signals relying on four working modes: Rx/Tx on A, Rx/Tx on B, Rx on A Tx on B, Rx on B Tx on A.

- **Micro USB**. This interface can be used to connect the RCM directly to a PC for communication and control (much like a crossover Ethernet connection). On the one hand, this communication method requires drivers on the machine side and thus makes the configuration more complex. On the other hand, it allows multiple RCMs connected to the same machine without the need of setting up an IP network.

- **Serial**. The serial port allows the RCM to be controlled by rudimentary peripheral hardware specifically targeted at embedded hosts. Due to the fact that serial functions are highly standardized and basic, this eliminates the need for special devices drivers.

The flexibility granted by an IP network for communication between the Host and the RCMs is what makes this the preferred choice for connecting the devices together.

Round-trip Time of Flight Ranging

Once requested by the host, an RCM will perform a range measurement. This is a built-in feature of these modules and consists in sending a UWB packet (i.e. train of UWB pulses) transmitted at a rate and phase determined by Pseudo-Random Code node to both requester and target RCM in a way resembling a Code-Division Multiple Access (CDMA) technique. The target RCM identifies the leading edge of the received pulse stream, which is the point in time when the first edge of the direct path pulse emerges from the background noise on the receiver. Clocks on both RCMs are synchronized as this is a coherent system. The target RCM sends the information on the leading-edge information back to the requester. With this information, the requester RCM computes the Round-trip Time of Flight by subtracting the sum of both leading-edges (from the request packet received by the target and the response packet received by the requester) from the time difference between the request and response packet. The distance is estimated dividing this time by 2 and multiplying by the speed of light.

As expected, this system is subject to errors in distance measurement. These are due to three main factors:

- **Clock jitter**. Although precise up to picoseconds to allow distance resolution up to millimetres, the clock jitter of the devices may cause synchronism errors between the requester and target node.
- **Finite bandwidth**. The impulse finite bandwidth limits the slope of the leading-edge which influences the output of leading-edge offset detection algorithms. Moreover, frequency selective channels also contribute to overall inaccuracy by distorting the UWB impulse shape.
- **Noise**. The presence of noise can distort the leading-edge slope contributing to inaccuracies in its measurement.

The objective of the mathematical tools employed in this work is to limit the effects of these error inducing factors and provide a localization system as accurate as possible.

6.2.2 Network environment and communication

Network Layout

Each RCM has an IP address assigned and has a service listening on the 21210 port in order to receive UDP packets from the host which is running the developed control software. Figure 6.3 gives a graphical overview of a possible RCM network. In this example, RCM 1 and 2 are wired to the switch and are acting as Base Stations. A third RCM is acting as target as it will respond to RF range requests from 1 and 2 originated at the host.

The exchange of information between the network of RCMs and the host works in an imperative fashion. The host sends a *request* packet and the RCM responds with a *confirm* packet. The kind of response packet is always a *confirm* packet followed by other packet types depending on the request. In the previous example, in an attempt to get the distance between RCMs 1 and 3, the host would send a request packet to 1 with the information to measure distance to 2. RCM 1 would respond with an

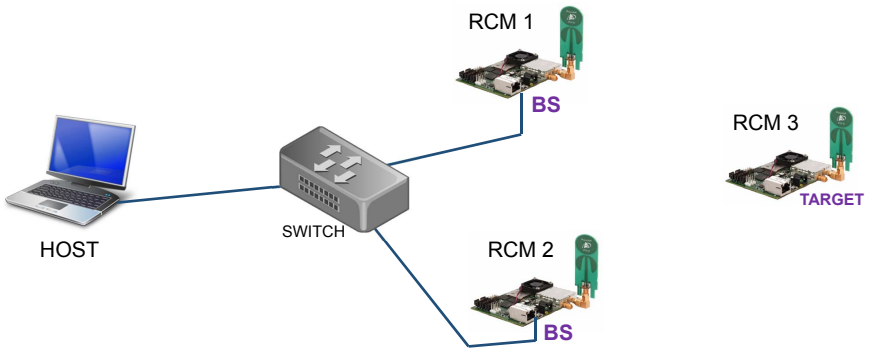

Figure 6.3: Network of RCMs.

confirm packet to acknowledge the request reception. A few moments later RCM 2 responds with a data packet with the distance information - the conversation ends here. Sporadic packets sent by the RCM to the host may happen in some circumstances but only if configured to do so, otherwise a conversation is always initiated by the host.

The described network diagram in Figure 6.3 is the trivial and most simple solution for connecting the devices in a network. However, the particular set of RCMs used in this dissertation came with the same Media Access Control (MAC) Addresses. This detail prevents the well functioning of these devices in a network environment where only simple switches are used because packet delivery on single ports depends on the switch MAC Table entries that are overwritten once a packet originating from a RCM arrives at the switch. Since it's not possible to modify the MAC Burned-In Address (BIA) of the RCMs, the obvious solution was to broadcast a range request all over the network and discard responses at the host from unwanted devices. This way, since the MAC Address destination is the broadcast address, it is guaranteed that every RCM will receive the packet whether it was intentional or not, independent of the current switch MAC Table. A software and hardware problem arise. First, although not substantial, there would be an additional overhead on the host side that overcomplicates the code on packet processing. Additionally, a target RCM is only able to respond to one range request at a time. This is a problem because the RCM requesters would receive the broadcast request almost simultaneously and only one will get a valid response from the target - the others time out. The firmware does not allow a modification of the time out which makes this solution infeasible.

In order the minimize extra hardware in the network, the RCMs have to be separated in their own broadcast domains so that, for each one, a separate MAC Table on the switch exists. Simply put, each RCM had to be in its own Virtual Local Area Network (VLAN) in a separate IP subnet. This kind of Layer 2 functionality is native of managed switches. Moreover, a router would also be necessary to allow the VLANs to communicate with each other. To achieve all this in a single device, an Asus RT-N12 D1 router, a relatively cheap device, with a custom firmware was used. The final network diagram is depicted in Figure 6.4.

A different VLAN with its own IP subnet was assigned to each router port with a /24 address space. Traffic between all of the VLANs is allowed in the router firewall by default. Additionally, presumably a bug in the RCM firmware prevents outbound communication from their respective subnet when IP

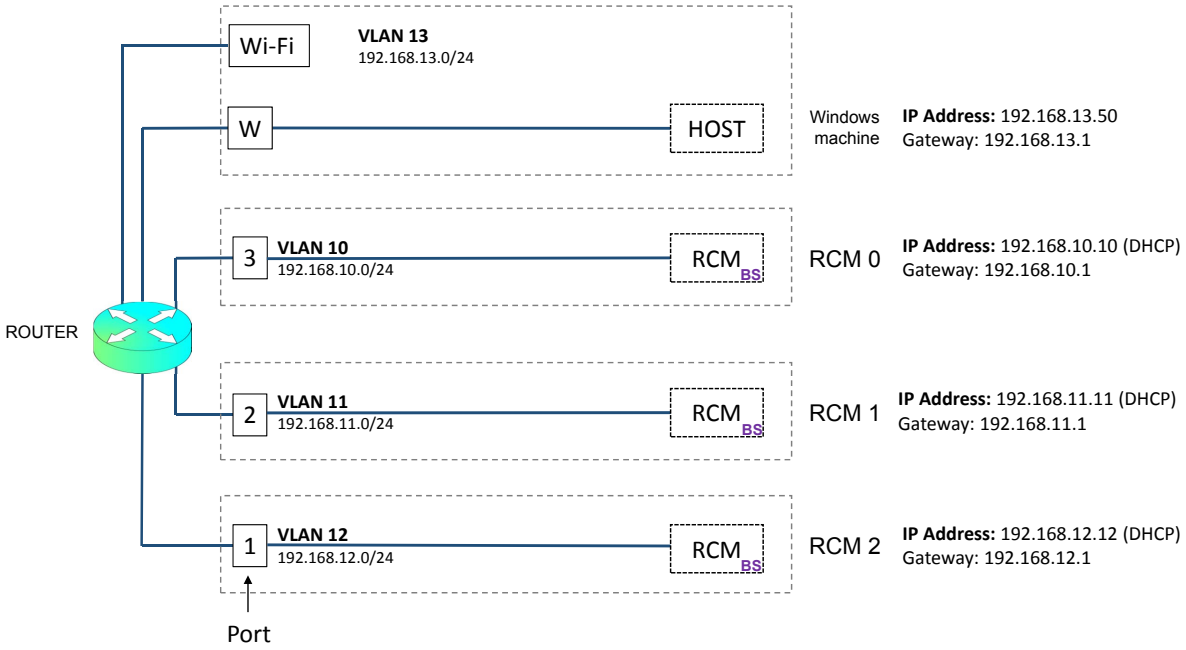

Figure 6.4: Network Layer 3 and Layer 4 structure (target not shown).

Addresses are configured manually. RCM response packets don't ever reach the gateway for proper routing. However, when network configuration details are sent through Dynamic Host Configuration Protocol (DHCP), the communication between Host and RCMs occurs flawlessly. As such, a DHCP server has been configured for each VLAN which assigns the same unique IP Address 192.168.x.x for VLAN x every time an RCM is connected to this VLAN.

Since the router used has Wi-Fi 2.4GHz capability, its corresponding interface was bridged to the Host's VLAN, so that a host computer could connect to the system wirelessly. Although available, this functionality was not tested as it introduces unnecessary packed delay and should only be used if a wired connection from the control PC to the router is not possible.

The proposed network and hardware configuration is constant throughout all operation scenarios.

Transmitted packet types

In this system there are two types of transmitted packets:

- **UDP Packets**. These are the packets that flow through the wired network (or via Wi-Fi), whose endpoints are the host and the RCMs. The interface used is the Ethernet NIC on each endpoint. There is no UDP communication between RCMs themselves.
- **UWB Packets**. These packets are utilized by the RCMs that participate in ranging conversation, i.e. two RCM communicate via UWB Packets when performing a distance measurement. The interfaces used are the RF ports on either device. Details on ranging conversation and how it is handled by the host are described in section 6.3.1.

The software developed in this dissertation only handles the network UDP part. The UWB connection is managed by the stock internal RCM firmware.

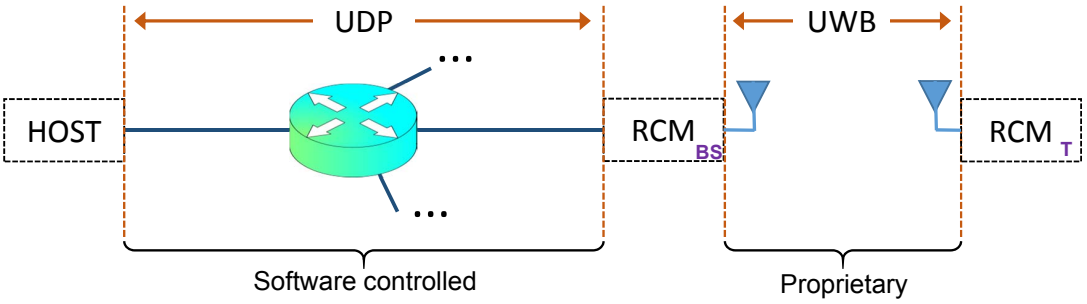

Figure 6.5: System packet transmission.

There are three types of UDP packets that make up a Host-RCM conversation:

- **Request**. Always originates at the host and it can be interpreted as an execution order of a particular RCM function. These packets have the suffix `_REQUEST`.
- **Confirm**. Responses sent by the RCM that acknowledge the reception of one request. These packets have the suffix `_CONFIRM`.
- **Sporadic**. Sent by the RCM sporadically, typically moments after sending a confirm packet to provide additional information. These packets have no suffix.

In what follows, a list and a brief description of the command packets involved in the communication between the RCMs and the host is presented.

- `GET_CONFIG_REQUEST (0x0002)`

  This command is sent by the Host to request for current configuration information. This is used for the software to check for RCM connectivity and configuration display.
  The corresponding acknowledgement is `GET_CONFIG_CONFIRM (0x0102)`.

- `SET_CONFIG_REQUEST (0x0001)`

  This command is sent by the Host with information on new configuration parameters.
  The corresponding acknowledgement is `SET_CONFIG_CONFIRM (0x0101)`.

- `SEND_RANGE_REQUEST (0x0003)`

  The command is sent by the Host in order for an RCM to perform a range measurement. This packet contains information on the target node.
  The corresponding acknowledgement is `SEND_RANGE_CONFIRM (0x0103)`.

- `RANGE_INFO (0x0201)`

  This is a sporadic packet sent by the RCM after performing a ranging operation with details on the measurement. It is expected at the Host just after a `SEND_RANGE_CONFIRM (0x0103)`.

  This packet provides the following relevant data fields:

  - **Channel Quality**. Qualitative measure of channel quality based on the rise time of the leading edge [79].
  - **RSSI**. Receive Signal Strength Indicator.
  - **Range Value**. Estimated distance in mm between the requested RCM and target node.

- `SCAN_INFO (0x0203)`

  This is a sporadic packet sent by the RCM to the Host whenever it receives a UWB packet. Useful information regarding channel quality and RSSI is available within this packet. The difference to `RANGE_INFO` is that this packet arrives without direct request and lacks range estimation. It can be used by hypothetical RSSI Fingerprinting methods to update data maps without explicitly requesting information.

A detailed list of available data fields within all used UDP packet types in this system is available in [79].

6.3 Software description

To control UDP traffic flow and use the information provided by the modules for target localization a software was developed that manages the request, confirm and sporadic packets. The application includes an extensive User Interface designed to interact with the system and it was developed in Visual C# 2012.

The choice of the C# language relies on vast and complete native libraries included in .NET Framework that facilitate interaction with Windows API. Moreover, due to the need of a complete and easy to assemble GUI, the tools provided by Visual Studio 2012 Integrated Development Environment, support the choice of C#. Furthermore, C# is an object-oriented language which provide the unique ability to divide the code in building-blocks known as classes, provides a better understanding on how the application is organized code-wise and promotes further foreign code integration, which simplifies future expansion of the software.

In addition, this application makes use of two foreign distinct pre-compiled assemblies developed for the .NET Framework platform that aid the mathematical operations carried out by the solving algorithms.

- **Math.NET Numerics**[1] which includes also Math.NET Symbolics, is a foreign .NET pre-compiled library with pre-coded mathematical tools such as matrix multiplication, matrix decomposition or runtime algebraic expressions evaluation. It is used by the solver to perform the mathematical operations required by the localization algorithms in an already optimized manner, without recurring to the very basic native mathematical .NET Math class. It also provides a probability distribution toolkit that is used by the simulation tool of the software (see Appendix C.5) to generate random samples normally distributed. The .DLL files needed to load this library are deployed with the application package.

- **MATLAB Runtime** is a set of pre-shared libraries compiled for a specific platform (in this case, the .NET Framework) that allow MATLAB programmed functions to run on computers that don't have MATLAB installed. However, the free MATLAB Runtime software package has to be installed. The application only requires these libraries for the execution of the Non-Linear Least Squares solver. This means the application is fully functional without MATLAB Runtime installed except for this specific solver. The availability of the libraries is checked at runtime.

6.3.1 Application structure

The application is structured into 12 classes all members of the same namespace *Path Tracker* which also shares its name with the application. Classes are divided in types as shown in Table 6.1.

The core classes of the software are the Packet, Solver and Tracker classes. The content of this classes are used by the *Tracking Algorithm* to perform measurements, localize the target and implement smoothing operations (see section 5.5). In what follows, these will be looked into in-depth while analysing the different stages of the *Tracking Algorithm*. Additionally, the main challenges faced on the development of the software will be also pointed out.

Tracker class

As described in section 5.5 the *Tracking Algorithm* is the iterative algorithm employed in the software that measures the distance between base stations and the target (stage A), initializes coordinates values for the solver in case an iterative algorithm was chosen (stage B), estimates target localization (stage C) and perform data smoothing operations (stage D). The stages A to D form a complete iteration and a general block diagram of the main operations of the algorithm is presented in Figure 5.3.

A new tracker class is instantiated each time a new tracking operation is initiated by the user. The methods and fields in this class are used in order to complete a tracking operation which involves a consistency validation upon user-entered algorithm preferences, entered base station layout and the execution of the *Tracking Algorithm* itself.

[1] Lincesed under MIT/X11: https://opensource.org/licenses/MIT

Table 6.1: Classes present in the application.

Class type	Name	Simultaneous instances	Description
non-static	MessageID	1	Provides a field for packet tagging so that pairing between request and confirm packets is possible.
	Packet	3	Provides the essential methods and data fields for UDP socket communication between the host and one module.
	Solver	1	Provides the localization algorithms used for tracking localization including Kalman filtering. It also uses Utilities class methods to draw on form class MainForm.
	Tracker	1	Contains the *tracking algortihm* which gathers measurements and calls solver localization algortihms.
static	Utilities	---	Contains methods which are called repeatedly by other classes. Such methods include drawing on Bitmaps or data conversion.
	Variables	---	Provides all static variables to the whole program (i.e. populate list boxes)
Form class	AdvConfig	1	Form that allows advanced modules and network configuration as well as diagnostic tools.
	KalmanConfig	1	Allows for configuration of Kalman filter properties.
	MainForm	1	This is the main class of the software which initializes all other classes. It controls the main user interface.
	ReportForm	1	After each run of the *tracking algorithm* this form gives options for saving current measurement and tracking data.
	SimulationForm	1	Used to test tracking and solver algorithms.

Packet class

This is the class responsible for creating the receive and send UDP socket to allow communication with a module. Each base station has a *Packet* object associated to it and each network communication with a specific module is carried out through the methods within its respective *Packet* object - this implies the use of distinct UDP sockets for each module and consequently different ports.

The methods in this class are called by the *Tracking Algorithm* to perform stage A, i.e. to get measurement reading from the base stations. An example of how the measurements are obtained and what packets are exchanged through the network is depicted in Figure 6.6.

The modules are named 100-103 and are assigned to each of the four available modules. In the example of Figure 6.6, the *Tracking Algorithm* begins measurements on base station 101 and proceeds up to 103. Each time the target is module 100. Which modules are base stations and which is the target are set by the user prior to tracking.

Every packet sent by the software has a Message ID field. The Message ID from an incoming *confirm* or *sporadic* packet is compared against the one on the *request* package to check for Request-Confirm

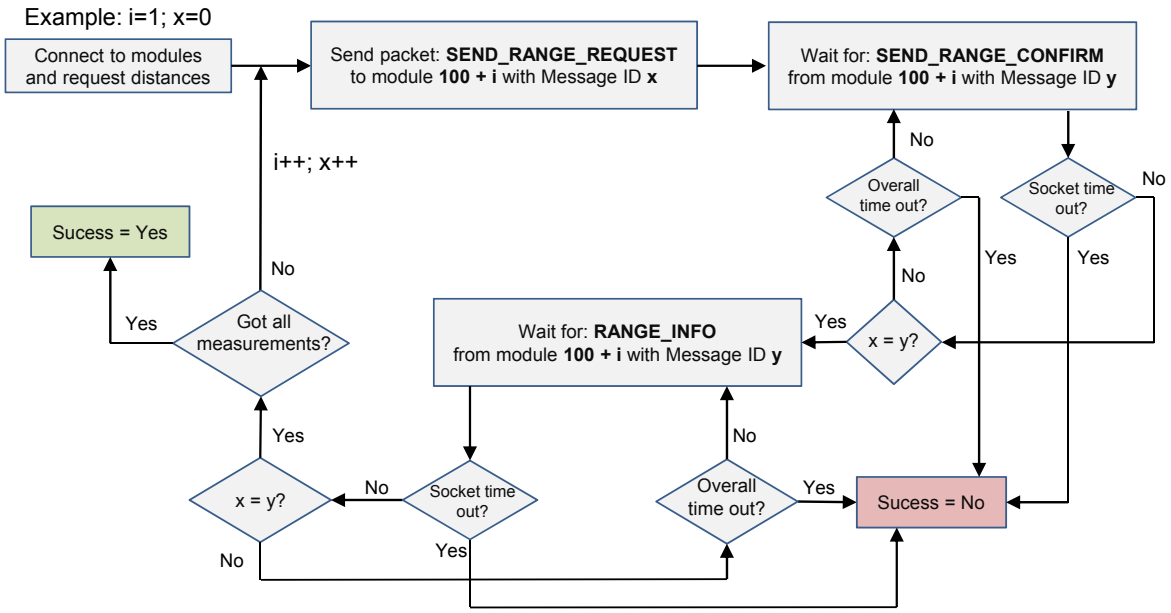

Figure 6.6: Block diagram of stage A of the *Tracking Algorithm*.

correspondence. Because the actual measurement information only arrives in the `RANGE_INFO` packet several milliseconds later after the *confirm*, the software ignores all other received packets on the current port in the meantime. Time out occurs if no valid packed is received (overall time out) or if no packet is received at all (socket time out).

Equally important is to mention that because the measurement operation is a variable time consuming operation and thus does not occur instantly, it is fully executed on a separate process thread. In fact, all stages of the *Tracking Algorithm* except for stage D (data smoothing operations) are executed in separate threads other than the thread that main User Interface (see Appendix C) is currently on. This non-trivial multi-threading aspect is essential since the *Tracking Algorithm* is of iterative nature. If no multi-threading were to be implemented, the User Interface would block and become unresponsive throughout the whole tracking process. As consequence, no real-time visualization of the target would be possible nor direct parameter update.

Solver class

The Solver class contains all methods and data fields necessary to perform location estimation. It is initialized once by the Tracker class and its object remains on use throughout the whole execution of the *Tracking Algorithm*.

To evaluate algebraic matrix and vector expressions, this class makes use of the Math.NET Numerics toolkit. To solve linear systems of equations the QR decomposition technique provided by this library is used. This is the most efficient way to solve linear equations system, since there is no Gaussian elimination available and matrix inversion is a costly operation.

In the scope of the *Tracking Algorithm*, the solver class contains the operations executed within the stage B, C and D. Moreover, it is responsible for drawing the target position estimation on the main User

Interface which also includes the linear interpolation lines and Kalman filter output. It is also at this stage that the *Tracking Algorithm* waits for the sampling period to complete if a specified sampling frequency has been set by the user. The sampling period corresponds to the duration of one full iteration of the *Tracking Algorithm*. By defining a sampling frequency, the measurements take place in a specified time slot. However, in case one iteration takes more time than the sampling period, it means that the solver will return already on the next time slot which will cause the measurements to get out of sync with the predefined time slots. To avoid such a situation, the solver only returns when there's a transition between periods. For instance, if the solver starts at the beginning of the third period and returns half-way through the fourth period, it will wait for the current period to finish and return only at the end of the fourth period actually skipping one full time slot. Figure 6.7 depicts the given situation where the red lines represent the beginning of a new *Tracking Algorithm* iteration.

The procedures of stages B, C and D can be summarized by the block diagram of Figure 6.8. In blocks where a red dot is in view have a failure check at the end of the execution of that block. The failure check is shown at the bottom of the diagram and it was left out of the main diagram due to clarification reasons.

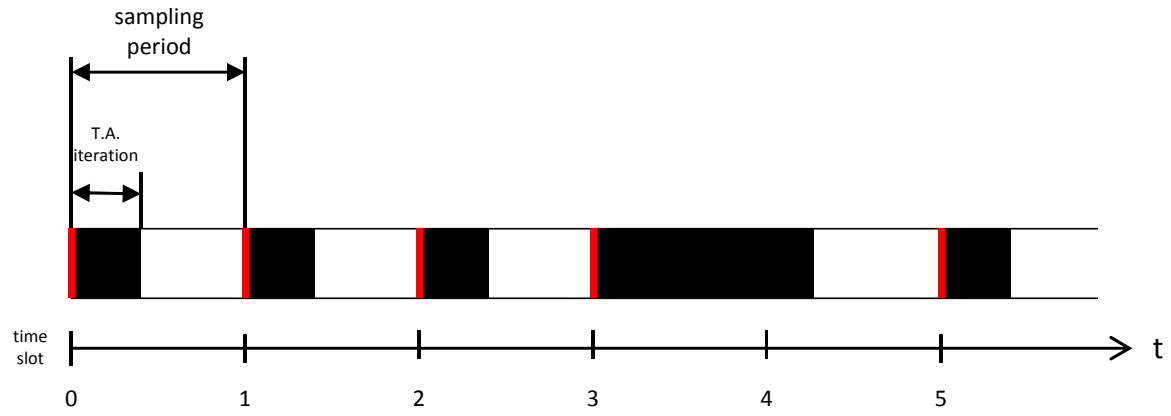

Figure 6.7: 4th time slot is skipped due to delay on stage A, B or C of the *Tracking Algorithm*.

6.4 Summary

In this Chapter, the hardware used in this work was described as well as the developed software. The network problem imposed by the modules' MAC has been addressed and it was solved by separating each module into its own VLAN. Moreover, the programming structure of the software has been shown and its main features pointed out. Finally, every stage of the *Tracking Algorithm* has been explained and analysed together with information on UDP, UWB packet exchange and application constituent classes. It can be concluded that the software is programmed in such a way as to facilitate further feature integration as well as to be adapted to other ranging systems. Additionally, the application is still fully functional without external hardware or software (except for MATLAB Runtime which has to be installed for certain algorithms to be available - see section 5.2.1).

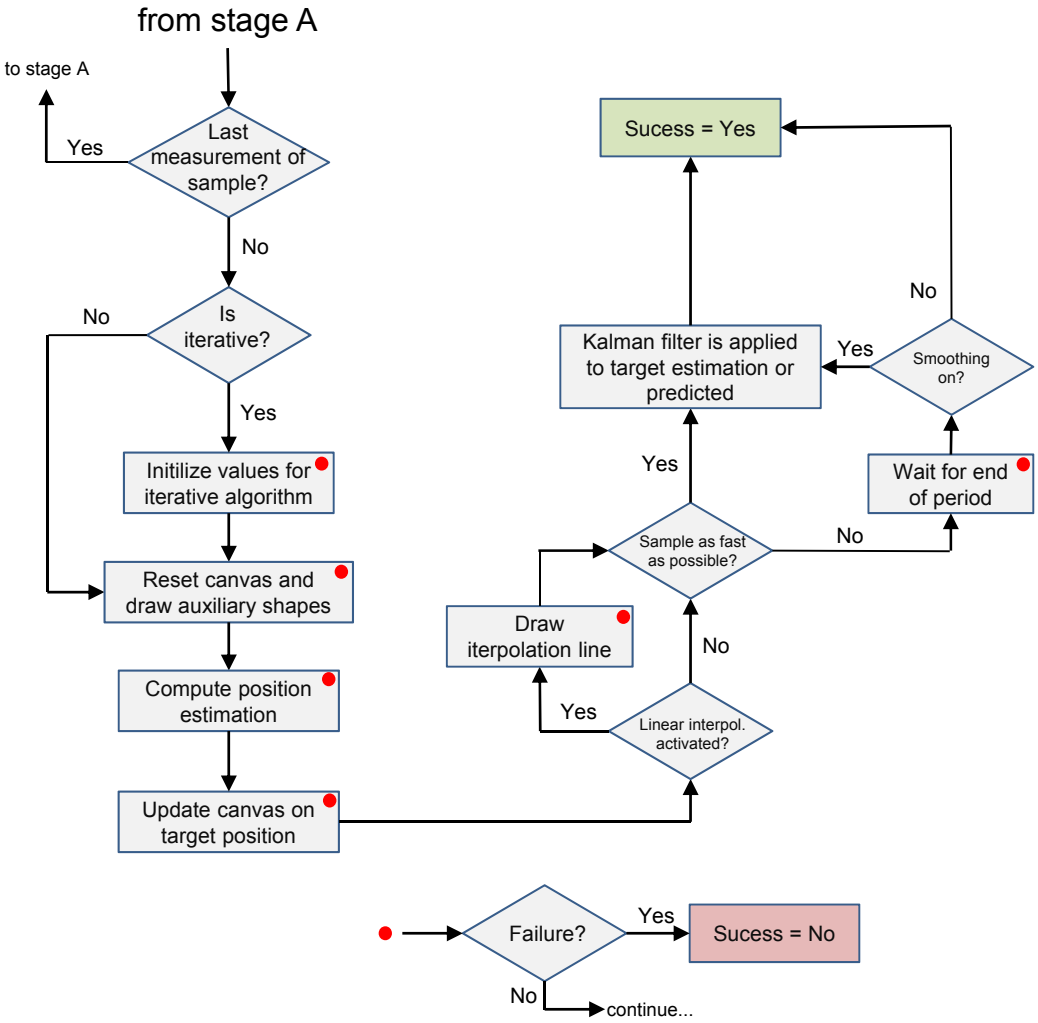

Figure 6.8: Block diagram of stage B, C and D of the *Tracking Algorithm*.

Chapter 7

Conclusion and future work

The main objective of this work was to provide a software control interface for a UWB indoor localization system based on commercially available wireless modules (TimeDomain P400) capable of distance measuring via an RToF protocol. A UWB antenna reflector antenna to be used with this system is also proposed. At the end, a fully functional RTLS is conceived without the use of any external hardware besides the modules and network material.

To achieve the stated goals, this dissertation is composed of three main parts. First, in Chapter 2 and 3, a thorough review on current localization systems and antennas was presented. This helped understanding the current state of art on the matter of wireless localization systems as well as their correspondent antenna requirements. The main challenges and details for antenna dimension were described and their correspondence to actual localization system was also presented.

The second part of this work is composed of Chapter 4 where a printed CPW UWB antenna was developed. The main goal of the proposed antenna was to investigate if a high gain and directional antenna has influence on ranging measurements variance of a UWB ranging system. Due to its radiative properties, the proposed antenna is also less susceptible to interference as well as multipath effects. To achieve high gain and a directive radiation pattern with main lobe oriented perpendicularly to the antenna, a reflector plane was placed behind the substrate. Distance and reflector inclination relative to the substrate were analysed in CST Microwave Studio. The Parameter Sweep tool available in CST helped to visualize the influence of the sweeped parameters, in order to choose the best combination and achieve the stated goals. The accomplished antenna model is matched in the frequency band 2.6GHz up to 10GHz. In the band of interest (3.1 - 5.3GHz), the developed antenna also achieves a theoretical maximum directivity of 8.1dBi. The model was then prototyped and tested in a real scenario. There was a slight discrepancy between the measured and theoretical S_{11} in the lower frequencies of the band, which can be explained by poor coaxial connector matching properties as well as prototype manufacturing imperfections. Additionally the antenna was tested in a real ranging system scenario and its performance compared to 3dBi stock UWB omni-directional monopole antennas. After evaluating the antenna performance, it has been observed that the variance of the measurements is on average 9mm lower when compared to the reference omni-directional monopole up to a distance of 3.8m. However,

the most improvement is in Received Signal Strength Indicator (RSSI) readings, which reached up to 3.3dB.

The third part of this work consists of Chapters 5 and 6 were the controlling software was developed. The goal of the proposed software is to provide a user interface and network controlling of UDP packets used by the Time Domain P400 ranging modules, effectively transforming simple distance measurements in a fully functional, ToA based, localization system. Furthermore, the developed software is stand alone which means that functionality is assured without any third-party software. At first, to process distance information, several localization algorithms were tested. It was given special attention to the Non-Linear Least Squares formulation as it corresponds to the Maximum Likelihood solution. To solve this non-linear localization problem, a linearization was presented (LLS and LWLS) alongside with an iterative Taylor-Series approximation. In addition, to solve the non-linear problem directly and compare results, the MATLAB Runtime external library was used to implement the non-linear least squares solver Trust Region Reflective. Additionally, a solution based on finding the centroid of a triangle formed by the intersection points of circumferences was proposed (SGP). The software was tested in a real and simulated scenario where the accuracy (for 90% precision) and Mean Distance Error (MDE) were measured for various algorithm combinations. For both tests, it has been concluded that the Taylor Series Approximation algorithm establishes a fair compromise between *Tracking Algorithm* iteration time and consistent results in terms of MDE and accuracy. Further, a Kalman filter state model was proposed for this RTLS. For the straight path test (simulated scenario), the filter was able to increase accuracy by approximately 40% for all algorithm combinations. However, filter results depend on base station configuration, propagation conditions and may vary substantially when tested in other scenarios. Also, proper initial filter parameter configuration has to be carried out depending on target behaviour.

The developed software is able to provide an intuitive user interface that controls the modules via UDP packets, processes distance information, applies verified and tested localization algorithms and performs target tracking employing a Kalman filter approach - all in a stand alone application. Furthermore, the software provides a Simulation Console where algorithm performance can be tested in different base station configurations and target behaviour without actually setting up a laboratory measurement. Moreover, the software provides a real time target location visualization as well as linear position interpolation. At the end of each tracking sequence, a report containing the gathered data and tracking statistics is presented to the user.

7.1 Future Work

The challenges regarding antennas and UWB indoor localization systems still have much potential for further investigation. In what follows, four main future work topics are suggested.

- At least two more prototypes of the proposed UWB reflector antenna for base stations should be manufactured so that its true influence on the variance of the measurements can be tested. Also the antennas should be tested under a different UWB localization system with different signal processing algorithms so that a benchmark can be developed. Moreover, the measurement of the

fidelity factor can also contribute to a more comprehensive comparison and understanding of UWB antenna design for indoor UWB localization.

- As mentioned in Chapter 5, a base station to target distance measurement of this RTLS takes approximately 50ms. Because measurements have to be taken sequentially due to inherent hardware limitations, a position sample takes at least approximately 150ms, which limits the system sampling frequency. Such a problem can be circumvented by using the available and implemented Kalman filter more actively. Requests to base stations could be replaced by filter predictions effectively improving sampling frequency and reducing amount of requests. Moreover, the current system state model assumes constant measurement noise covariance ($\boldsymbol{R}$) and constant process noise covariance ($\boldsymbol{Q}$). By modelling target behaviour correctly and predicting the noise values depending on target position, these parameters can be dynamically modified during tracking process to further improve Accuracy and MDE.

- The used Time Domain P400 modules have the capability of measuring Received Signal Strength. This information could be used to implement RSSI Fingerprinting. It has been shown that RSSI measurements are in general less accurate when compared to ToA. However, the performance of a hybrid solution RSSI/ToA could be investigated with the present RTLS and developed without the need for extra hardware.

- The software presented in this work, was developed in such a way that adding or modifying current features is easy even for someone who had not been in contact with the code. As described in Chapter 6, the main application functions are divided in classes and encapsulated from other code parts making the application modular. Therefore, the software can be adjusted dynamically to the necessities of the RTLS user by adding, removing or modifying features as needed. As such, the software can be used as new form of algorithm benchmarking and performance evaluation of other tracking procedures.

References

[1] United States of America - Department of Defense, "Global positioning system standard positioning service performance standard," 4th edition, September 2008.

[2] G. M. Giaglis, A. Pateli, K. Fouskas, P. Kourouthanassis, and A. Tsamakos, "On the Potential Use of Mobile Positioning Technologies in Indoor Environments," *15th Bled Electronic Commerce Conference*, pp. 413–429. Bled, Slovenia, June 17-19, 2002.

[3] H. M. Khoury and V. R. Kamat, "Evaluation of position tracking technologies for user localization in indoor construction environments," *Automation in Construction*, vol. 18, no. 4, pp. 444–457, 2009.

[4] L. Bras, "Desenvolvimento de um sistema de localização de baixo consumo," 2009. M.S. Thesis, Universidade de Aveiro.

[5] G. Jeyakumar and G. Gopinath, "Ad Hoc Mobile Wireless Networks Routing Protocols – A Review," in *Journal of Computer Science 3 (8)*, pp. 574–582, 2007.

[6] O. Hernandez, V. Jain, S. Chakravarty, and P. Bhargava, "Position Location Monitoring Using IEEE 802.15.4/ZigBee technology." `http://https://www.freescale.com/files/microcontrollers/doc/brochure/PositionLocationMonitoring.pdf`. [Accessed April 2015].

[7] A. KING, "Inertial Navigation – Forty Years of Evolution," *General Electric Company Review*, vol. 13, no. 3, 1998.

[8] J. Hightower and G. Borriello, "Location systems for ubiquitous computing," *Computer*, vol. 34, no. 8, pp. 57–66, 2001.

[9] S. Gezici and H. Poor, "Position estimation via Ultra-Wide-Band signals," *Proc. IEEE*, vol. 97, no. 2, pp. 386–403, 2009.

[10] A. Boukerche, H. A.B.F. Oliveira, E. F. Nakamura, and A. A.F. Loureiro, "Localization Systems For Wireless Sensor Networks," *IEEE Wireless Communications*, 2007.

[11] A. Savvides, C.-C. Han, and M. B. Strivastava, "Dynamic fine-grained localization in ad-hoc networks of sensors," in *Proceedings of the 7th annual international conference on Mobile computing and networking*, pp. 166–179, ACM, 2001.

[12] G. Pottie and W. Kaiser, “Wireless integrated network systems,” in *Communications of the ACM*, vol. 43, pp. 51–58, May 2000.

[13] L. Bras, N. B. Carvalho, P. Pinho, L. Kulas, and K. Nyka, “A Review of Antennas for Indoor Positioning Systems,” *International Journal of Antennas and Propagation*, vol. 2012, pp. 1–14, 2012.

[14] H. Liu, H. Darabi, P. Banerjee, and J. Liu, “Survey of Wireless Indoor Positioning Techniques and Systems,” *IEEE Trans. Syst., Man, Cybern. C*, vol. 37, no. 6, pp. 1067–1080, 2007.

[15] P. Kasebzadeh, G.-S. Granados, and E. Lohan, “Indoor localization via WLAN path-loss models and Dempster-Shafer combining,” in *Localization and GNSS (ICL-GNSS), 2014 International Conference on*, pp. 1–6, June 2014.

[16] Y. Fu, H. Liu, J. Qin, and T. Xing, “The Localization of Wireless Sensor Network Nodes Based on DSSS,” in *Electro/information Technology, 2006 IEEE International Conference on*, pp. 465–469, May 2006.

[17] K. Pahlavan, X. Li, and J. Makela, “Indoor geolocation science and technology,” *IEEE Communications Magazine*, vol. 40, no. 2, pp. 112–118, 2002.

[18] L. Yang and G. Giannakis, “Timing Ultra-Wideband signals with dirty templates,” *IEEE Trans. Commun.*, vol. 53, no. 11, pp. 1952–1963, 2005.

[19] J. Yang, X. Wang, S. I. Park, and H. M. Kim, “A Novel First Arriving Path Detection Algorithm Using Multipath Interference Cancellation in Indoor Environments,” in *Vehicular Technology Conference Fall (VTC 2010-Fall), 2010 IEEE 72nd*, pp. 1–5, Sept 2010.

[20] S. Gezici, “A Survey on Wireless Position Estimation,” *Wireless Personal Communications*, vol. 44, no. 3, pp. 263–282, 2008.

[21] S. Gezici, I. Guvenc, and Z. Sahinoglu, “On the Performance of Linear Least-Squares Estimation in Wireless Positioning Systems,” in *Communications, 2008. ICC ’08. IEEE International Conference on*, pp. 4203–4208, May 2008.

[22] B. Huang, L. Xie, and Z. Yang, “Analysis of TOA localization with heteroscedastic noises,” in *Control Conference (CCC), 2014 33rd Chinese*, pp. 327–332, July 2014.

[23] N. B. Priyantha, A. K. Miu, H. Balakrishnan, and S. Teller, “The Cricket Compass for Context-aware Mobile Applications,” in *Proceedings of the 7th Annual International Conference on Mobile Computing and Networking*, MobiCom ’01, (New York, NY, USA), pp. 1–14, ACM, 2001.

[24] B. Fang, “Simple solutions for hyperbolic and related position fixes,” *IEEE Trans. Aerosp. Electron. Syst.*, vol. 26, no. 5, pp. 748–753, 1990.

[25] S. Gezici, Z. Sahinoglu, H. Kabayashi, and H. V. Poor, *Ultra Wideband Wireless Communication*, ch. 3, pp. 43–71. Wiley, 2010.

[26] B. Van Veen and K. Buckley, “Beamforming: a versatile approach to spatial filtering,” *IEEE ASSP Magazine*, vol. 5, no. 2, pp. 4–24, 1988.

[27] M. Cheney, “The linear sampling method and the MUSIC algorithm,” *Inverse Problems*, vol. 17, no. 4, pp. 591–595, 2001.

[28] A. Tsz Yin Lok, Z. Aliyazicioglu, and H. Hwang, “Multiple Signal Detection using the ESPRIT Algorithm,” *World Congress on Engineering*, vol. II, 2010.

[29] A. Cidronali, S. Maddio, G. Giorgetti, and G. Manes, “Analysis and Performance of a Smart Antenna for 2.45-GHz Single-Anchor indoor positioning,” *IEEE Transactions on Microwave Theory and Techniques*, vol. 58, no. 1, pp. 21–31, 2010.

[30] X. Sun, Y. Ma, J. Xu, J. Zhang, and J. Wang, “A high accuracy mono-station UWB positioning system,” in *Ultra-Wideband, 2008. ICUWB 2008. IEEE International Conference on*, vol. 1, pp. 201–204, Sept 2008.

[31] R. J. Orr and G. D. Abowd, “The Smart Floor: A mechanism for natural user identification and tracking,” in *Proc. Conf. Human Factors in Computing Systems (CHI 2000)*, pp. 1–6, IEEE, 2000.

[32] J. Krumm, S. Harris, B. Meyers, B. Brumitt, M. Hale, and S. Shafer, “Multi-camera multi-person tracking for EasyLiving,” in *Visual Surveillance, 2000. Proceedings. Third IEEE International Workshop on*, pp. 3–10, 2000.

[33] Y.-C. Tseng, S.-L. Wu, W.-H. Liao, and C.-M. Chao, “Location awareness in ad hoc wireless mobile networks,” *Computer*, vol. 34, pp. 46–52, Jun 2001.

[34] R. Want, A. Hopper, V. Falcao, and J. Gibbons, “The active badge location system,” *TOIS*, vol. 10, no. 1, pp. 91–102, 1992.

[35] M. Kaur, M. Sandhu, N. Mohan, and P. S. Sandhu, “RFID Technology Principles, Advantages, Limitations and its Applications,” *IJCEE*, pp. 151–157, 2011.

[36] K. Curran, E. Furey, T. Lunney, J. Santos, D. Woods, and A. McCaughey, “An evaluation of indoor location determination technologies,” *Journal of Location Based Services*, vol. 5, no. 2, pp. 61–78, 2011.

[37] A. Bekkelien, “Bluetooth Indoor Positioning,” 2012. M.S. Thesis, University of Geneva.

[38] Zonith A.S., “ZONITH Indoor Postitioning Module.” `http://media.teldio.com/pdfs/Teldio_Indoor%20Positioning%20White%20Paper_v2.1a.pdf`, 2006. [Accessed April 2015].

[39] Ubiquity Networks, “Ubisense Hardware Datasheet.” `http://mpg.ndlab.net/wp-content/uploads/2009/11/mocap_ubisense_hardware.pdf`, 2006. [Accessed April 2015].

[40] STANLEY Healthcare, “AeroScout Location Engine 4.5.” `http://www.zencontech.cn/documents/datasheet/1434_Location%20engine%204.5.pdf`. [Accessed April 2015].

[41] P. Mercier, D. Daly, M. Bhardwaj, D. Wentzloff, F. Lee, and A. Chandrakasan, "Ultra-low-power UWB for sensor network applications," in *Circuits and Systems, 2008. ISCAS 2008. IEEE International Symposium on*, pp. 2562–2565, May 2008.

[42] L. Brás, "A survey of indoor location systems antennas," *Electrónica e Telecomunicações*, vol. 5, no. 2, pp. 243–250, 2013.

[43] A. Andersen, "2.4GHz Inverted F Antenna," *Texas Instruments - Design Note DN0007*.

[44] A. Andersen, "Small Size 2.4GHz PCB Antenna," *Texas Instruments - Application Note AN043*.

[45] Freescale Semiconductor Inc., "Compact Integrated Antennas." `http://cache.freescale.com/files/rf_if/doc/app_note/AN2731.pdf`. [Accessed April 2015].

[46] M. Ma and K. Deng, "The Study and Implementation of Meander-line Antenna for an Integrated Transciever Design," 2010. M.S. Thesis, University of Gävle.

[47] M. Shamim Shahriar Hossain and N. Karmakar, "An Overview on RFID Frequency Regulations and Antennas," in *Electrical and Computer Engineering, 2006. ICECE '06. International Conference on*, pp. 424–427, Dec 2006.

[48] A. M. Salama, *Radio Frequency Identification Fundamentals and Applications Design Methods and Solutions*, ch. 6, pp. 93–110. InTech, 2010.

[49] B. Chauhan, S. Vijay, and S. Gupta, "Comparative Analysis of Microstrip Patch Antenna using different substrates and observe effect of chaging parameter at 5.4 GHz," in *Conference on Advances in Communication and Control Systems 2013*, 2013.

[50] Nasimuddin, X. Qing, and Z. N. Chen, "Compact circularly polarized microstrip antenna for RFID handheld reader applications," in *Microwave Conference, 2009. APMC 2009. Asia Pacific*, pp. 1950–1953, Dec 2009.

[51] R. Ibrahim, M. Yagoub, and R. Habash, "Microstrip patch antenna for RFID applications," in *Electrical and Computer Engineering, 2009. CCECE '09. Canadian Conference on*, pp. 940–943, May 2009.

[52] C. Medeiros, J. Costa, and C. Fernandes, "UHF RFID smart conveyor belt with confined detection range," in *Antennas and Propagation Society International Symposium, 2009. APSURSI '09. IEEE*, pp. 1–4, June 2009.

[53] M. Abu, N. Masrom, E. Hussin, A. Othman, N. Yatim, F. Johar, and R. Munawar, "2.45 GHz RFID reader array antenna with hexagonal geometry arrangement," in *Applied Electromagnetics (APACE), 2012 IEEE Asia-Pacific Conference on*, pp. 338–341, Dec 2012.

[54] H. M. El Misilmani, M. Al-Husseini, K. Y. Kabalan, and A. El-Hajj, "Compact circularly polarized multiband antennas for RFID applications," *International Journal of Antennas and Propagation*, vol. 2014, pp. 1–10, 2014.

[55] Y. Rahayu, T. Rahman, R. Ngah, and P. Hall, “Ultra wideband technology and its applications,” in *Wireless and Optical Communications Networks, 2008. WOCN ’08. 5th IFIP International Conference on*, pp. 1–5, May 2008.

[56] E. Karapistoli, F.-N. Pavlidou, I. Gragopoulos, and I. Tsetsinas, “An overview of the IEEE 802.15.4a Standard,” *Communications Magazine, IEEE*, vol. 48, pp. 47–53, January 2010.

[57] X. Li and K. Pahlavan, “Super-resolution TOA estimation with diversity for indoor geolocation,” *IEEE Transactions on Wireless Communications*, vol. 3, no. 1, pp. 224–234, 2004.

[58] V. Matos, “Antennas and test-bed for new generation UWB localization systems,” 2012. M.S. Thesis, Instituto Superior Técnico - Universidade de Lisboa.

[59] S. M. Abbas, I. Saleem, B. Ahmed, and H. Khurshid, “UWB antenna with parasitic patch and asymmetric feed,” *Information Sciences Letters*, vol. 2, no. 1, pp. 27–33, 2013.

[60] M. Peyrot-Solis, G. Galvan-Tejada, and H. Jardon-Aguilar, “State of the art in WItra-Wideband antennas,” in *Electrical and Electronics Engineering, 2005 2nd International Conference on*, pp. 101–105, Sept 2005.

[61] E. G. Lim, Z. Wang, C.-U. Lei, Y. Wang, and K. Man, “Ultra Wideband Antennas–Past and Present,” *IAENG International journal of computer science*, vol. 37, no. 3, pp. 304–314, 2010.

[62] J. Liang, C. Chiau, X. Chen, and C. Parini, “Study of a printed circular disc monopole antenna for UWB systems,” *IEEE Transactions on Antennas and Propagation*, vol. 53, no. 11, pp. 3500–3504, 2005.

[63] H. Zhang, G. Li, J. Wang, and X. Yin, “A novel coplanar CPW-fed square printed monopole antenna for UWB applications,” in *Microwave and Millimeter Wave Technology (ICMMT), 2010 International Conference on*, pp. 352–354, May 2010.

[64] J. Jung, W. Choi, and J. Choi, “A Small Wideband Microstrip-fed Monopole Antenna,” *IEEE Microwave and Wireless components letters*, vol. 15, no. 10, pp. 703–705, 2005.

[65] H.-N. Lin, C.-M. Shao, and J.-L. Chen, “Design of ultra-wideband monopole antenna with band-notched and GPS circular polarization characteristics,” in *PIERS Proceedings*, pp. 151–156, 2008.

[66] S.-G. Mao, J.-C. Yeh, and S.-L. Chen, “Ultrawideband circularly polarized spiral antenna using integrated balun with application to Time-Domain target detection,” *IEEE Transactions on Antennas and Propagation*, vol. 57, no. 7, pp. 1914–1920, 2009.

[67] M. Koohestani, N. Pires, A. Skrivervik, and A. Moreira, “Band-reject ultra-wideband monopole antenna using patch loading,” *Electronic Letters*, vol. 48, no. 16, 2012.

[68] L. Bras, M. Oliveira, N. Carvalho, and P. Pinho, “Improved sectorised antenna for indoor localization systems,” in *Microwave Conference (EuMC), 2011 41st European*, pp. 1003–1006, Oct 2011.

[69] H. Kawakami and T. Ohira, "Electrically steerable passive array radiator (ESPAR) antennas," *IEEE Antennas Propag. Mag.*, vol. 47, no. 2, pp. 43–50, 2005.

[70] C. Sun, A. Hirata, T. Ohira, and N. Karmakar, "Fast beamforming of electronically steerable parasitic array radiator antennas: Theory and Experiment," *IEEE Transactions on Antennas and Propagation*, vol. 52, no. 7, pp. 1819–1832, 2004.

[71] K. Iigusa, K. Sato, and M. Fujise, "A Slim Electronically Steerable Parasitic Array Radiator Antenna," in *ITS Telecommunications Proceedings, 2006 6th International Conference on*, pp. 386–389, June 2006.

[72] R. Lourenço, "Projecto de Agregado Conforme a uma Superfície Cilíndrica," 2015. M.S. Thesis, Instituto Superior Técnico, Universidade de Lisboa.

[73] Time Domain, "P400 Documentation — Broadspec UWB Antenna." `http://www.timedomain.com/datasheets/TD_Broadspec_Antenna.pdf`. [Accessed February 2015].

[74] G. Quintero, J. F. Zurcher, and A. K. Skrivervik, "System fidelity factor: A new method for comparing uwb antennas," *IEEE Transactions on Antennas and Propagation*, vol. 59, pp. 2502–2512, July 2011.

[75] K. Cheung, H. So, W.-K. Ma, and Y. Chan, "Least squares algorithms for time-of-arrival-based mobile location," *Signal Processing, IEEE Transactions on*, vol. 52, pp. 1121–1130, April 2004.

[76] F. K. Chan, H. So, J. Zheng, and K. W. Lui, "Best Linear Unbiased Estimator Approach for Time-of-Arrival Based Localisation," *IET Signal Processing*, vol. 2, pp. 156–163, June 2009.

[77] S. Kay, *Fundamentals of Statistical Signal Processing: Estimation Theory*. NJ: Prentice-Hall, 1993.

[78] N. Han and J.-Y. Pyun, "Improved target detection for moving object in IR-UWB radar," in *Proceedings of the International Conference on Green and Human Information Technology (ICGHIT '13)*, pp. 69–73 vol.1, February 2015.

[79] Time Domain, "P400 Documentation — RCM Application Programing Interface." `http://www.timedomain.com/datasheets/320-0282F%20RCM%20API%20Specification.pdf`. [Accessed September 2015].

Appendix A

Connector model

Figure A.1: SMA connector.

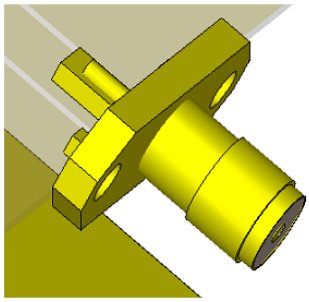

Figure A.2: CST model of SMA connector.

Appendix B

Radiation patterns of UWB antenna

In what follows, the radiation patters for the frequencies 3.1GHz, 4.3GHz and 5.3GHz are shown. The patters are shown in terms of θ for $\phi = 0$ and $\phi = 90$ (see Figure B.1).

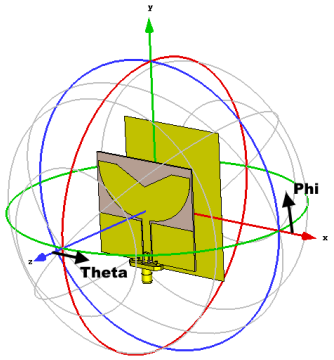

Figure B.1: Antenna spherical coordinate system.

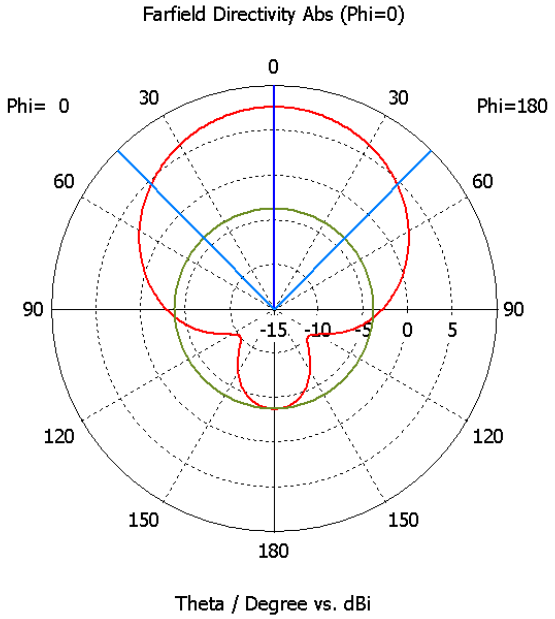

Figure B.2: $f = 3.1GHz$ for $\phi = 0$.

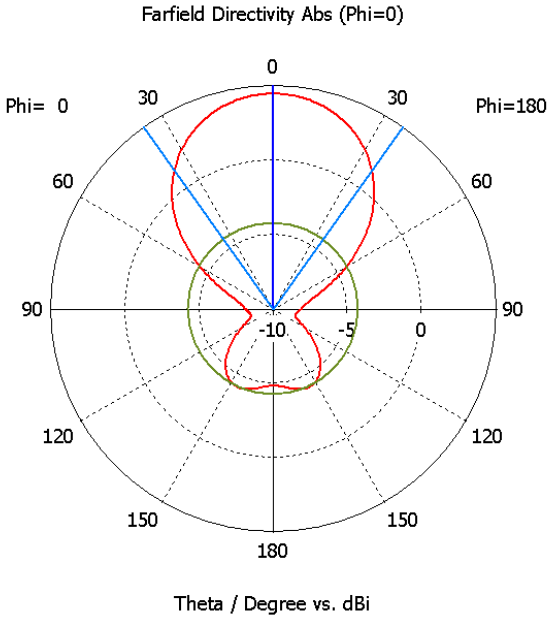

Figure B.3: $f = 4.3GHz$ for $\phi = 0$.

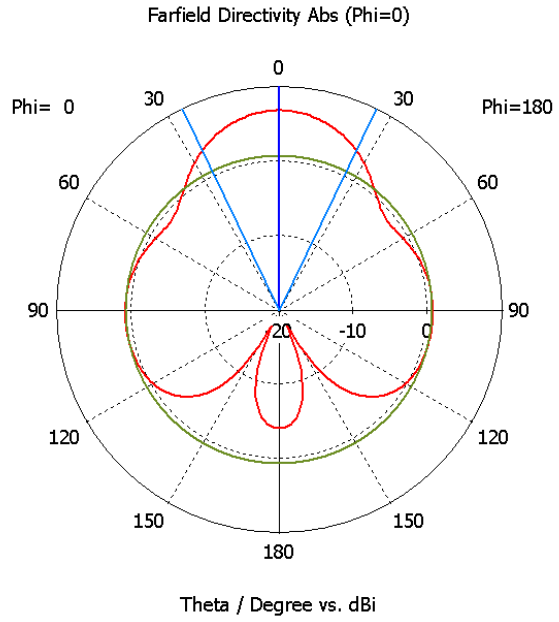

Figure B.4: $f = 5.3GHz$ for $\phi = 0$.

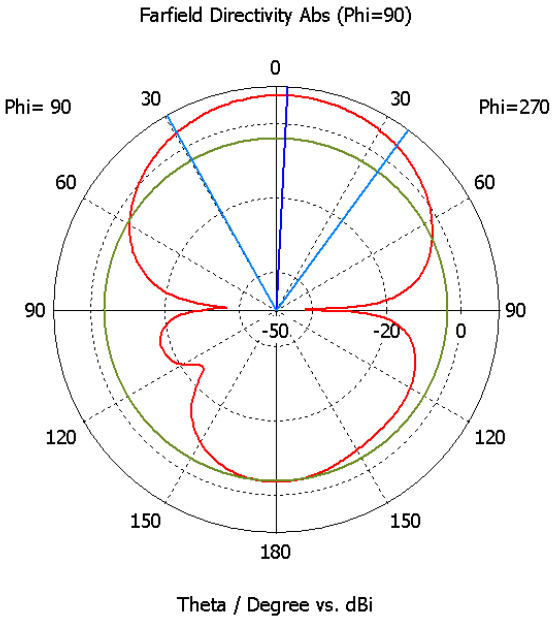

Figure B.5: $f = 3.1GHz$ for $\phi = 90°$.

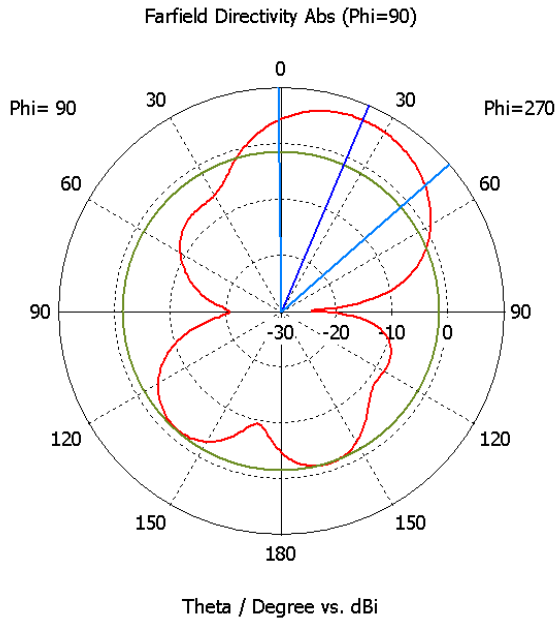

Figure B.6: $f = 4.3GHz$ for $\phi = 90°$.

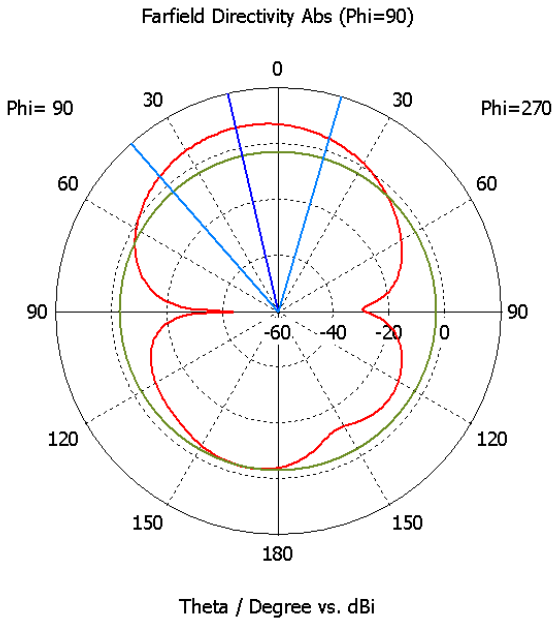

Figure B.7: $f = 5.3GHz$ for $\phi = 90°$.

Appendix C

Software User Interface

The developed software is composed of several interfaces to provide user control and configuration options. In this section the implemented interfaces or windows are presented along with their functionality and purpose.

C.1 Main User Interface

The main User Interface is depicted in Figure C.1. This is the initial window of the application and contains most the program's features.

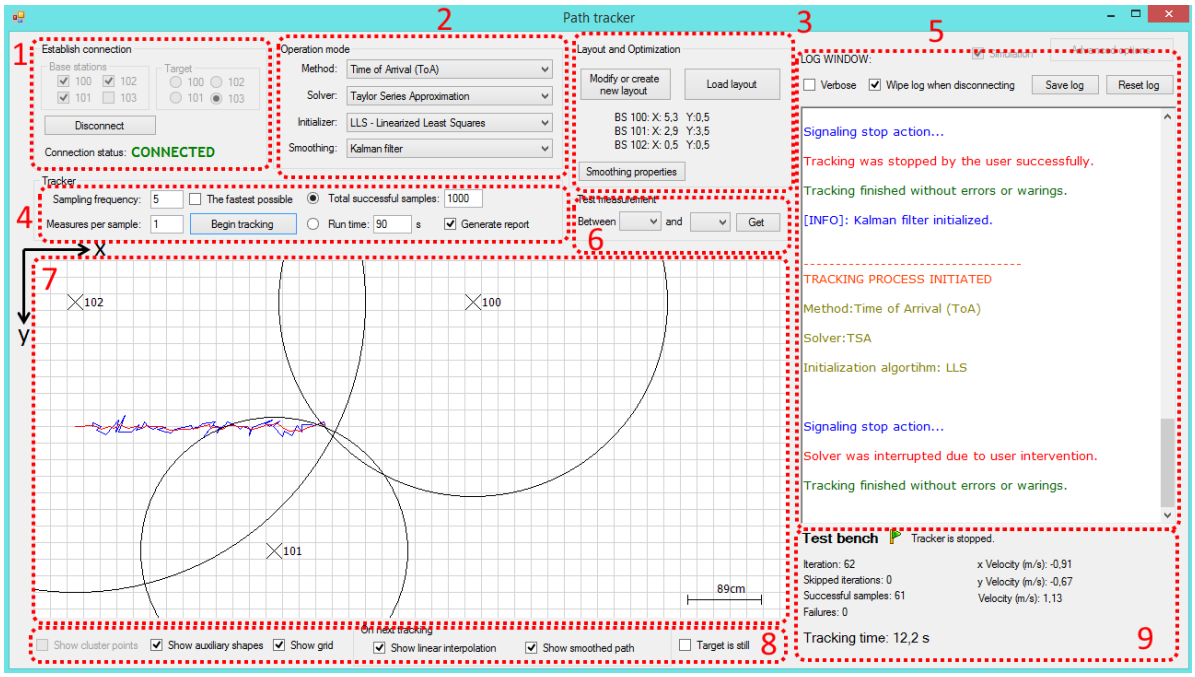

Figure C.1: Main User Interface.

- **Box 1**. Assignment of base stations and target modules.
- **Box 2**. Selection of:

  - **Method**. Tracking method (only option available is ToA).
  - **Solver**. Solving algorithm (SGP, LLS, TS, NLLS, ...).
  - **Initializer**. Initializer options in case an iterative algorithm is chosen in Solver.
  - **Smoothing**. Allows Kalman filter activation (only option available).

- **Box 3**. Selection, loading (see Appendix D) or modification of base station layout as well as Kalman filter properties.
- **Box 4**. Tracker configuration options.
- **Box 5**. Log window. Informations, warning or errors are displayed in this textbox. A verbose mode is available.
- **Box 6**. Tool to get one time distance between two modules.
- **Box 7**. Main canvas where tracking is displayed in real time.
- **Box 8**. Canvas options.
- **Box 9**. Test bench where current tracking statistics are displayed.

C.2 Advanced Options

This window includes special configuration settings of the modules for specific system needs. All experiments carried out in this work use default configuration values [79].

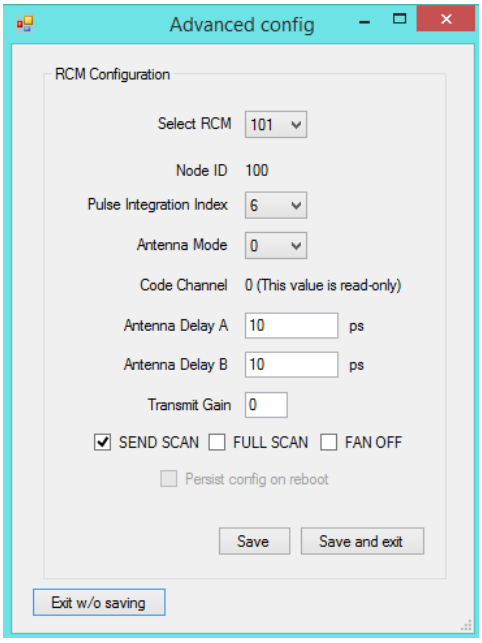

Figure C.2: Advanced configuration interface.

C.3 New base station layout

This window is accessed though Box 3 and allows configuration of base station layout including modules' coordinates, scale in pixels/m for canvas representation, scale size and grid size.

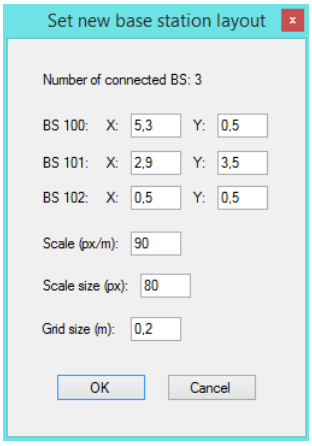

Figure C.3: Set new base station layout interface.

C.4 Smoothing options

This window is accessed through Box 3 and holds Kalman filter configuration options.

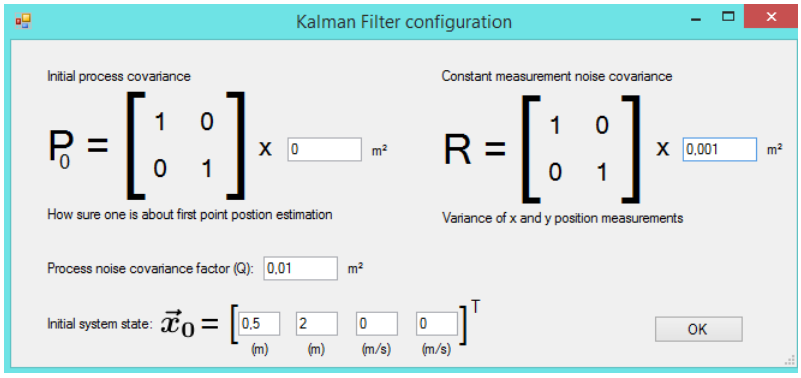

Figure C.4: Kalman filter options interface.

C.5 Simulation console

The window provide target behaviour simulation options.

- **Box 1**. Simulation options.
  - **Mouse hovering**. Simulates target behaviour by acquiring mouse position over canvas (Box 5).
  - **Circle**. Simulates a circular behaviour for the target.

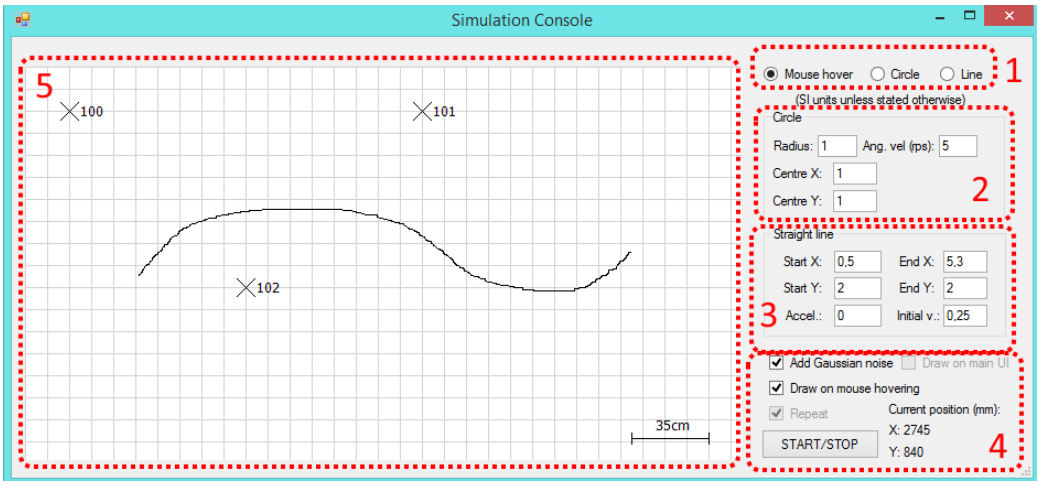

Figure C.5: Simulation console interface.

  - **Line**. Simulates a straight path for the target.

- **Box 2**. Circular behaviour options.
- **Box 3**. Straight line behaviour options.
- **Box 4**. Other options and Start/Stop simulation button.
- **Box 5**. Canvas where base stations and simulation path is displayed.

C.6 Tracking report

This window presents the user with tracking statistics at the end of each run of the *Tracking Algorithm*.

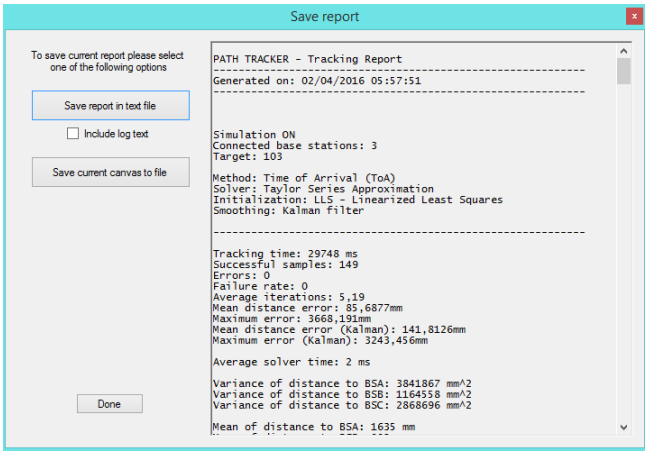

Figure C.6: Save tracking report window.

The following tracking statistics are provided in the report.

- **Tracking time**. Total time in milliseconds the tracker was active.
- **Successful samples**. Total amount of successful *Tracking Algorithm* iterations.

- **Errors**. Total amount of unsuccessful *Tracking Algorithm* iterations.
- **Failure rate**. Percentage of errors relative to every taken sample (successful or not).
- **Average iterations.** Only displayed if an iterative solver is chosen.
- **Mean distance error.** Mean error in millimetres to true target location (only computed if simulating).
- **Maximum error.** Maximum error in millimetres to true target position (only computed if simulating).
- **Mean distance error (Kalman)**. Mean error in millimetres to true target location from Kalman filtered position points (only computed if smoothing is activated).
- **Maximum error (Kalman)**. Maximum error in millimetres to true target location from Kalman filtered position points (only computed if smoothing is activated).
- **Average solver time.** Average time in milliseconds of stage C of the *Tracking Algorithm*.

Additionally, the tracking report contains a *tracking log file* which is composed of statistics for each *Tracking Algorithm* iteration. Each iteration corresponds to a line which contain the information in Table C.1 separated by a semi-colon.

Table C.1: Fields of tracking log file.

Position	Field
1	Elapsed tracker time [ms]
2	Distance to 1st B.S. (ID order) [mm]
3	Distance to 2nd B.S. (ID order) [mm]
4	Distance to 3rd B.S. (ID order) [mm]
5	Time to get measurement from 1st B.S. (ID order) [mm]
6	Time to get measurement from 2st B.S. (ID order) [mm]
7	Time to get measurement from 3st B.S. (ID order) [mm]
8	Tracking Algorithm current iteration
9	1 = Error; 0 = successful sample
10	X-coordinate of target position [m]
11	Y-coordinate of target position [m]
12	X-coordinate of target position after Kalman filtering [m]
13	Y-coordinate of target position after Kalman filtering [m]
14	Solver running time [ms]

Position	Field
15	RSSI from 1st B.S. (ID order)*
16	RSSI from 2st B.S. (ID order)*
17	RSSI from 3st B.S. (ID order)*
18	Channel Quality from 1st B.S. (ID order)*
19	Channel Quality from 2st B.S. (ID order)*
20	Channel Quality from 3st B.S. (ID order)*
21	(not used)
22	(not used)
23	(not used)
24	Number of iterations if solver is iterative. 0 if not.
25	X-coord. of true target position [m]
26	Y-coord. of true target position [m]
27	X-coord. of true target position after Kalman filtering [m]
28	Y-coord. of true target position after Kalman filtering [m]

* Provided by the internal firmware of the modules.

Appendix D

Example of layout input file

In order to load predefined settings to the software without setting up manually for every application instance, it is possible to load a text file with multiple configuration commands. This feature is accessible through the button 'Load Layout' in Box 3 of the main User Interface (Figure 5.7). The following code is an example of the expected configuration file.

```
1 N.BS:3
2 X:5,3;Y:0,5
3 X:2,9;Y:3,5
4 X:0,5;Y:0,5
5 scale:90
6 2ScaleSize:80
7 GridSize:0,2
```

- **Line 1**: Number of connected base stations. For the current software version this a constant number (3).
- **Line 2**: X and Y coordinate of first base station (ID order).
- **Line 3**: X and Y coordinate of second base station (ID order).
- **Line 4**: X and Y coordinate of third base station (ID order).
- **Line 5**: Scale in pixels per metre of canvas to real scenario.
- **Line 6**: Size in pixels of scale drawn on canvas.
- **Line 7**: Size in metres of grid squares drawn on canvas.

In this context, canvas refers to Box 7 of the main User Interface (Figure 5.7). Also, coordinate origin lies on the top left corner of canvas.

Any type of comments are not allowed and will render the file invalid.